



Title	CONSTRUCTION OF A PRECISION CALORIMETER ADAPTED TO CONDENSED GASES FROM 1.8 K TO ROOM TEMPERATURE AND HERMODYNAMIC PROPERTIES OF SOME SIMPLE MOLECULAR CRYSTALS
Author(s)	Atake, Tooru
Citation	大阪大学, 1973, 博士論文
Version Type	VoR
URL	https://hdl.handle.net/11094/2122
rights	
Note	

The University of Osaka Institutional Knowledge Archive : OUKA

<https://ir.library.osaka-u.ac.jp/>

The University of Osaka

DOCTORAL DISSERTATION

CONSTRUCTION OF A PRECISION CALORIMETER ADAPTED TO CONDENSED
GASES FROM 1.8 K TO ROOM TEMPERATURE AND THERMODYNAMIC PROPERTIES
OF SOME SIMPLE MOLECULAR CRYSTALS

by

TOORU ATAKE

Faculty of Science

Osaka University

Doctoral Committee:

Professor Hideaki Chihara, Chairman

Professor Syūzō Seki

Professor Tatsuo Miyazawa

Associate Professor Hiroshi Suga

(1973)

Acknowledgement

The author would like to express his sincere thanks to Professor Hideaki Chihara, who has guided him in his investigation, for fruitful suggestions and experimental assistance throughout the course of this work, as well as for excellent leading in refining this dissertation. He also wishes to thank Professor Syūzō Seki, Associate Professor Hiroshi Suga and Assistant Professor Nobuo Nakamura for their valuable suggestions and discussions. The author is indebted to Dr. M. Furue for his assistance in fractional distillation of tetramethylstannane. The author feels grateful to Dr. Michio Sorai, Dr. Takasuke Matsuo and Dr. Gen Soda for their kindhearted discussions. The author is also indebted to Mr. Yoshiyuki Higashigaki and Mr. Akira Inaba for their assistances in experiments of heat capacity measurements of dinitrogen oxide and of calibration of the temperature scale of germanium resistance thermometer β , and to Miss Hiroko Shimizu for typewriting the tables in this thesis. Finally, the author expresses his hearty thanks to his wife Tomiko Atake for her encouragement.

Contents

	page
Chapter 1. Introduction	1
Chapter 2. Construction of a precision adiabatic Nernst type calorimeter adapted to condensed gases from 1.8 K to room temperature	6
2.1. Introduction	7
2.2. Calorimeter and cryostat	9
2.2.1. General assembly	9
2.2.2. Calorimeter vessel and its surroundings ...	14
2.3. System of measurements	21
2.3.1. Sample filling and vapor pressure measurements	21
2.3.2. Electrical measurements	23
2.4. Temperature scales	27
2.4.1. Platinum resistance thermometer	27
2.4.2. Germanium resistance thermometer	28
2.5. Operation and performance	39
2.5.1. Operation	39
2.5.2. Performance	41
Chapter 3. The heat capacity, vapor pressure and related thermodynamic properties of dinitrogen oxide .	44
3.1. Introduction	45
3.2. Experimental	47
3.2.1. Material	47
3.2.2. Calorimetry	47
3.3. Results	52
3.3.1. Heat capacity	52
3.3.2. Fusion	52
3.3.3. Heat of vaporization	67
3.3.4. Vapor pressure	67
3.3.5. Thermodynamic functions	78

3.4.	Analysis and discussion	80
3.4.1.	Residual entropy	80
3.4.2.	Structure and librational motion in solid state	83
3.4.3.	Zero point properties	94
3.4.4.	Lattice modes in the low temperature region	98
3.4.5.	Premelting	110
3.4.6.	General discussion	115
Chapter 4. The heat capacity, vapor pressure and related thermodynamic properties of tetramethylstannane		123
4.1.	Introduction	124
4.2.	Experimental	127
4.2.1.	Material	127
4.2.2.	Calorimetry	128
4.2.3.	Vapor pressure measurement	130
4.2.4.	Raman spectra	131
4.3.	Results	132
4.3.1.	Heat capacity	132
4.3.2.	Fusion	132
4.3.3.	Vapor pressure and heat of vaporization ..	141
4.3.4.	Thermodynamic functions	145
4.3.5.	Raman spectra	149
4.4.	Analysis and discussion	154
4.4.1.	The third-law entropy and internal rotation of methyl groups	154
4.4.2.	Zero point properties	160
4.4.3.	Premelting	164
References		170

Chapter 1
Introduction

Chapter 1

Introduction

The classical thermodynamics based on the First and Second Law of Thermodynamics forms a completely closed system. In 1906 Nernst put forward the Heat Theorem, which has become the Third Law of Thermodynamics. The entropy derived in the Second Law appears also in the Third Law of Thermodynamics, where the thermodynamics and the statistics are connected by the entropy. The history of the third-law entropy is that of the investigations of simple molecular substances on modern thermodynamics. In the early stage of the history (in the 1920's and the 1930's), the Third Law enunciated by F.E.Simon²⁸⁾ was verified by experiments carried out by W.F.Giauque,¹⁾ F.E.Simon and several other investigators and their coworkers.^{2),3)} The calorimetry and related thermodynamic measurements on simple molecular substances were made with high precision, and the values of the third-law entropy compared favorably with those of the spectroscopic entropy calculated from the structural and spectroscopic data. Sometimes, however, there have been the non-zero residual entropies defined as the difference between the two kinds of entropies. The explanation for the differences has been one of the principal problems in such investigations. After eliminating the causes for errors in the measurements and calculations, there still remain

two possibilities; (a) non-equilibrium state frozen in solid state, (b) anomaly of heat capacity below the lowest temperature measured. Glassy states certainly belong to the first category. In the case of some molecular crystals, however, the explanations for the residual entropies have been made insufficiently because of several causes; the insufficient precision of calorimetry and the rather high temperature to which the calorimetry was limited, etc. Many efforts have been devoted by several investigators for obtaining more precise data down to lower temperature region. In the history, one of most brilliant works was made by J.A. Morrison, et al. on methane and the deuterated derivatives.⁷⁾ They obtained precise heat capacity data of methane and the deuterated derivatives down to about 2.5 K, and found some anomalies in the lowest temperature region, which required to take the contribution of nuclear spins into consideration. More recently, the heat capacities of deuterated methanes have been measured down to about 0.4 K.^{19),20)} However, the entire features of the anomalies are still to be explored.

The precise heat capacity measurements for obtaining the residual entropies have also brought about the investigations of molecular dynamics in crystals, which dealt with the relation between the macroscopic-thermodynamic properties and the molecular or atomic behaviors in crystals. The investigation of lattice dynamics in crystals has been started by the splendid achievement of A.Einstein in 1907.⁴⁵⁾ This was extended by P.

Debye in 1912.⁴⁾ Both these two models have been widely used as yet particularly in phenomenological analyses. At the same time as that of P. Debye (in 1912), M. Born and Th. von Karman⁴⁶⁾ published their investigation of the lattice dynamics based on the microscopic model where each individual atomic interaction was taken explicitly into account. Based on this atomic model, many theoretical investigations of lattice dynamics have been developed for obtaining the frequency distribution $g(\nu)$. The root sampling method was devised by M. Blackman.⁷⁵⁾ The moment trace method has been developed by H. Thirring,⁴²⁾ E. W. Montroll,⁴⁷⁾ and others.⁴⁸⁾ W. V. Houston⁷⁶⁾ introduced an approximate method for calculating $g(\nu)$ for a few symmetric directions in a cubic crystal. The numerical calculations have been made by using high speed computers. Lately, self-consistent phonon approximation has been developed. In the case of molecular crystals, inert gas crystals have been widely investigated, and recently, the investigation has been extended to diatomic molecular crystals.

There has been no commercial precision calorimeter for heat capacity determination available. For determining third-law entropies of simple molecular substances, of which almost all substances are gaseous at room temperature, the heat capacities and related thermodynamic quantities should be measured with high precision. The first aim of this investigation is to construct a new precision calorimeter for use with condensed gases from 1.8 K to room temperature. The author wishes to report the

performance of the condensed gas calorimeter, of which the precision and accuracy are higher than any previous apparatus.^{5),8),10),12),etc.} The second is to measure the heat capacities and related thermodynamic properties of simple molecular substances; dinitrogen oxide and tetramethylstannane. The present thesis gives the results of the measurements and the analyses and discussions in detail.

Chapter 2

Construction of a precision adiabatic Nernst type calorimeter
adapted to condensed gases from 1.8 K to room temperature

2.1. Introduction

2.2. Calorimeter and cryostat

2.2.1. General assembly

2.2.2. Calorimeter vessel and its surroundings

2.3. System of measurements

2.3.1. Sample filling and vapor pressure measurement

2.3.2. Electrical measurements

2.4. Temperature scales

2.4.1. Platinum resistance thermometer

2.4.2. Germanium resistance thermometer

2.5. Operation and performance

2.5.1. Operation

2.5.2. Performance

Chapter 2

Construction of a precision adiabatic Nernst type calorimeter
adapted to condensed gases from 1.8 K to room temperature

2.1. Introduction

Because of their simple molecular and crystal structures, some molecular crystals which are gaseous at room temperature have been widely investigated. The precision calorimetry and related thermodynamic measurements on condensed gases provide basic information about their properties, but the construction and operation of these apparatus are very difficult and complicated. There is no commercial precision calorimeter available. The heat capacities and related thermodynamic data of these substances by W.F.Giauque,¹⁾ K.Clusius²⁾ and other several investigators³⁾ and their coworkers have been receiving high reputation for a long time. However, their measurements were limited to above 15 K, and heat capacities were extrapolated to 0 K by the Debye T^3 law⁴⁾ to obtain the third-law entropies, on the assumption that there were no anomaly below the lowest temperatures measured. It seemed desirable that more complete and more accurate information on the thermodynamic properties of some of condensed gases should be provided. In 1961 J.A.Morrison et al.^{5),6)} reported the precise heat capacities and related thermodynamic

properties of argon and krypton together with a detailed analysis.ⁱ
 The heat capacities of CH_4 ,⁷⁾ Ne ,⁸⁾ Xe ,⁸⁾ CO ,^{9),10),11)} NO ,¹¹⁾
 N_2 ,^{11),12)} O_2 ,^{11),13)} SiH_4 ,¹⁴⁾ CF_4 ,^{15),16)} CO_2 ,¹⁷⁾ NH_3 ,¹⁸⁾ etc.
 have been measured more precisely down to about 3 K. More
 recently, the heat capacities of deuterated methanes have been
 measured down to about 0.4 K,^{19),20)} tracing out the low temper-
 ature heat capacity anomalies which had been partly detected in
 the earlier work of Morrison et al.⁷⁾

In this investigation, a new calorimeter for use with con-
 densed gases from 1.8 K to room temperature which is the more
 improved than the earlier one,¹⁰⁾ has been constructed, and the
 measuring system described in the earlier paper²¹⁾ has been
 modified and improved. The present chapter deals with detailed
 description of the cryostat and calorimeter, and their design
 and performance.

2.2. Calorimeter and cryostat

2.2.1. General assembly

Several types of cryostats for calorimetry on condensed gases have been developed,^{5),8),10),12),etc.} and the temperature region of measurements has been extended to liquid helium region.

However, the precision of measurements in this region is much lower than that in higher temperature region. In this investigation, a new type of cryostat for calorimetry by the adiabatic Nernst method has been devised and constructed, which proved to give an improved performance. It can be used for continuous measurements from 1.8 K to room temperature.

The general calorimeter assembly is shown as a sectional drawing and as a photograph of the interior of the cryostat in Figures 1 and 2, respectively. The feature of the cryostat is that it has a cooling system of vertical cascade type with two refrigerant containers E (brass, internal volume = 430 cm^3) and I (brass, internal volume = 1770 cm^3), which we call the helium can and the hydrogen can, respectively, above the calorimeter vessel A (gold, internal volume = 44 cm^3) and its surroundings B (copper) and C (copper). This cascade system is very economical of liquid helium at low temperature region. The radiation shield D (0.2 mm in wall thickness) and the inner jacket H (1 mm in wall thickness) are made of copper to maintain thermal homogeneity and connected with Wood's alloy to the helium can and the hydrogen can, respectively, while the outer

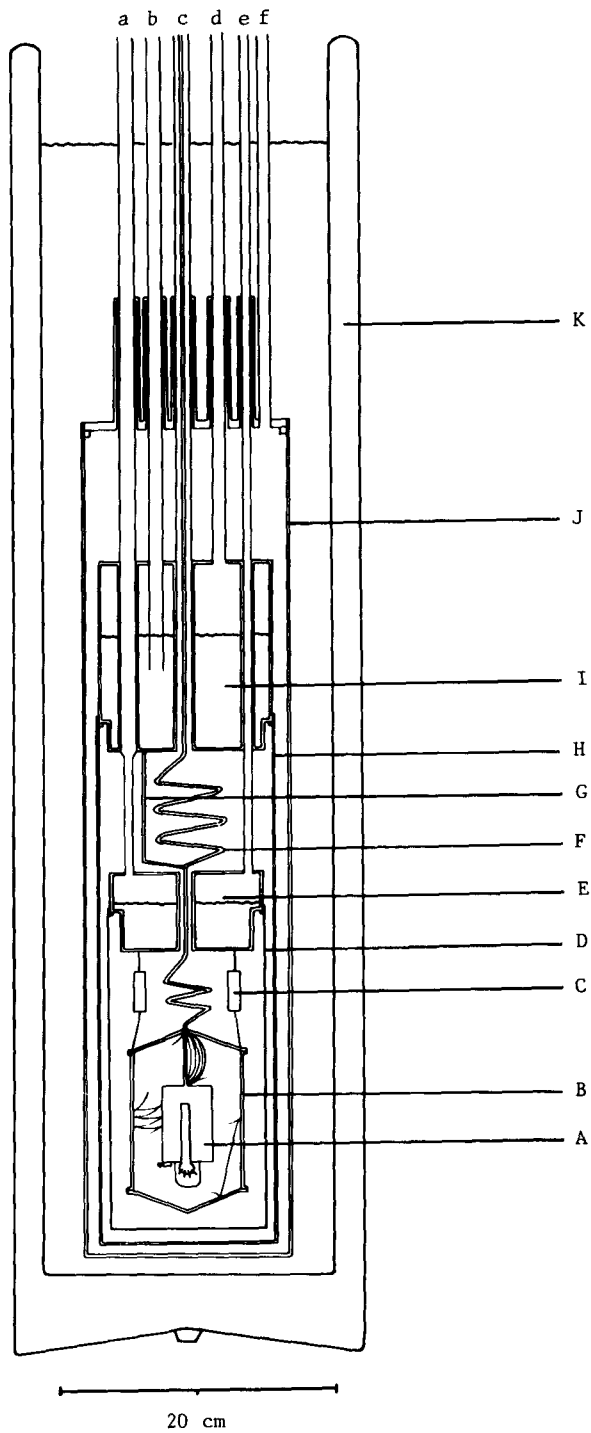


FIGURE 1. The calorimeter assembly. A, Calorimeter cell; B, Adiabatic shield; C, Floating ring; D, Radiation shield; E, Helium can; F, Sample filling tube; G, Thermal shunt; H, Inner jacket; I, Hydrogen can; J, Outer jacket; K, Liquid nitrogen Dewar; a, Helium can transfer tube; b, Hydrogen can transfer tube; c, Inner jacket evacuation tube; d, Hydrogen can evacuation tube; e, Helium can evacuation tube; f, Outer jacket evacuation tube.

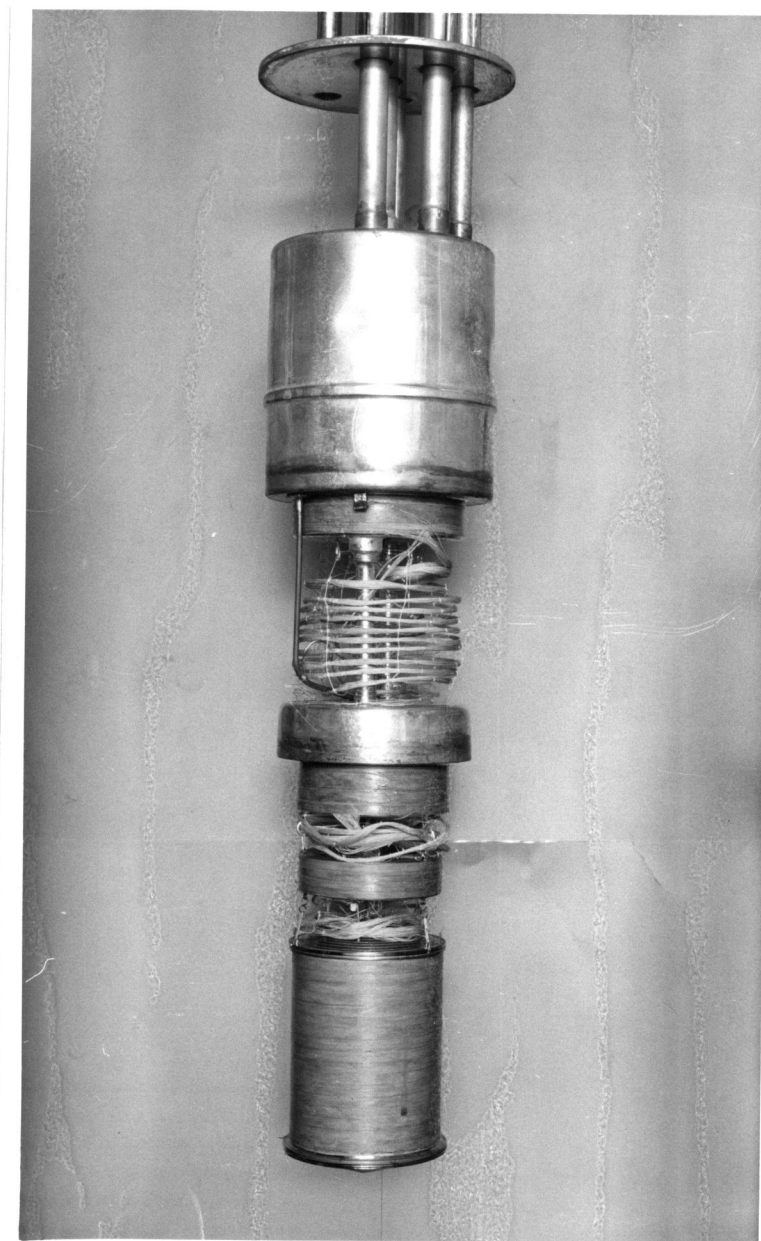


FIGURE 2. A PHOTOGRAPH OF THE INTERIOR OF THE CRYOSTAT.

jacket J (1.2 mm in wall thickness, conneted to the top plate (brass) of the cryostat with Wood's alloy) is made of brass. All these cans and jackets are chromium plated and polished. In order to minimize the heat exchange through gases, the entire system can be evacuated through the pipes c (SUS-27 stainless steel, 13 mm in outer diameter, 0.15 mm in wall thickness) and f (15 mm in outer diameter). These inner jacket and outer jacket evacuation pipes are connected separately to the different evacuation systems, each of which consists of a mechanical pump (Tokuda Seisakusho Ltd., type MG-50A, 50 liter/min), an oil diffusion pump (Shimadzu Seisakusho Ltd., type OD-4, 400 liter/s), liquid nitrogen traps and the several other equipments. All the tubes a-f are made of SUS-27 stainless steel, non-plated, and non-polished, and have outer diameters of 10-16 mm and 0.15 mm in wall thickness. These tubes a-e except the outer jacket evacuation tube f have thermal economy sheaths (brass, 1 mm in wall thickness, 100 mm in length). The sample filling tube F (German silver, 1 mm in outer diameter, 0.1 mm in wall thickness) connects the calorimeter vessel A with the outside system for sample-measuring and pressure determinations (Figure 6). The length of the filling tube from the calorimeter vessel A to the point just outside the cryostat at room temperature is 1630 mm. Heat leak along the filling tube is anchored through the thermal shunt G (copper tube, 4 mm in outer diameter, 1 mm in wall thickness, 150 mm in length) to the bottom of the hydrogen can I.

Over the entire length of the filling tube F, is closely wound non-inductively double silk-insulated B.S. #36 manganin wire heaters from the point where F emerges from the cryostat to the top of the adiabatic shield (Figure 3), the wire varnished with glyptal lacquer (G.E. adhesive No. 7031). The heaters are wound in 7 separate parts so that each portion may be heated independently; This was necessary to maintain the tube at a predetermined temperature. The temperatures of different parts of the filling tube are monitored and measured with seven constantan versus chromel-P thermocouples of which ^{the} temperature scale has been established in our laboratory (Figure 7). The temperatures of the 4 lower parts of the filling tube are also measured by carbon resistance thermometers (Allen-Bradley, nominal value of $10\ \Omega$) in the low temperature region. The temperatures of several other points in the cryostat are also measured with the constantan versus chromel-P thermocouples. The total number of the electric lead wires including some spares are 76, and each runs about 10 m from the calorimeter vessel to the terminal box outside the cryostat. All lead wires except for the thermocouples are double silk insulated B.S. #36 copper wires. The lead wires enter the cryostat at the head of the cryostat through picein cement (Figure 5), and pass through the evacuation tube c, turning around the sample filling tube F. They are brought to the temperature of the refrigerant container I, being wound closely at its bottom and fixed with glyptal lacquer. They are also in good thermal

contact with the refrigerant container E at its bottom.

2.2.2. Calorimeter vessel and its surroundings

Figure 3 shows the lower part of the cryostat. After heat exchange with the helium can P at the bottom, lead wires B are wound closely on the thermal station ring N (copper, weighing 450 g), of which the temperature is maintained in between the temperatures of the helium can and of the adiabatic shield I, in order to minimize the temperature gradient on the adiabatic shield and help to make adiabatic controlling operation easy. The ring N is of three year-ring shaped construction for^{securing} good thermal contact between wires and the ring. The adiabatic shield consists of three parts, top L, side I and bottom A, which are made of copper, the wall being 2 mm thick and its total weight is 750 g. The lead wires are wound closely on the side of the adiabatic shield I, and enter the inside of the shield through the small holes on the circumference around the bottom of the side I. The lead wires between the calorimeter vessel and the side of the adiabatic shield I except for the thermocouples, D, H and K are double silk insulated B.S. #38 copper wires and about 500 mm long. The lead wires from the calorimeter vessel are soldered inside the adiabatic shield and have not any other soldered connections between the calorimeter vessel and the terminal box outside the cryostat. In the adiabatic Nernst type calorimetry, the adiabatic shield must be maintained at the same temperature as the calorim-

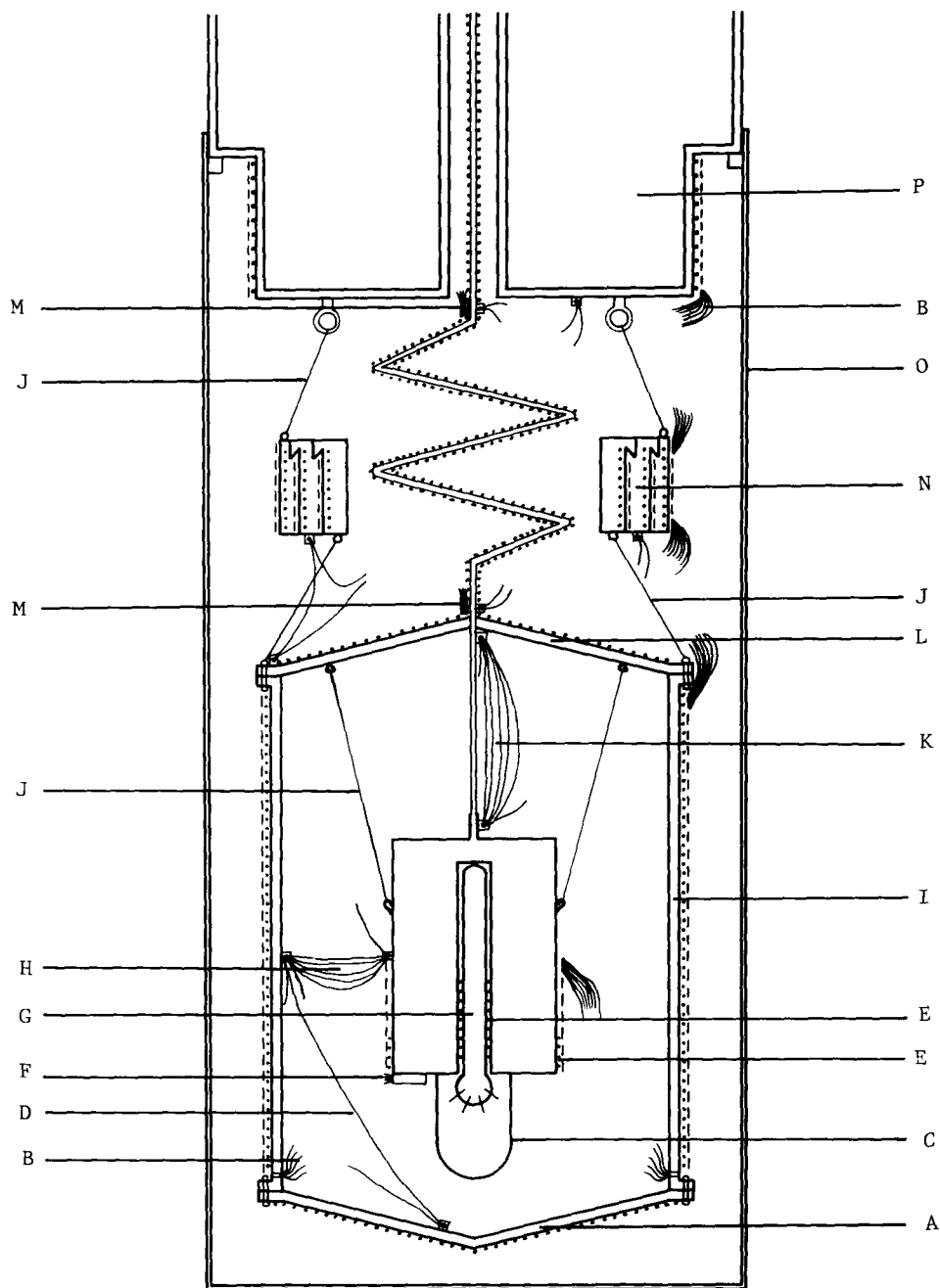



FIGURE 3. A DETAIL SECTIONAL DRAWING OF THE CALORIMETER CELL AND THE SURROUNDINGS. ----, Lead wires;, Heater wires; , Thermocouple junction point; A, Adiabatic shield (Bottom); B, Lead wires; C, Radiation cap; D, Difference thermocouple between side and bottom; E, Calorimeter heater; F, Germanium thermometer; G, Platinum thermometer; H, Difference thermocouple between side and calorimeter; I, Adiabatic shield (Side); J, Nylon thread; K, Difference thermocouple between top and calorimeter; L, Adiabatic shield (Top); M, Carbon thermometer and thermocouple for filling tube; N, Thermal station ring; O, Radiation shield; P, Helium can.

eter vessel all the time. The temperature differences if any are detected with gold + 2.1 mole per cent cobalt versus copper thermocouples (one thermocouple D, three thermopiles H and K), and temperatures of the three parts, top, side and bottom are controlled separately. The adiabatic condition is controlled automatically.²²⁾ The block diagram of the system is shown in Figure 4 (a), together with a chart trace of controller performance in Figure 4 (b). The e.m.f. of the thermocouples is amplified and fed into a thyatron relay. The relay energizes the switch that short-circuits a resistance in the circuit of the shield heater. The rheostats A and B, the switches D and E, and the Slidac C are controlled manually. The switch E, on closing, increases the heater current by about three times and the switch D makes the heater current zero when the relay is off. These two switches help to make manual operation easy. Similar amplifier-relay circuits are used for the side and the bottom. A recorder chart trace of controller performance in Figure 4 (b) shows the temperature difference between the calorimeter and the side of the adiabatic shield. The oscillation of the temperature is small enough to ensure that no correction is necessary for heat input. The calorimeter vessel is made of gold, internal volume of about 44 cm³, about 76 g in weight, and has eight vanes for the inside thermal uniformity. The calorimeter vessel is equipped with a platinum resistance thermometer G (Leeds & Northrup Company, type 8164, calibrated at the U. S. National Bureau of Standards on the

FIGURE 4 (a). BLOCK DIAGRAM OF THE ADIABATIC CONTROLLING SYSTEM.

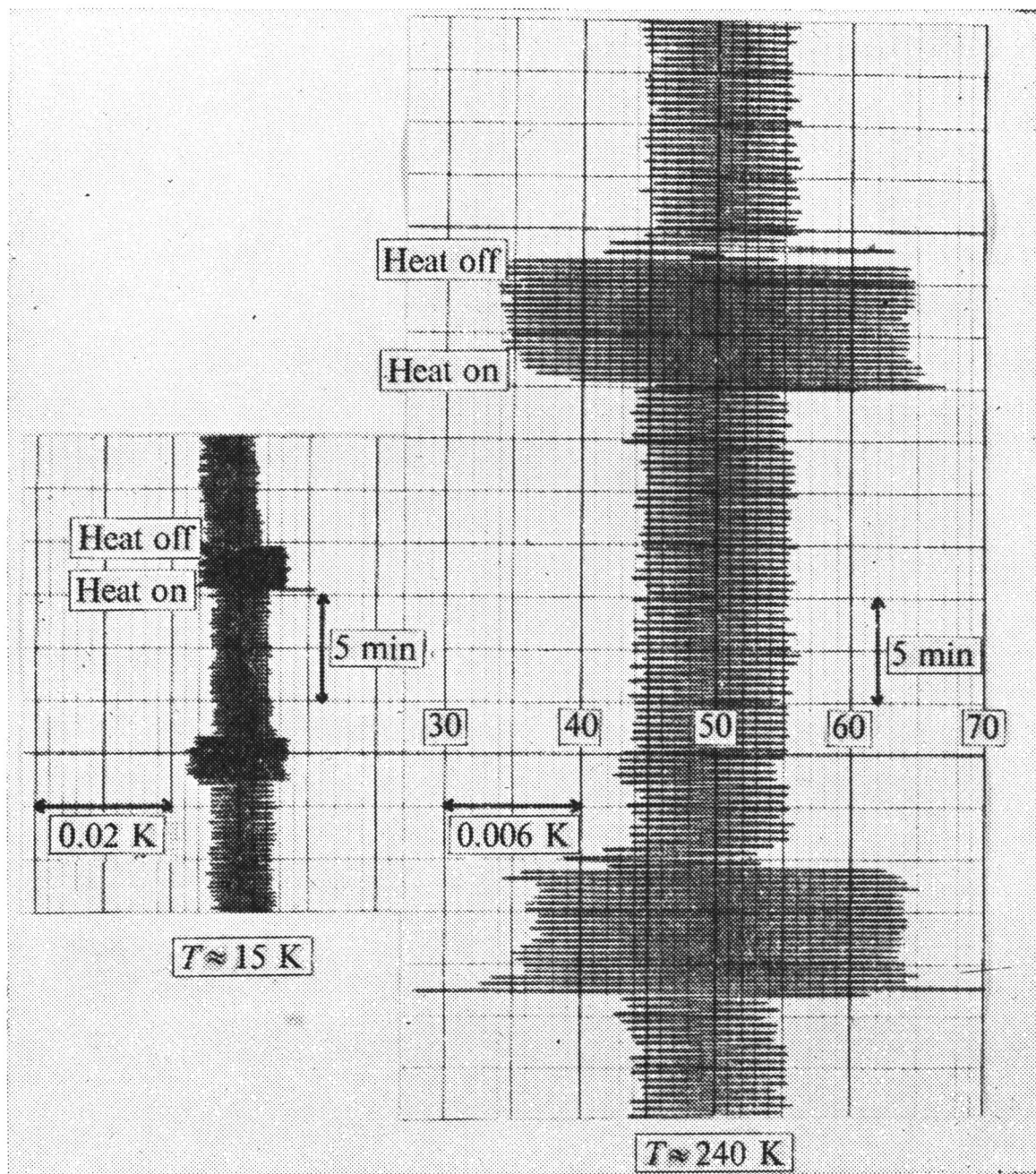


FIGURE 4 (b). A RECORDER CHART TRACE OF CONTROLLER PERFORMANCE.

NBS-55 temperature scale), a germanium resistance thermometer (in the early stage of this investigation, Minneapolis-Honeywell Regulator Company, type MHSP 2401, and later, Cryocal, Inc., CryoResistor type CR 1000), the calorimeter heater E (B.S. #36 KARMA wire, Driver-Harris Company, resistance of about 150 Ω) which is wound non-inductively around the platinum resistance thermometer and also ^{wound} the bottom quarter of the calorimeter vessel. The cap C (copper, 0.2 mm in wall thickness) serves as a radiation trap and thermocouple junction post is soldered on the side of the vessel. The platinum resistance thermometer wound with the KARMA heater wire is cast in the re-entrant well at the center of the vessel with Wood's alloy and the germanium resistance thermometer is placed in the copper sheath with high vacuum silicone grease for good thermal contact, the sheath being soldered on to the bottom face. The sample filling tube runs down through the top of the adiabatic shield L, being thermally connected to the top, and connected to the top of the calorimeter vessel. The calorimeter vessel is suspended with three nylon threads from the top of the adiabatic shield.

Figure 5 (a) is a photograph of the head of the cryostat. A photograph of the calorimeter vessel is given in Figure 5 (b).



FIGURE 5 (a). A PHOTOGRAPH OF THE TOP OF THE CRYOSTAT.

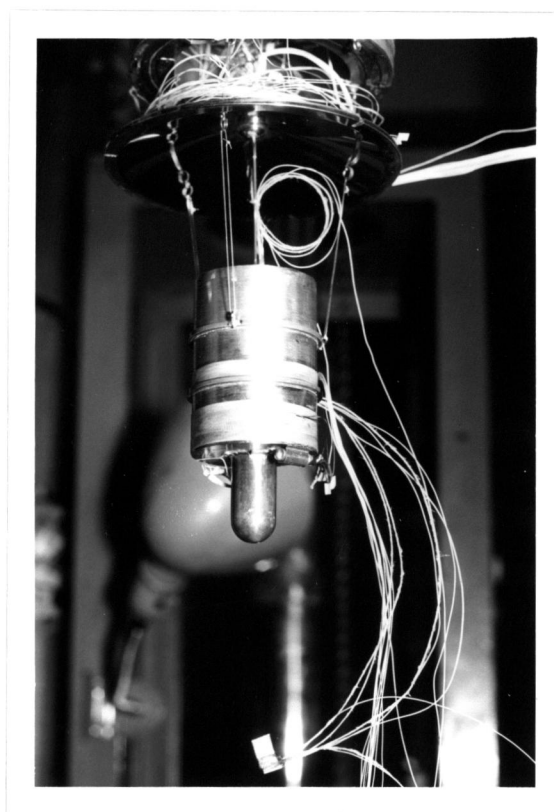


FIGURE 5 (b). A PHOTOGRAPH OF THE CALORIMETER VESSEL.

2.3. System of measurements

2.3.1. Sample filling and vapor pressure measurement

The system for sample purification and measurement and for measurements of vapor pressure and of heat of vaporization is shown in Figure 6. The whole system is made of pyrex glass, and high vacuum grease (silicone lubricant, Dow Corning Co.) is used for stop-cocks and joints. The outer diameters of the pyrex glass tubes are 20-10 mm for sample preparation part, while capillary tubes with 2 mm inner diameter are used for pressure measurement part to make the volume of dead space as small as possible. The sample gas was stored in 5 dm³ flask before condensing it into the calorimeter vessel. In the case of dinitrogen oxide, for example, the gas was first dried over P₂O₅, and then condensed at the trap 1 which is immersed in liquid nitrogen Dewar vessel (not shown in Figure 6). The traps 1-4 were then used for distillation of the condensed gas. The amount of the sample gas is determined by the P-V-T measurements using the calibrated 5 liter volume (5372.01 cm³ at 23.8 °C). The 5 liter volume was determined by weighing the flask filled with freshly distilled water. The flask is contained in a thermally insulated box. Pressures were measured with the mercury manometer A and also in the later stage of investigation by the quartz Bourdon gauge (Texas Instruments Incorporated, type 144-01). The mercury manometer A was designed so as not to require corrections for capillary depression. The meniscus height of

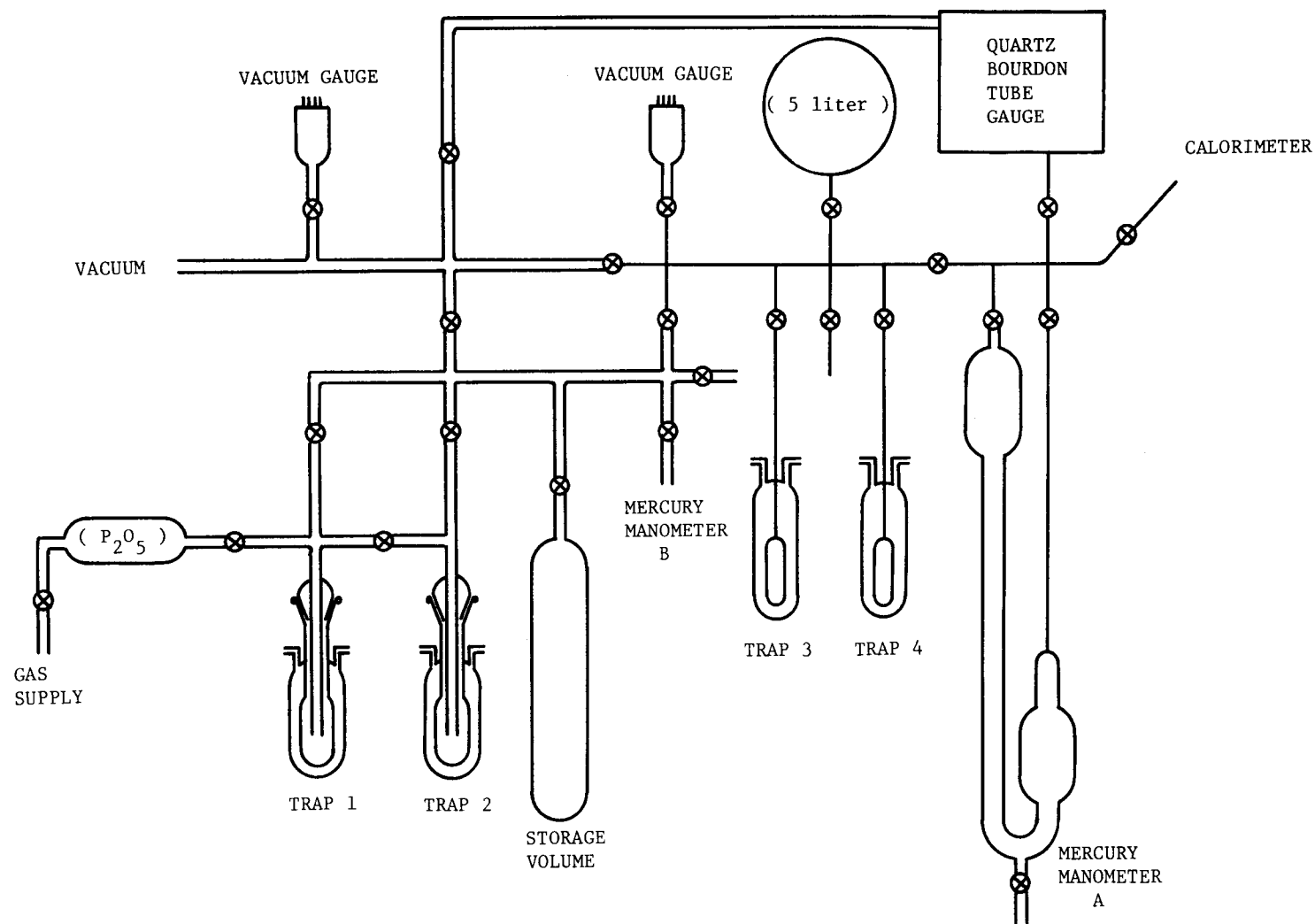


FIGURE 6. THE PYREX GLASS SYSTEM FOR SAMPLE-FILLING AND FOR MEASUREMENTS OF VAPOR PRESSURE AND HEAT OF VAPORIZATION.

either arm was measured by a pair of travelling telescopes cathetometer (± 0.01 mm precision, Rika Seiki Kogyo Co.) by locating the meniscus in reference to a calibrated steel scale mounted between the manometer arms (not shown in Figure 6). The quartz Bourdon gauge has a precision of ± 0.01 Torr^{*}; it has advantages of small and unchanged dead volume (1.536 cm^3) and simplicity in operation. Another mercury manometer B (not illustrated) was used for monitoring the pressure over the condensed gas during distillation. The total dead volume of the capillary line except the manometer A is 9.779 cm^3 . The capillary line is connected to the German silver filling tube of the cryostat with picein cement.

* 1 Torr is defined as $(101325/760)\text{Pa}$.

2.3.2. Electrical measurements

Because part of the sample gas is in the filling tube and the pressure gauge at higher temperatures, it is necessary to determine the amount of the gas outside of the calorimeter vessel and to apply corrections to the solid heat capacity. This was done by measuring the temperature gradient along the length of the filling tube with seven thermocouples. The measurements were also necessary while the sample gas was being condensed in the calorimeter vessel in order to prevent the gas from condensing in the filling tube. The thermocouple outputs and also the potential and current across the calorimeter heater were recorded

on the automatic data acquisition system, the block diagram of which is shown in Figure 7. The system has ten channels which are scanned for their d.c. e.m.f. with a scanner (Takeda Riken Industry Co., Ltd., type TR-7216-20S and TR-7513) which consists of crossbar switches (James Cunningham Son and Company, Inc., type A crossbar, specially modified for lowering thermal e.m.f. (about 0.3 μ V) and contact resistance) and controller, and has several kinds of program functions. The e.m.f.s are determined by a digital voltmeter (Hewlett-Packard, type 3450 A, multifunction meter) which has 5 full digits, 20 per cent overrange and 1 μ V sensitivity on the 100 mV range. The output levels of the HP-3450A are converted to the same voltages of the TR-system by the TR-level converter to connect to the TR-system with BCD (1-2-4-8) codes. The digital clock (TR-7414, with several options) operates as both a clock and a timer. The digital printer records the time (minutes and seconds), channel number (0-9), and the outputs of the multifunction meter HP-3450A. The nominal sensitivity is better than ± 1 μ V on the 100 mV range. The heating time is determined by an electronic counter (TR-124B) to the nearest 1/100 s. Resistances of the platinum and germanium resistance thermometers are determined by the potentiometric method using a six-dial double thermofree microvolt potentiometer (Minneapolis Honeywell Regulator Co., Rubicon Instruments Division). The current through the thermometer and the standard resistor is reversed at each reading in order to cancel the possible extra-

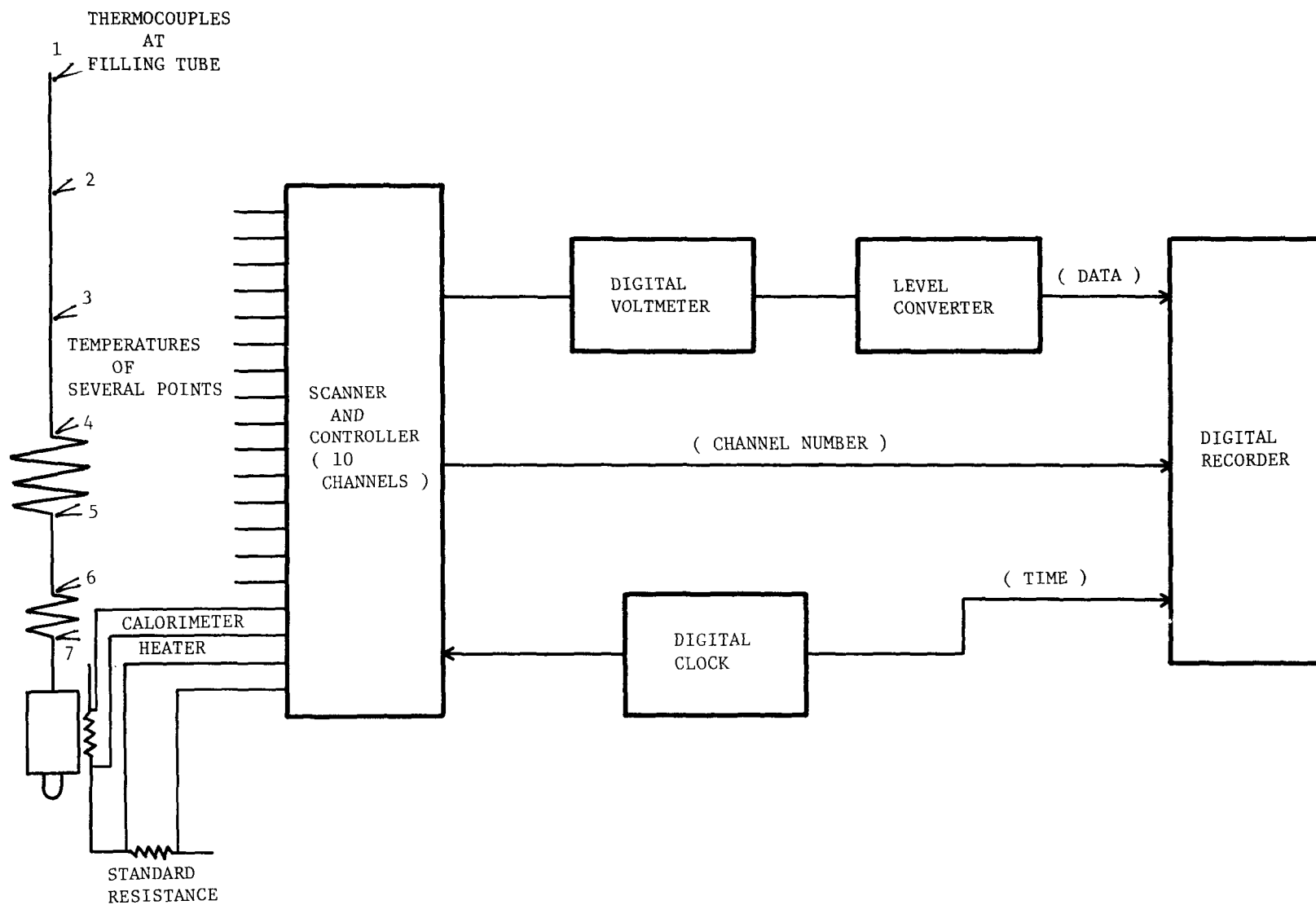


FIGURE 7. THE DATA ACQUISITION SYSTEM.

neous e.m.f. Unsaturated cadmium standard cells (The Epply Laboratory, Inc. Scientific Instruments) and standard resistors (Shimadzu Seisakusho Ltd.) were used, which are stored in a thermostat regulated at 29 °C. For all high precision circuits, electrically shielded wires (Fujikura Cable Works, Ltd., type 3C-2V) are used outside the cryostat, and low thermal e.m.f. and contact resistance switches (Leeds & Northrup Company, type 3294, pinch-type switch) are also used. All dc power was supplied from a bank of batteries.

2.4. Temperature scales

2.4.1. Platinum resistance thermometer

The International Practical Temperature Scale of 1968 (IPTS-1968) was adopted at the meeting of the International Committee on Weight and Measures, after the recommendation of its International Committee on Thermometry, in October 1968.²³⁾ Since January 1, 1969, it has replaced the International Practical Temperature Scale of 1948 (IPTS-1948, amended in 1960). The following changes have been introduced:

- a). The name kelvin and the symbol K are used as the unit of temperature.
- b). All values of the defining fixed points except of the triple point of water (273.16 K = 0.01 °C) are changed.
- c). The lower limit of Range 1 is extended to the triple point of hydrogen (13.81 K = -259.34 °C).
- d). The lower limit of resistance ratio R_{100}/R_0 of the platinum resistance thermometer for Ranges 1 and 2 is changed to 1.3925.
- e). Range 1 is divided into four parts; the triple point of hydrogen — the boiling point of hydrogen (20.28 K) — the triple point of oxygen (54.361 K) — the boiling point of oxygen (90.188 K) — the freezing point of water (273.15 K = 0 °C).
- f). In Range 1, the Callender - Van Dusen equation is replaced by a new reference function which is calculated

by an electronic computer in each part.

g). In Range 2 (0 °C — 630.74 °C), the Callendar equation is modified by a correction term.

h). In Range 4 (above 1064.43 °C), the second radiation constant c_2 is changed to 0.014388 meter kelvins.

The platinum resistance thermometer on the present calorimeter (calibrated at the U.S. National Bureau of Standards; laboratory designation, thermometer β) is the one calibrated against the IPTS-48 and the NBS-55 temperature scale below the temperature of the boiling point of oxygen. The relationship between the IPTS-68 and the NBS-55 temperature scale is given in the reference 23). (c). Therefore, the temperature scale of the platinum thermometer β has been converted to the IPTS-68 using the NEAC 2200-500 computer system at the Computer Center of Osaka University.

2.4.2. Germanium resistance thermometer

Recently, germanium resistance thermometers have been used widely in the world below about 20 K because of their high sensitivity and good reproducibility with respect to time and thermal cycling.²⁴⁾ Because there is no simple relation between the resistance and the temperature, which is one disadvantage of germanium resistance thermometers, an electronic computer was used to determine the calibration formula.

In this investigation the germanium scale was fixed by using different method for each of the three temperature regions:

(a) the 1958 ^4He vapor pressure temperature scale²⁵⁾ below 4.2 K, (b) the ^4He gas thermodynamic temperature scale between 4.2 K and 13.81 K, (c) the IPTS-68 above 13.81 K.

The germanium resistance thermometer used in the early stage of this investigation bears the laboratory designation, the germanium thermometer α , and the one used at a later stage the germanium thermometer γ . The germanium thermometer γ is of a better quality than the α : small size and high sensitivity, etc.

The germanium thermometer α was calibrated by the following methods.

(a). Below 4.2 K, the thermometer α was calibrated against the ^4He vapor pressure. The apparatus is illustrated in Figure 8. Here, pure helium is condensed into the copper block (about 1.5 cm³ in volume) through the stainless steel tubing (2 mm in outer diameter, 0.15 mm in wall thickness) which is used also for vapor pressure measurements and which has an outer sheath for preventing the film flow of liquid helium-II below the λ -point from causing the pressure fluctuation. The sensor α is placed in a hole drilled in the copper block. The outer liquid helium bath is pumped on with a mechanical pump, and the lowest calibration point was at 1.425 K (Table 1).

(b). Between 4.2 K and 13.81 K, the thermometer α was calibrated against the ^4He gas thermometer. This condensed gas calorimeter can be used as a gas thermometer. The sensor α is mounted on the calorimeter vessel, purified helium gas is introduced into

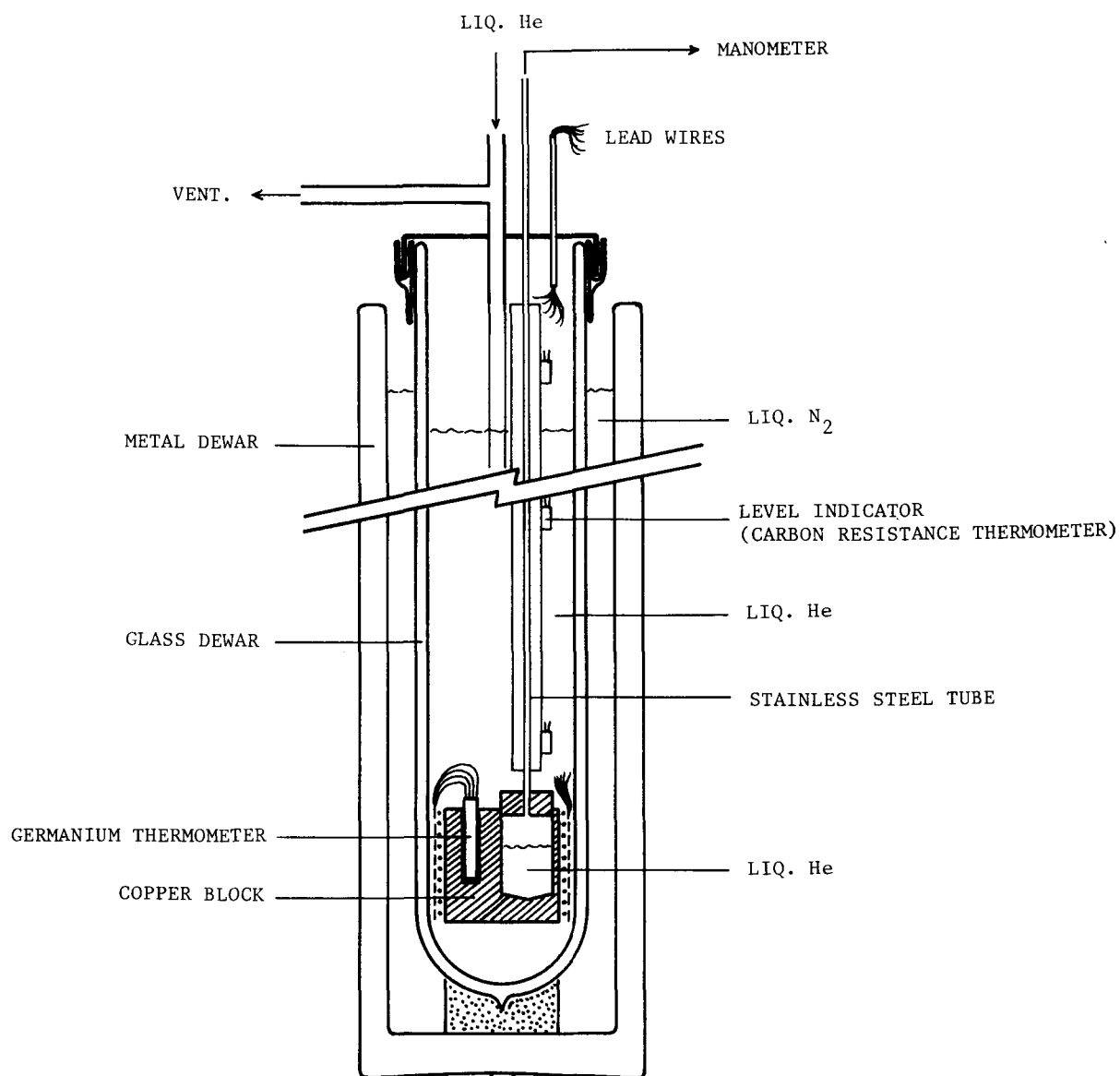


FIGURE 8. THE APPARATUS FOR CALIBRATION OF THE GERMANIUM THERMOMETER α ON THE 1958 ⁴He VAPOR PRESSURE TEMPERATURE SCALE BELOW 4.2K.

the calorimeter vessel through the sample filling tube, and the vapor pressure measurement system is used. Due to the large volume of the calorimeter vessel (44 cm^3) compared with the volume of the filling tube (1 cm^3 altogether) and of the dead space at room temperature (about 30 cm^3 in the case of mercury manometer, 10 cm^3 in the case of Bourdon gauge), the calibration sensitivity was sufficiently high (Tables 1,2). The corrections for thermal expansion of the volume of the calorimeter vessel²⁶⁾ and for the second virial coefficient of helium²⁷⁾ were applied. No correction was made for the adsorption of gas on the inside wall.

(c). Above 13.81 K, the thermometer α was calibrated on the IPTS-68. The germanium resistance thermometer α and the platinum resistance thermometer β , both of which are mounted on the calorimeter vessel, can be compared with each other in situ.

Although the germanium thermometer was used only below 13.81 K, its calibration procedure was extended up to 15 K to assure smooth connection between these two regions. The calibration points obtained (27 points) are tabulated in Table 1. The following two functions were examined for computer fitting by the method of least squares,

$$\log_{10} R = \sum_{i=1}^b A_i T^{i-a}, \quad (1, a)$$

$$\log_{10} R = \sum_{i=1}^b A_i (\log_{10} T)^{i-a}, \quad (1, b)$$

TABLE 1. THE CALIBRATION POINTS FOR THE GERMANIUM RESISTANCE THERMOMETER α .

T	R	T	R
K	Ω	K	Ω
1.42523	9638.97	4.20917	777.101
1.71508	5822.21	4.21386	776.263
1.92602	4346.47	4.8345	584.833
1.98909	3984.63	5.8930	391.717
2.27736	2858.57	6.9134	278.877
2.46599	2383.28	8.1060	195.9521
2.47337	2370.20	8.7864	163.1749
2.98178	1567.87	9.6426	131.9649
2.99615	1482.612	10.4617	109.9944
3.35981	1185.175	12.2714	78.1906
3.55492	1090.482	13.3073	65.9716
3.89230	908.795	14.2191	57.7029
4.0979	807.104	15.1988	50.6600
4.20879	776.533		

TABLE 2. THE CALIBRATION FORMULA FOR THE GERMANIUM RESISTANCE THERMOMETER α .

$$\log_{10} R = \sum_{i=1}^{10} A_i T^{i-2}$$

$$\begin{aligned} A_1 &= -0.0722156087 & A_6 &= 0.0281957798 \\ A_2 &= 6.1827664995 & A_7 &= -0.0025095935 \\ A_3 &= -2.4344128577 & A_8 &= 0.0001371840 \\ A_4 &= 0.8842873514 & A_9 &= -0.0000042058 \\ A_5 &= -0.1998328862 & A_{10} &= 0.0000000553 \end{aligned}$$

$$\sum_{i=1}^{27} (\log_{10} R_{i(\text{calc.})} - \log_{10} R_{i(\text{obs.})})^2 = 0.00042887$$

where R is the resistance in absolute ohm and A_i are constants.

The best fit was obtained by employing the formula:

$$\log_{10} R = \sum_{i=1}^{10} A_i T^{i-2} \quad . \quad (2)$$

The ten coefficients A_1 - A_{10} are listed in Table 2, together with the sum of deviations:

$$\Delta \log_{10} R = \log_{10} R_{\text{calc.}} - \log_{10} R_{\text{obs.}} \quad . \quad (3)$$

The deviation plot is given in Figure 9.

This germanium resistance thermometer α was used as the working thermometer for the heat capacity measurements of dinitrogen oxide in its first series of runs. Later, in the second series of the heat capacity measurements of dinitrogen oxide, the α has been replaced by the germanium resistance thermometer γ , which was calibrated by comparison with the resistance of the α . However, below 4.2 K it was recalibrated on the 1958 ^4He vapor pressure temperature scale. For this purpose this condensed gas calorimeter was used as a vapor pressure thermometer. Purified helium was condensed into the calorimeter vessel through the sample filling tube, and the vapor pressure was measured. The lowest calibration temperature was 1.819 K (Table 3). The calibration points are tabulated in Table 3, and the coefficients of the formula that gave the best fit between 1.8 K and

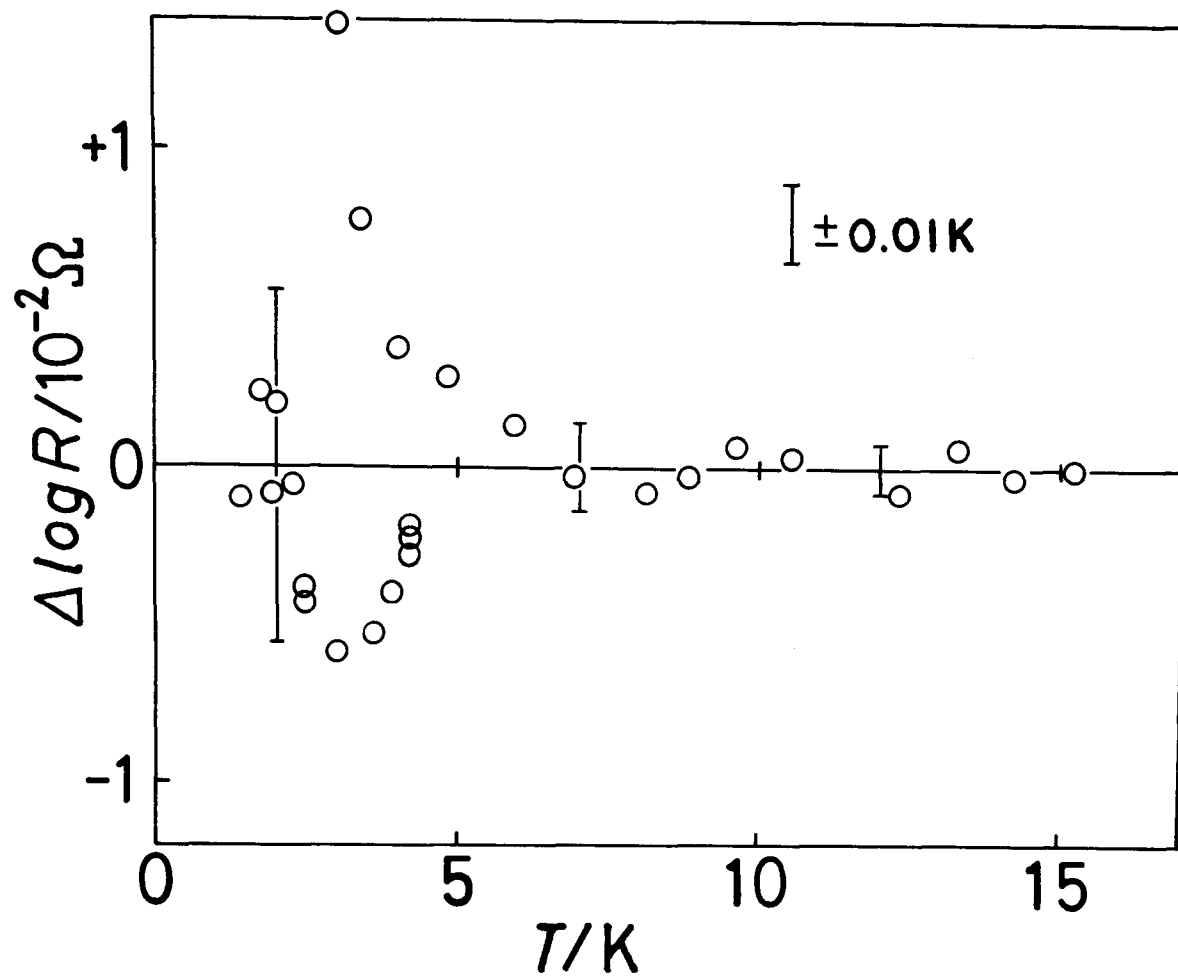


FIGURE 9. THE DEVIATION PLOTS FOR THE GERMANIUM RESISTANCE THERMOMETER α FITTED WITH THE FORMULA : $\log_{10} R = \sum_{i=1}^8 A_i \cdot T^{i-2}$.

TABLE 3. THE CALIBRATION POINTS FOR THE GERMANIUM RESISTANCE THERMOMETER γ BETWEEN 1.8 K AND 4.2 K.

T	R	T	R
K	Ω	K	Ω
1.81921	5206.052	3.13460	1533.056
1.88212	4791.032	2.27461	3054.186
2.00745	4089.195	2.99370	1686.293
2.15459	3454.223	3.30217	1380.678
2.44269	2598.533	3.51371	1219.183
2.75215	2007.690	3.73901	1079.971
2.95518	1730.737	4.20917	853.295

TABLE 4. THE CALIBRATION FORMULA FOR THE GERMANIUM RESISTANCE THERMOMETER γ BETWEEN 1.8 K AND 4.2 K.

$$\log_{10} R = \sum_{i=1}^7 A_i T^{i-4}$$

$$\begin{aligned} A_1 &= -11.2661447706 & A_5 &= -2.7850755249 \\ A_2 &= 24.1382990601 & A_6 &= 0.3716358040 \\ A_3 &= -19.8015576148 & A_7 &= -0.0211956379 \\ A_4 &= 13.1433175470 \end{aligned}$$

$$\sum_{i=1}^{14} (\log_{10} R_{i(\text{calc.})} - \log_{10} R_{i(\text{obs.})})^2 = 0.00000077$$

4.2 K:

$$\log_{10} R = \sum_{i=1}^7 A_i T^{i-4} , \quad (4)$$

are given in Table 4. By including the calibration points at higher temperatures which are based on the α scale, a single formula good between 1.7 K and 15 K was determined as

$$\log_{10} R = \sum_{i=1}^{10} A_i T^{i-4} . \quad (5)$$

The calibration points are tabulated in Table 5, and the ten coefficients are given in Table 6. The difference between the two formulas (4) and (5) for the temperature region from 1.8 K to 4.2 K was negligible. The deviation plots are given in Figure 10.

TABLE 5. THE CALIBRATION POINTS FOR THE GERMANIUM RESISTANCE THERMOMETER γ BETWEEN 1.7 K AND 15 K.

T	R	T	R
K	Ω	K	Ω
1.71508	6013.514	4.20879	852.674
1.81921	5206.052	4.20917	853.295
1.88212	4791.032	4.21386	852.379
2.00745	4089.195	4.8345	642.094
2.15459	3454.223	5.8930	428.712
2.44269	2598.533	6.9134	304.676
2.75215	2007.690	8.1060	214.784
2.95518	1730.737	8.7864	179.704
3.13460	1533.056	9.6426	146.545
2.27461	3054.186	10.4617	123.310
2.99370	1686.293	12.2714	89.705
3.30217	1380.678	13.3073	76.754
3.51371	1219.183	14.2191	67.958
3.73901	1077.971	15.1988	60.427

TABLE 6. THE CALIBRATION FORMULA FOR THE GERMANIUM RESISTANCE THERMOMETER γ BETWEEN 1.7 K AND 15 K.

$$\log_{10} R = \sum_{i=1}^{10} A_i T^{i-4}$$

$$\begin{array}{ll} A_1 = -9.9045028235 & A_6 = 0.3418143002 \\ A_2 = 19.5189446673 & A_7 = -0.0374955679 \\ A_3 = -14.3988441226 & A_8 = 0.0025284079 \\ A_4 = 10.2554923447 & A_9 = -0.0000934843 \\ A_5 = -2.0933249566 & A_{10} = 0.0000014433 \end{array}$$

$$\sum_{i=1}^{28} (\log_{10} R_{i(\text{calc.})} - \log_{10} R_{i(\text{obs.})})^2 = 0.00000791$$

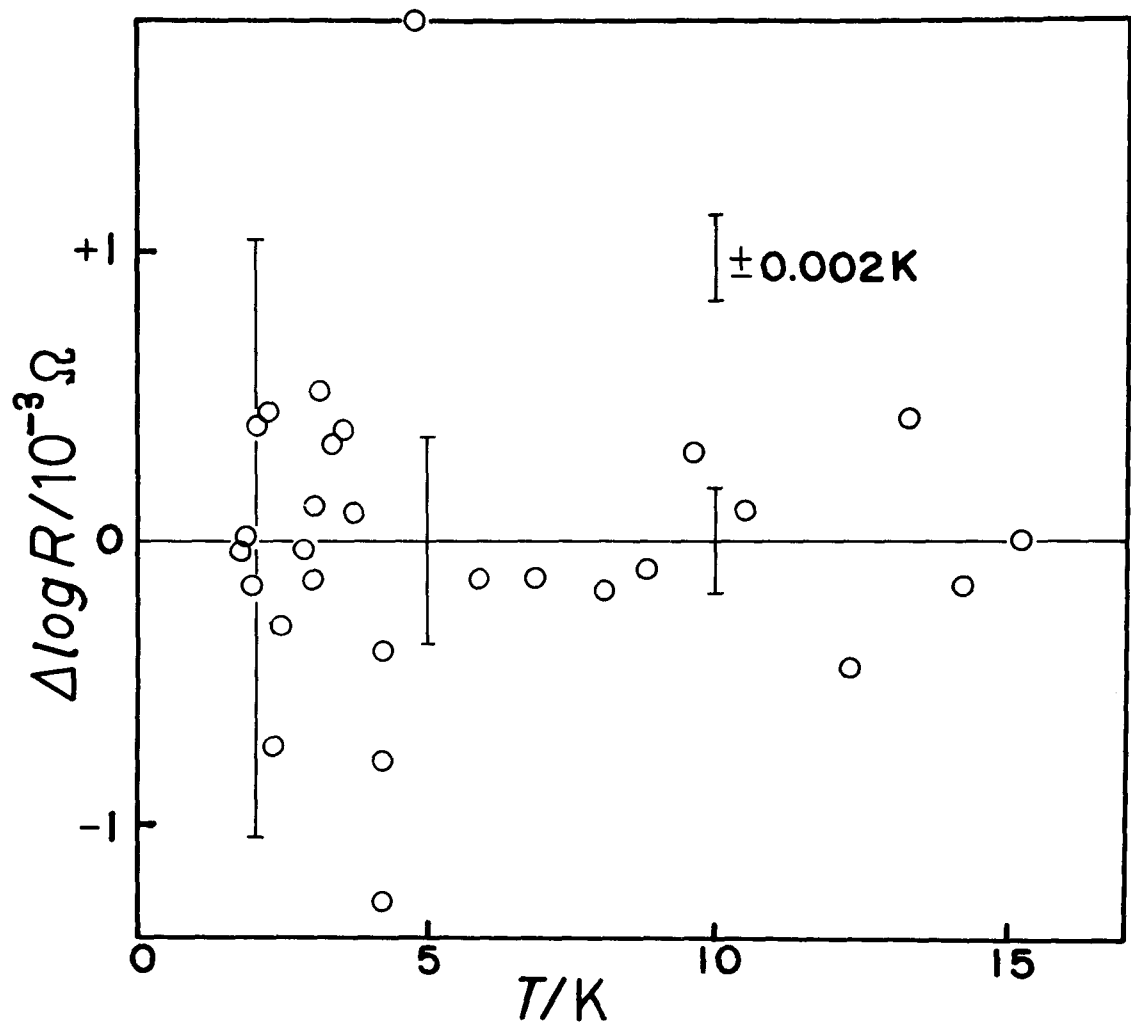


FIGURE 10. THE DEVIATION PLOTS FOR THE GERMANIUM RESISTANCE THERMOMETER γ FITTED WITH THE FORMULA : $\log_{10} R = \sum_{i=1}^{16} A_i \cdot T^{i-4}$.

2.5. Operation and performance

2.5.1. Operation

The standard method of operation of the cryostat is as follows. The metal Dewar vessel K (Figure 1) is filled with liquid nitrogen, and different refrigerants are introduced into the refrigerant containers E and I (Figure 1) depending on the temperature region to be studied. For the measurements above 200 K, the E and I contained no liquids, but helium gas at atmospheric pressure. The container I is filled with liquid nitrogen and solid nitrogen for the temperature region from 100 K to 200 K and from 55 K to 100 K, respectively, while the container E is empty. Liquid and solid hydrogen are charged in the hydrogen can I for the measurements between 22 K and 55 K, and between 11 K and 22 K, respectively, while the helium can E contained helium gas at atmospheric pressure. For the measurements from 2.6 K to 11 K, the helium can E is filled with liquid helium which, by a single charging, lasts about twenty hours, whereas the hydrogen can contains solid hydrogen. For the measurements of the lowest temperature region down to 1.8 K, both containers, the helium can E and the hydrogen can I, are filled with liquid helium in which case the refrigerants last about ten hours. Containers E and I can be pumped on ⁿ ~~and~~ off separately. The inside and outside vacuums are maintained better than 1×10^{-6} Torr during measurements. The calorimeter is cooled by breaking the vacuum with small amount of helium exchange gas at about 1×10^{-2} Torr down to about 15 K. Below

about 15 K, the calorimeter is cooled only by the heat conduction through the electrical lead wires. In the temperature region where the vapor pressure of the sample in the calorimeter vessel is negligibly small, the heat capacity measurements are carried out under strict adiabatic conditions as for the solid calorimeter.²²⁾ However, when the vapor pressure of the material in the calorimeter vessel cannot be ignored, the temperature of filling tube is maintained above its boiling point, and the top of the adiabatic shield L (Figure 3) is maintained about 0.5 K on the warmer side compared with the calorimeter vessel to prevent distillation of the specimen. The heat leak due to such a temperature head can be adequately taken into account of by tracing the temperature drift after the heat input was turned off. The temperature of the thermal station ring (Figure 3) is controlled manually. However, in the low temperature region below about 150 K, it does not need heat supply to maintain the temperature of the ring in between the temperatures of the helium can and of the adiabatic shield I (Figure 3), while in the higher temperature region to room temperature, significant current must be supplied. The time of the heat input to the calorimeter vessel for heat capacity measurement is about two minutes in the lowest temperature region below about 15 K, and increases to twelve minutes in the higher temperature region at room temperature. No helium gas is introduced into the calorimeter vessel for heat exchange.

2.5.2. Performance

This condensed gas calorimeter can be used for continuous measurements from 1.8 K to room temperature. The time for thermal equilibrium in the calorimeter vessel is a few seconds at the lowest temperature region, about one minute at about 20 K, a few minutes at about 50 K, and increases to ten or more minutes at room temperature.

The precision of this calorimeter is very high. The scatter of the measured points of heat capacity of dinitrogen oxide is at most ± 3 per cent at 4 K, ± 1 per cent at 10 K, ± 0.1 per cent above 20 K, and ± 0.3 per cent in the high temperature region where vapor pressure of dinitrogen oxide is significantly high. In the case of the first series of measurements on dinitrogen oxide, the calorimeter vessel contributed about 40 per cent of the total heat capacity. The comparison of the present results with the previously published reliable data by Blue and GIAUQUE¹⁾ will give some idea about the accuracy of our measurements (Table 9). The more sensitive comparison can be made in terms of the Debye characteristic temperature, which is shown in Figure 11 in the low temperature region below 50 K. In the lowest temperature region below 4 K, there are large differences between the ^{data} of the two series of measurements obtained with the germanium thermometers α and γ (± 10 -20 per cent of C_p). There may be two reasons for this systematic discrepancy:

- a). the nature of dinitrogen oxide related to thermal history.

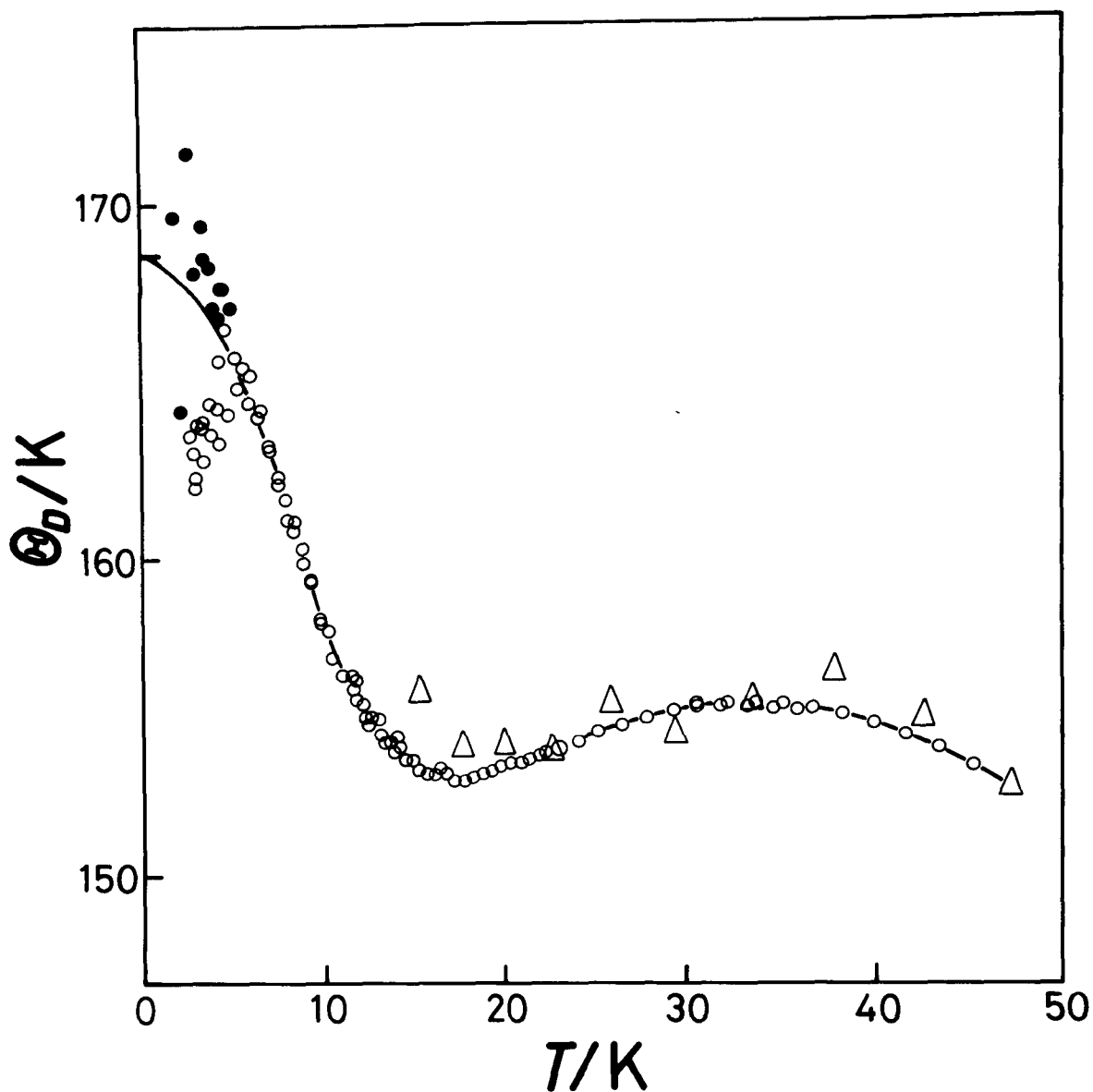


FIGURE 11. THE DEBYE CHARACTERISTIC TEMPERATURES OF NITROUS OXIDE DERIVED FROM THE MEASURED HEAT CAPACITIES, ASSUMING 5N DEGREES OF FREEDOM. O, THIS RESEARCH, MEASURED WITH THE GERMANIUM THERMOMETER α AND THE PLATINUM THERMOMETER β ; ●, THIS RESEARCH, MEASURED WITH THE GERMANIUM THERMOMETER γ ; Δ, R.W. BLUE AND W.F. GIAUQUE.⁽¹⁾

b). difference in the temperature scale between the germanium thermometers α and γ .

The temperature scale differences due to the formulas (2), (4), (6) can not cause such large differences, because the discrepancies in the temperature scales which are very small distribute at random. At present, the origin of the discrepancy can not be assessed. In the absence of other sensible measures, the differences may be considered as the accuracy. Nevertheless, the precision and the accuracy of this condensed gas calorimeter may be higher than any previous apparatus.^{5),8),10),12),etc.}

Chapter 3

The heat capacity, vapor pressure and related thermodynamic
properties of dinitrogen oxide

3.1. Introduction

3.2. Experimental

3.2.1. Material

3.2.2. Calorimetry

3.3. Results

3.3.1. Heat capacity

3.3.2. Fusion

3.3.3. Heat of vaporization

3.3.4. Vapor pressure

3.3.5. Thermodynamic functions

3.4. Analysis and discussion

3.4.1. Residual entropy

3.4.2. Structure and librational motion in solid state

3.4.3. Zero point properties

3.4.4. Lattice modes in the low temperature region

3.4.5. Premelting

3.4.6. General discussion

Chapter 3

The heat capacity, vapor pressure and related thermodynamic
properties of dinitrogen oxide

3.1. Introduction

The entropy of a gaseous system can be calculated by the statistical thermodynamics using the structural and spectroscopic data, while the calorimetry and related thermodynamic measurements of it provide the third-law entropy. Comparison between these two kinds of entropies have been made by F.E.Simon, W.F.Giauque and several other investigators and their coworkers, verifying the Third Law of Thermodynamics.²⁸⁾ On some simple molecular systems, however, there have been the residual entropies defined as:

$$S_0^\circ = S_{(\text{statistical})}^\circ - S_{(\text{third-law})}^\circ \quad , \quad (6)$$

which have been explained in terms of the orientational disorder frozen in solid state.

In 1964, Melhuish and Scott²⁹⁾ calculated electrostatic energies of some molecular crystals, and provided the Curie temperatures of 5 K and 11 K for dipole orientation in CO and N₂O, respectively. In 1966, the heat capacity and related thermodynamic properties of carbon monoxide were reported by

the author and J.A.Morrison and their coworkers.^{9),10)} The third-law entropy of carbon monoxide was determined and the residual entropy was estimated as $S_0^\circ = (3.3 \pm 0.8) \text{ JK}^{-1}\text{mol}^{-1}$, which showed significant difference from the value of $4.7 \text{ JK}^{-1}\text{mol}^{-1}$ approximating to $R \ln 2 = 5.76 \text{ JK}^{-1}\text{mol}^{-1}$ obtained by J.O.Clayton and W.F.Giauque.¹⁾ K.S.Pitzer et al.³⁰⁾ considered the kinetics of the order-disorder transition in solid carbon monoxide by a tunneling mechanism in 1968. In 1969, J.C.Burford and G.M. Graham¹¹⁾ reported the heat capacity of carbon monoxide in the lower temperature region from 0.8 K to 4.2 K, where no anomalous behavior was found. At present, there is no reasonable explanation of the residual entropy of carbon monoxide.

Dinitrogen oxide has similar aspects to carbon monoxide; linear molecule with small electric dipole moment of $0.166 \times 10^{-18} \text{ e.s.u. cm}$, cubic crystal structure of $P2_13$, etc. Recently, the molecular dynamics in simple molecular crystals has been improved, and the precision calorimetry and related thermodynamic measurements seemed fruitful investigations. In this chapter, the measurements of heat capacity and related thermodynamic properties of dinitrogen oxide are described, and are analyzed in detail.

3.2. Experimental

3.2.1. Material

The sample of dinitrogen oxide which was in 13 glass flasks (1 liter, at 760 Torr, equipped with breakable seal) was purchased from Takachiho Kagaku Kogyo Co., Ltd. and the claimed purity was 99.9 mol per cent. It was further purified in the sample preparation system described in the preceding chapter (Figure 6). Dried over P_2O_5 , dinitrogen oxide was distilled twice by means of the traps 1 - 4. The final purity was 99.997 mol per cent determined by the fractional melting method in the calorimetry. Gas-chromatographic and mass-spectrographic analyses gave no detectable impurities. The quantities of the purified dinitrogen oxide used in the calorimetry were determined by the P-V-T measurements, corrected for non-ideality using published values of the second virial coefficients;³¹⁾ (0.4265 ± 0.0016) mol in the first series and 0.1800 mol in the second series.

3.2.2. Calorimetry

In the first series of the calorimetry, the germanium resistance thermometer α was used, and the pressure was measured with the mercury manometer. The calorimetry in the whole temperature region from 2.6 K to 184 K (heat capacity, heat of fusion, heat of vaporization and vapor pressure measurements) was carried out in the first series.

In the second series, the germanium resistance thermometer

γ was used, and the pressure was measured with the quartz Bourdon gauge. The heat capacity measurement below 5 K down to 1.9 K, and the calorimetry above the triple point were carried out in the second series.

Above 120 K, where the vapor pressure of dinitrogen oxide was significant, the following corrections were necessary: (a) the heat of vaporization caused by the vapor pressure increase during heat input, (b) the heat of compression of the dinitrogen oxide gas in the free vapor volume over the condensed dinitrogen oxide in the calorimeter vessel, and (c) heat capacity of the gas of dinitrogen oxide. After a heat input, the dinitrogen oxide in condensed state (liquid and solid) decreased by the amount of these contributions, of which value was used for the calculation of heat capacity of condensed dinitrogen oxide. For these corrections, the distributions of dinitrogen oxide in the calorimeter vessel, in the filling tube and in the dead volume for pressure measurement were determined. The free volume in the calorimeter vessel was calculated by means of the densities of liquid and solid dinitrogen oxide.³²⁾ (Because only two values of density of solid dinitrogen oxide at 20 K and 83 K were available, the value of density at any temperature was obtained by the method of linear extrapolation.) The heat of vaporization at each temperature was estimated by Kirchhoff's law:

$$d(\Delta H)/dT = C_{p(\text{gas})} - C_{p(\text{condensed})} \quad , \quad (7)$$

where ΔH denotes enthalpy change, and the $C_{p(\text{gas})}$ was calculated from the classical model for translational and rotational molecular motions and from the infrared and Raman spectral data for intramolecular vibrations in the harmonic approximation. The gas imperfection corrections were made by using the second virial coefficients.³¹⁾ (Because the second virial coefficients were given only above 197 K, the values below this temperature were obtained by the method of smooth extrapolation.) A typical example of these corrections is given in Table 7. The operation and performance of the calorimetry are described in Section 2.5. The heat capacity value obtained is not C_p at constant pressure but C_s under its saturated vapor pressure. However, the difference between C_s and C_p given by the equation,

$$C_s - C_p = [(\delta H / \delta P)_T - V] \cdot (\delta P / \delta T)_S, \quad (8)$$

is negligible, and the data are tabulated as C_p .

The system for sample filling and vapor pressure measurement shown in Figure 6 was used for measurement of heat of vaporization. The calibrated 5 liter flask was used as sample storage volume of the dinitrogen oxide evaporated from the calorimeter vessel, and during heat input, the pressure was controlled manually within ± 1 Torr by adjusting a stop-cock, being monitored with the pressure gauge.

In the lowest temperature region below 10 K, the adiabatic

condition between the calorimeter and the shield was controlled manually, because of the rather poor sensitivity of the thermocouples.

TABLE 7. A TYPICAL EXAMPLE OF THE CORRECTIONS FOR THE CALORIMETRY OF THE SECOND SERIES. The n_{gd} , n_{gf} and n_{gc} denote the amount of the gaseous dinitrogen oxide in the dead volume for the vapor pressure measurements at room temperature, in the filling tube and in the free volume (V_{gc}) in the calorimeter vessel, respectively. The n_{cc} is the amount of the condensed dinitrogen oxide in the calorimeter vessel.

STARTING POINT:	FINAL POINT:
TEMPERATURE $T_1 = 183.9367$ K	TEMPERATURE $T_2 = 184.9170$ K
VAPOR PRESSURE $P_1 = 724.208$ Torr	VAPOR PRESSURE $P_2 = 768.207$ Torr
DISTRIBUTION OF DINITROGEN OXIDE;	DISTRIBUTION OF DINITROGEN OXIDE;
$n_{gd1} = 0.0004093$ mol	$n_{gd2} = 0.0004341$ mol
$n_{gf1} = 0.0000356$ mol	$n_{gf2} = 0.0000379$ mol
$n_{gc1} = 0.0024206$ mol	$n_{gc2} = 0.0025566$ mol
$n_{cc1} = 0.1771345$ mol	$n_{cc2} = 0.1769714$ mol

TEMPERATURE INCREASE $\Delta T = 0.98032$ K

VAPOR PRESSURE INCREASE $\Delta P = 43.999$ Torr

HEAT INPUT $\Delta E = 31.937$ J

CORRECTIONS:

$$\Delta n_{gd} \cdot \Delta H_{vap} = -0.411 \text{ J}$$

$$\Delta n_{gf} \cdot \Delta H_{vap} = -0.038 \text{ J}$$

$$\Delta n_{gc} \cdot \Delta H_{vap} = -2.256 \text{ J}$$

$$n_{gc} \cdot C_{p(gas)} \cdot \Delta T = -0.078 \text{ J}$$

$$\Delta P \cdot V_{gc} = +0.219 \text{ J}$$

3.3. Results

3.3.1. Heat capacity

The measured heat capacity values of dinitrogen oxide without curvature corrections are tabulated in Table 8. The data are shown graphically in Figure 12. The smoothed values at rounded temperatures are given in Table 9, together with the deviations derived from the comparison with the values obtained by Blue and GIAUQUE.¹⁾ The values show very good agreement in the entire temperature region. The more sensitive comparison in the temperature region below 50 K is shown in Figure 11 in section 2.5.2., which is given in terms of the Debye characteristic temperatures derived from the measured heat capacity values. The scatter of the present results is much smaller than that of the results by Blue and GIAUQUE. The comparison of the measured heat capacities in the region of liquid dinitrogen oxide given in Figure 13 shows rather large scatter of the present data, which is caused by the large corrections in the first series of the calorimetry, where the mercury manometer A was used for the vapor pressure measurements (section 2.3.1.).

3.3.2. Fusion

The heat of fusion of dinitrogen oxide was determined in the usual manner illustrated schematically in Figure 14. Two series of measurements are summarized in Table 10, where the average value is compared with that of Blue and GIAUQUE.¹⁾

TABLE 8. Measured heat capacity values of dinitrogen oxide.

1 mol N₂O = 44.0128 g , IPTS-1968

$\frac{T}{K}$	$\frac{C_p}{JK^{-1}mol^{-1}}$	$\frac{T}{K}$	$\frac{C_p}{JK^{-1}mol^{-1}}$
SERIES I		(Run 2)	
(Run 1)		2.935	0.0189
2.676	0.0142	3.355	0.0279
3.002	0.0205	3.762	0.0388
3.414	0.0299	4.202	0.0542
3.824	0.0414	4.688	0.0723
4.260	0.0575	5.173	0.0985
4.755	0.0788	5.650	0.1292
5.306	0.1082	6.110	0.1638
5.881	0.1484	6.567	0.2074
6.437	0.1958	7.028	0.2587
6.969	0.2523	7.481	0.3170
7.454	0.3148	7.920	0.3810
7.887	0.3801	8.353	0.4515
8.315	0.4480	8.802	0.5361
8.768	0.5341	9.274	0.6386
9.261	0.6350	9.775	0.7645
9.787	0.7653	10.329	0.9057
10.352	0.9243	(Run 3)	
10.979	1.1130	3.017	0.0209
11.650	1.3294	3.447	0.0302

TABLE 8 (continued)

$\frac{T}{K}$	$\frac{C_p}{JK^{-1}mol^{-1}}$	$\frac{T}{K}$	$\frac{C_p}{JK^{-1}mol^{-1}}$
(Run 4)		(Run 7)	
3.078	0.0215	11.675	1.3547
3.487	0.0326	12.374	1.6295
3.895	0.0438	13.062	1.922
4.339	0.0583	13.755	2.261
(Run 5)		14.467	2.624
11.582	1.3062	15.203	3.040
12.105	1.5114	15.957	3.490
12.725	1.766	16.744	3.984
13.342	2.054	17.650	4.605
13.970	2.343	18.650	5.309
(Run 6)		19.658	6.045
11.647	1.3362	(Run 8)	
12.257	1.5789	20.886	7.006
12.871	1.830	21.911	7.817
13.491	2.121	22.948	8.654
14.125	2.431	24.011	9.519
14.795	2.800	25.114	10.424
15.509	3.221	26.356	11.437
16.290	3.682	27.718	12.563
17.163	4.275	29.064	13.655
18.130	4.936	30.374	14.701
19.215	5.720	31.731	15.78
20.305	6.544	33.133	16.85
21.272	7.299	34.491	17.88
22.148	8.000	35.824	18.84

TABLE 8 (continued)

$\frac{T}{K}$	$\frac{C_p}{JK^{-1}mol^{-1}}$	$\frac{T}{K}$	$\frac{C_p}{JK^{-1}mol^{-1}}$
(Run 9)		70.316	34.72
30.436	14.74	72.047	35.22
31.997	15.97	73.815	35.69
33.524	17.13	75.625	36.16
35.033	18.24	77.478	36.62
36.537	19.32	79.358	37.09
38.152	20.43	81.249	37.52
39.866	21.57	83.134	37.94
41.598	22.65	(Run 11)	
43.378	23.71	82.159	37.71
45.198	24.75	84.241	38.19
47.069	25.77	86.295	38.62
49.003	26.77	88.321	39.07
51.050	27.79	90.322	39.47
52.018	28.16	92.301	39.86
(Run 10)		94.260	40.19
50.375	27.41	96.195	40.61
52.383	28.35	98.111	41.03
54.468	29.28	(Run 12)	
56.481	30.11	96.437	40.62
58.433	30.87	98.436	40.98
60.332	31.59	100.419	41.36
61.769	32.11	102.404	41.66
63.471	32.68	104.372	42.01
65.184	33.23	106.325	42.42
66.894	33.74	108.274	42.81
68.604	34.25	110.225	43.22

TABLE 8 (continued)

$\frac{T}{K}$	$\frac{C_p}{JK^{-1}mol^{-1}}$	$\frac{T}{K}$	$\frac{C_p}{JK^{-1}mol^{-1}}$
112.159	43.54	181.097	58.74
114.080	43.85	(fusion)	
116.005	44.20	183.215	76.79
117.936	44.52	184.241	77.43
(Run 13)		(Run 15)	
118.749	44.57	183.096	76.45
120.936	44.83	183.993	76.46
123.228	45.44	(Run 16)	
125.873	45.92	72.756	35.37
128.812	46.53	74.656	35.90
131.789	47.04	76.611	36.39
134.878	47.64	78.563	36.93
138.008	48.25	80.517	37.32
141.181	48.87	82.485	37.82
144.437	49.55	84.448	38.28
(Run 14)		86.560	38.75
147.686	50.19	88.823	39.18
150.933	50.93	(Run 17)	
154.174	51.67	163.421	53.62
157.408	52.38	167.246	54.58
160.634	53.19	171.131	55.63
163.841	53.99	174.742	56.56
167.025	54.85	177.929	57.58
170.194	55.46	180.558	58.29
172.864	56.27	(fusion)	
175.018	56.85	183.062	76.19
177.132	57.57		
179.199	58.14		

TABLE 8 (continued)

$\frac{T}{K}$	$\frac{C_p}{JK^{-1}mol^{-1}}$	$\frac{T}{K}$	$\frac{C_p}{JK^{-1}mol^{-1}}$
---------------	-------------------------------	---------------	-------------------------------

SERIES II

(Run 1)

1.907	0.0046
2.193	0.0077
2.570	0.0109
2.988	0.0182
3.400	0.0262
3.830	0.0382
4.248	0.0535
4.655	0.0693

(Run 2)

3.453	0.0279
3.957	0.0430
4.490	0.0622
5.009	0.0873

(Run 3)

184.427	78.00
---------	-------

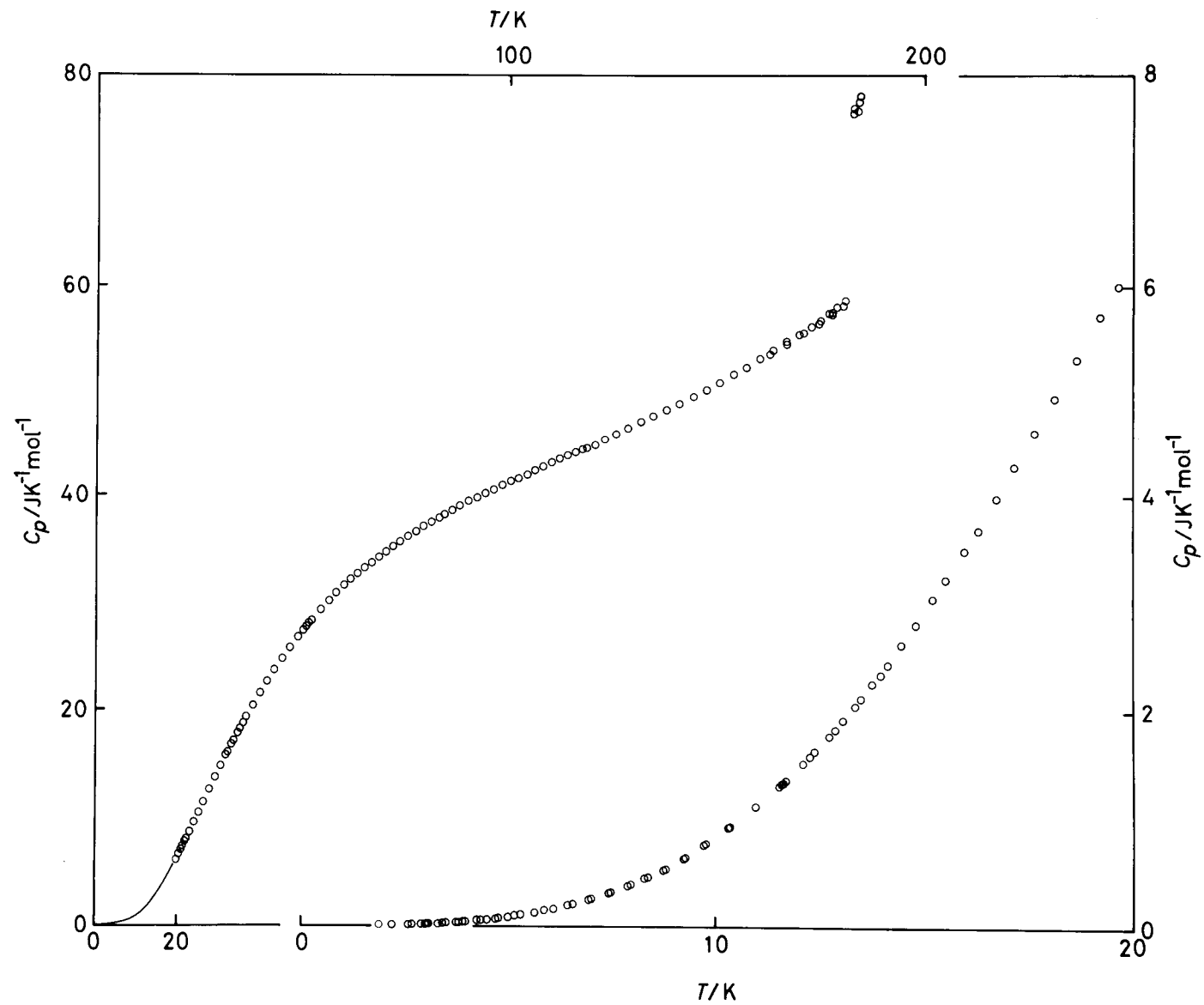


FIGURE 12. HEAT CAPACITY OF DINITROGEN OXIDE.

TABLE 9. Smoothed heat capacity values of dinitrogen
oxide at rounded temperatures.

1 mol N₂O = 44.0128 g , IPTS-1968

<u>T</u> K	<u>C_p^o</u> JK ⁻¹ mol ⁻¹	<u>Deviation*</u> %
2	0.005 ₅	
3	0.019	
4	0.045	
5	0.089	
6	0.156	
7	0.256	
8	0.395	
9	0.580	
10	0.822	
11	1.117	
12	1.472	
13	1.892	
14	2.374	
15	2.918	
16	3.516	
17	4.162	
18	4.847	
19	5.563	
20	6.309	+ 0.16
21	7.090	

* Deviation = $\left[\frac{C_p(\text{Blue and Giauque}) - C_p(\text{This})}{C_p(\text{This})} \right] \times 100$

TABLE 9 (continued)

$\frac{T}{K}$	$\frac{C_p^o}{JK^{-1}mol^{-1}}$	$\frac{Deviation^*}{\%}$
22	7.885	
23	8.694	
24	9.511	
25	10.326	
26	11.14	
27	11.97	
28	12.79	
29	13.60	
30	14.40	+ 0.56
31	15.20	
32	15.97	
33	16.74	
34	17.50	
35	18.23	
36	18.95	
37	19.65	
38	20.33	
39	21.00	
40	21.65	- 0.84
41	22.28	
42	22.90	
43	23.50	
44	24.08	
45	24.65	
46	25.20	
47	25.73	
48	26.25	

TABLE 9 (continued)

$\frac{T}{K}$	$\frac{C_p^o}{JK^{-1}mol^{-1}}$	$\frac{Deviation^*}{\%}$
49	26.76	
50	27.25	+ 0.13
51	27.72	
52	28.18	
53	28.63	
54	29.07	
55	29.50	
56	29.92	
57	30.32	
58	30.71	
59	31.10	
60	31.47	+ 0.54
61	31.83	
62	32.18	
63	32.52	
64	32.85	
65	33.17	
66	33.48	
67	33.78	
68	34.07	
69	34.36	
70	34.64	+ 0.52
71	34.92	
72	35.19	
73	35.46	
74	35.73	
75	35.99	

TABLE 9 (continued)

<u>T</u> K	<u>C_p^o</u> JK ⁻¹ mol ⁻¹	<u>Deviation*</u> %
76	36.25	
77	36.50	
78	36.75	
79	36.99	
80	37.23	+ 0.62
81	37.46	
82	37.69	
83	37.92	
84	38.14	
85	38.36	
86	38.58	
87	38.79	
88	39.00	
89	39.21	
90	39.41	+ 0.25
91	39.61	
92	39.80	
93	39.99	
94	40.18	
95	40.37	
96	40.55	
97	40.73	
98	40.92	
99	41.10	
100	41.28	+ 0.36
101	41.46	
102	41.64	
103	41.82	

TABLE 9 (continued)

$\frac{T}{K}$	$\frac{C_p^o}{JK^{-1}mol^{-1}}$	$\frac{Deviation^*}{\%}$
104	42.00	
105	42.18	
106	42.36	
107	42.54	
108	42.72	
109	42.90	
110	43.07	+ 0.28
111	43.24	
112	43.42	
113	43.60	
114	43.78	
115	43.96	
116	44.14	
117	44.32	
118	44.50	
119	44.68	
120	44.86	+ 0.47
121	45.04	
122	45.22	
123	45.40	
124	45.58	
125	45.77	
126	45.96	
127	46.14	
128	46.32	
129	46.51	
130	46.70	+ 0.81

TABLE 9 (continued)

$\frac{T}{K}$	$\frac{C_p^o}{JK^{-1}mol^{-1}}$	$\frac{Deviation^*}{\%}$
131	46.89	
132	47.08	
133	47.27	
134	47.46	
135	47.65	
136	47.84	
137	48.03	
138	48.23	
139	48.43	
140	48.63	+ 0.86
141	48.83	
142	49.03	
143	49.23	
144	49.44	
145	49.65	
146	49.86	
147	50.07	
148	50.28	
149	50.49	
150	50.70	+ 0.63
151	50.92	
152	51.14	
153	51.36	
154	51.58	
155	51.80	
156	52.02	
157	52.25	

TABLE 9 (continued)

$\frac{T}{K}$	$\frac{C_p^o}{JK^{-1}mol^{-1}}$	$\frac{Deviation^*}{\%}$
158	52.48	
159	52.71	
160	52.95	+ 0.45
161	53.19	
162	53.43	
163	53.68	
164	53.93	
165	54.18	
166	54.43	
167	54.69	
168	54.95	
169	55.21	
170	55.48	+ 0.32
171	55.75	
172	56.02	
173	56.29	
174	56.57	
175	56.85	
176	57.13	
177	57.41	
178	57.70	
179	57.99	
180	58.28	+ 0.39
181	58.58	
182	58.88	
183	76.75	
184	77.10	
185	77.50	+ 0.28

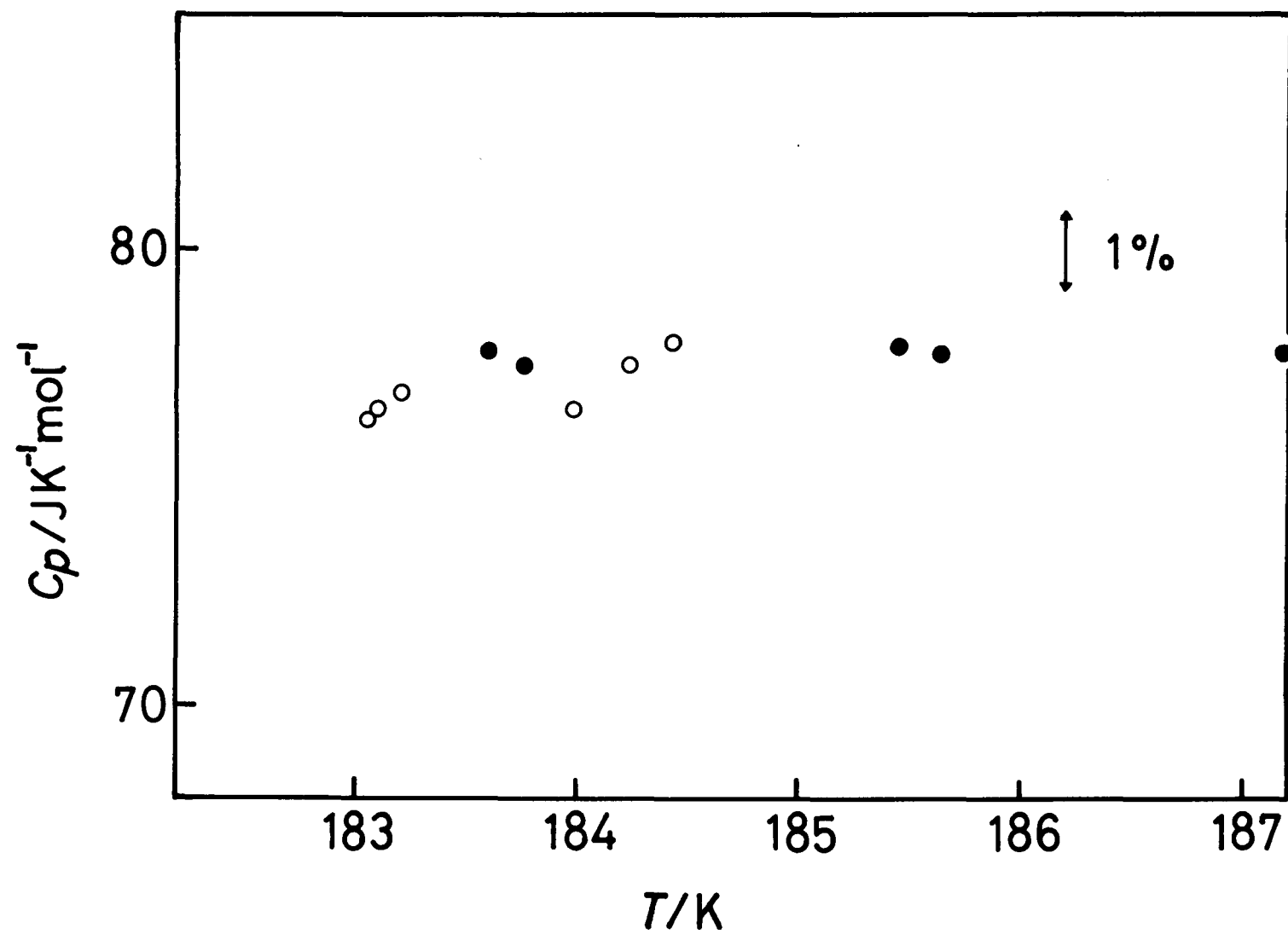


FIGURE 13. HEAT CAPACITY OF LIQUID DINITROGEN OXIDE.
 ○, THIS RESEARCH; ●, BLUE AND GIAUQUE.¹⁾

The value of the heat of fusion of dinitrogen oxide is $(6516 \pm 20) \text{ Jmol}^{-1}$.

The triple point of pure dinitrogen oxide was determined as $(182.408 \pm 0.002) \text{ K}$ from the fractional melting curve, which is given in Figure 15. (The melting point of the dinitrogen oxide used in this calorimetry was 182.4077 K .) The amount of impurity was estimated as 0.003 mol per cent from this curve. The data of the triple point of dinitrogen oxide are summarized in Table 11.

3.3.3. Heat of vaporization

The heat of vaporization at fixed temperatures and vapor pressures were measured and the corrections were applied in the same manner as for the heat of fusion illustrated in Figure 14. The measurements of heat of vaporization are summarized in Table 12, together with the data of Blue and Giauque.¹⁾ The value of the heat of vaporization of dinitrogen oxide is $(16544 \pm 20) \text{ J mol}^{-1}$ at 184.81 K and 763 Torr .

3.3.4. Vapor pressure

The vapor pressure of solid and liquid dinitrogen oxide were measured concurrently with the heat capacity measurements. The data are tabulated in Table 13, together with the deviations compared with the values derived from the equations (9) and (10), and shown graphically in Figure 16. (The gravitational accel-

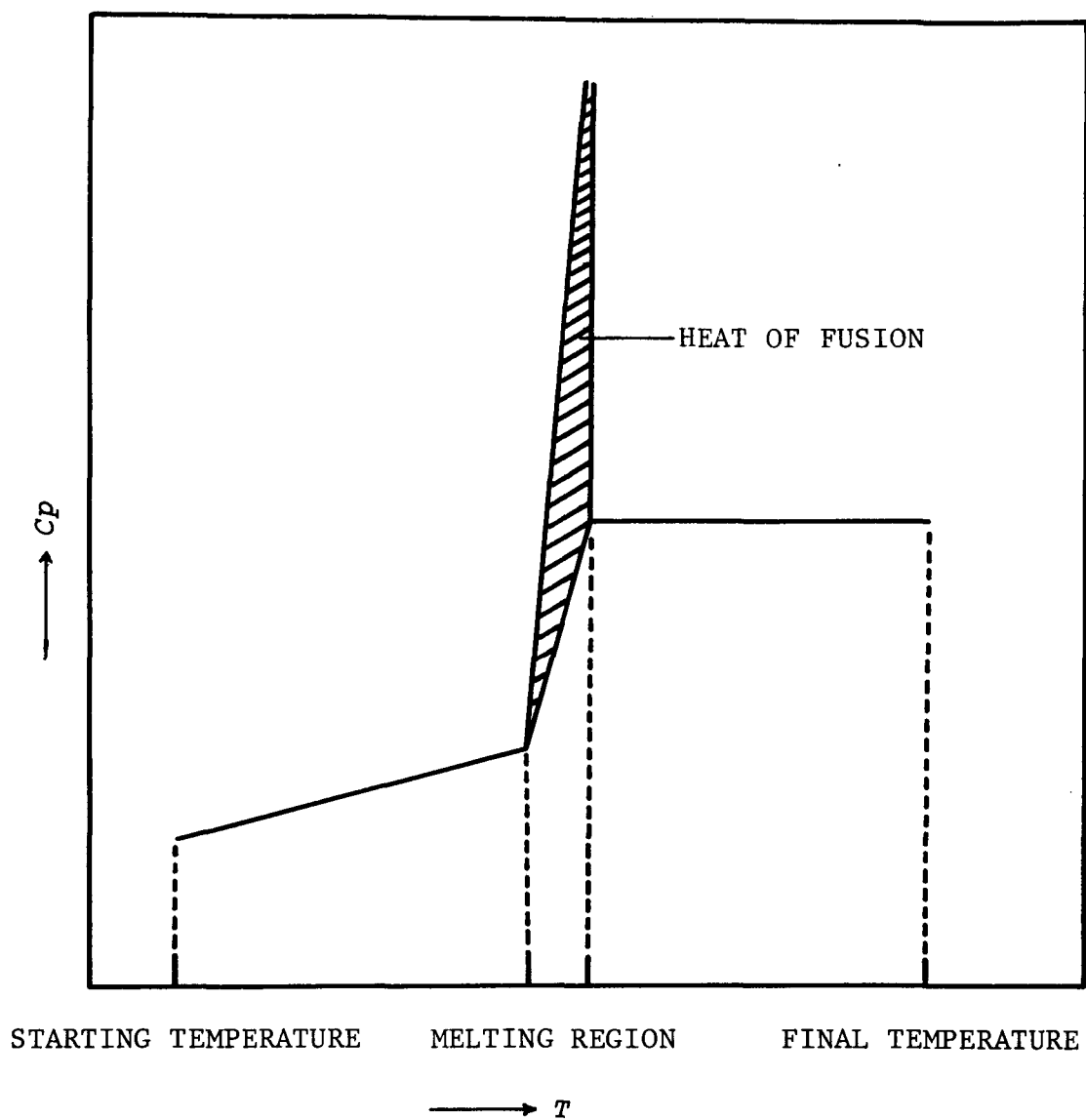


FIGURE 14. Schematic diagram for the determination of the heat of fusion.

TABLE 10. THE HEAT OF FUSION OF DINITROGEN OXIDE.

(1). 0.4265 mol, 2). 0.2007 mol)

Temperature interval	Heat input	$\int C_p dT$	$\Delta n_g \cdot \Delta H_v$	ΔH_f
K	J	J	J	J·mol ⁻¹
182.2100 - 184.2946	2864.77	99.87	4.96	6511
181.6269 - 183.8208	1368.43	65.97	12.26	6521
average				6516 ± 20

R.W.Blue and W.F.Giauque (1935)

6541

TABLE 11. THE TRIPLE POINT OF DINITROGEN OXIDE.

Fraction melted	Temperature	Pressure
	K	Torr
0.169	182.4040	659.72
0.302	182.4043	659.79
0.435	182.4049	659.39
0.568	182.4054	659.37
0.702	182.4059	659.36
0.835	182.4065	659.99
0.968	182.4075	659.45
(1.000)	(182.4077)	

The triple point of pure dinitrogen oxide = (182.408 ± 0.02) K

K.Clusius, et al. (1930) 182.4 K ; Blue and Giauque (1935) 182.26K.

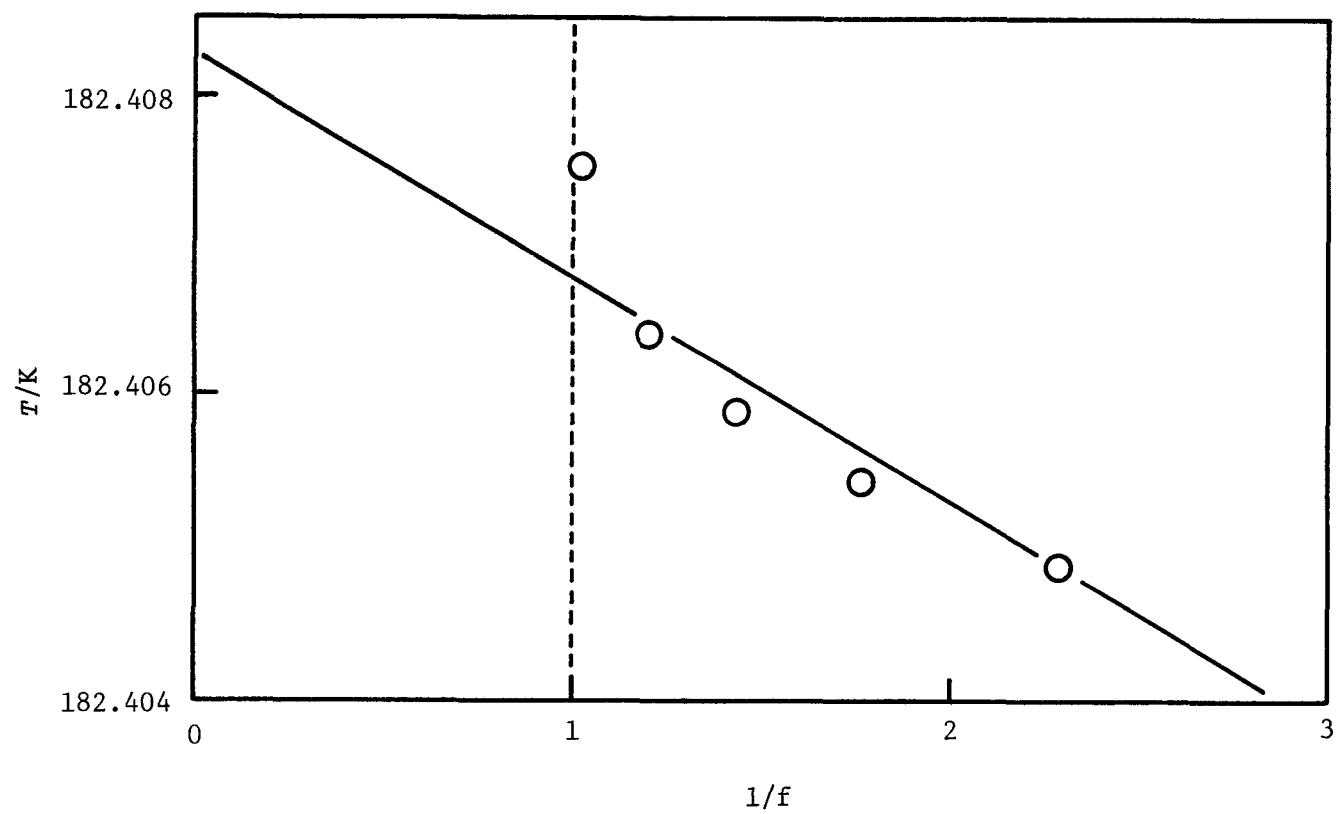


FIGURE 15. MELTING CURVE OF DINITROGEN OXIDE.

TABLE 12. THE HEAT OF VAPORIZATION OF DINITROGEN OXIDE.

STARTING POINT (T/K, P/dyne cm ⁻²)	FINAL POINT (T/K, P/dyne cm ⁻²)	HEAT INPUT (ΔE/J)	AMOUNT OF EVAPORATED N ₂ O (Δn/mol)
i). T ₁ = 184.4132 P ₁ = 993589	T ₂ = 184.6673 P ₂ = 1008573	ΔE = 1096.05	Δn = 0.0653615
ii). T ₁ = 184.8003 P ₁ = 1017080	T ₂ = 184.8162 P ₂ = 1017802	ΔE = 1070.96	Δn = 0.0647080
iii). T ₁ = 184.6745 P ₁ = 1009276	T ₂ = 184.6841 P ₂ = 1009503	ΔE = 1066.27	Δn = 0.0644931
Average ΔH _v = (16544 ± 20) J mol ⁻¹ at 184.81 K			

Blue and Giaugue (1935)

$$\Delta H_v = (16564 \pm 13) \text{ J} \cdot \text{mol}^{-1} \text{ at } 184.59 \text{ K}.$$

eration at our laboratory was taken as 979.71 cm^{-2} for the mercury manometer which was used in the first series of the calorimetry.) The following equations for temperature dependence of the vapor pressures of dinitrogen oxide were determined by the method of least squares:

a) 146 K — triple point (solid)

$$\log_{10}(P/\text{Torr}) = -1270.4/T + 9.95563 - 0.00094122T \quad , \quad (9)$$

b) triple point — 185 K (liquid)

$$\log_{10}(P/\text{Torr}) = -1036.6/T + 9.31608 - 0.0044602T \quad . \quad (10)$$

The normal boiling point of dinitrogen oxide is obtained as 184.74 K from the equation (10). The smoothed values at rounded temperatures derived from these equations are given in Table 14, together with the equations obtained by Blue and Giauque.¹⁾ From the temperature dependence of vapor pressure described above, the heat of vaporization can be obtained by Clapeyron-Clausius equation:

$$dP/dT = \Delta H_V / T \Delta \bar{V} \quad , \quad (11)$$

which is compared with the value calculated from Kirchhoff's law in Figure 17, showing good agreement.

TABLE 13. VAPOR PRESSURE OF DINITROGEN OXIDE.

$\frac{T}{K}$	$\frac{P}{\text{dyne}\cdot\text{cm}^{-2}}$	$\frac{\text{deviation}}{\log_{10}(P_{\text{obs.}}-P_{\text{smoothed}})}$
(Solid)		
146.071	17648	-0.00095
149.301	26977	-0.00010
152.566	40602	0.00137
155.781	59904	0.00132
159.034	87458	0.00071
162.234	124788	0.00090
165.447	176001	0.00059
168.603	243407	0.00054
171.784	333341	0.00053
171.783	333254	0.00060
173.945	409968	0.00049
176.091	500974	0.00041
178.174	605579	0.00044
180.222	726880	0.00025
181.973	846778	0.00011
181.758	831359	0.00006
182.210	864616	-0.00007
161.506	116182	-0.00269
165.335	174887	-0.00176
169.155	258296	-0.00120
173.105	379415	-0.00050
173.115	379591	-0.00031
176.369	514637	-0.00017
179.489	682008	-0.00017
181.626	822453	-0.00022

TABLE 13 (continued)

$\frac{T}{K}$	$\frac{P}{\text{dyne}\cdot\text{cm}^{-2}}$	$\frac{\text{deviation}}{\log_{10}(P_{\text{obs.}} - P_{\text{smoothed}})}$
181.627	822453	-0.00019
	(Liquid)	
184.295	986531	0.00002
182.405	879115	0.00025
182.408	879226	0.00026
184.875	1021437	-0.00001
182.617	890853	0.00013
183.813	958044	0.00015
183.822	958408	0.00024
184.660	1008075	0.00013
183.577	944722	0.00003
184.410	993589	-0.00008
184.413	993589	0.00001
184.667	1008573	0.00011
183.821	959165	-0.00015
182.482	885024	-0.00061
183.643	949018	-0.00021
184.679	1009759	-0.00011
184.089	974774	-0.00013
182.407	879782	-0.00004
182.407	879718	-0.00001
183.937	965506	0.00003
183.937	965560	0.00003
184.917	1024222	-0.00011
184.800	1017080	-0.00009
184.816	1017802	0.00002
184.674	1009276	-0.00000 ₄
184.684	1009503	0.00015

TABLE 14. SMOOTHED VALUES OF VAPOR PRESSURE OF DINITROGEN
OXIDE AT ROUNDED TEMPERATURES.

I). 146 K — triple point (solid)

$$\log_{10}(P/\text{Torr}) = -1270.4/T + 9.95563 - 0.00094122T$$

II). triple point — 185 K (liquid)

$$\log_{10}(P/\text{Torr}) = -1036.6/T + 9.31608 - 0.0044602T$$

T	P	T	P
K	dyne.cm ⁻²	K	dyne.cm ⁻²
I			
146	17443	180	713233
150	29504	182	849001
155	54751	II	
160	97683	182.5	884754
165	168160	183	912246
170	280203	184	969255
175	453193	185	1029038

Blue and Giauque (1935)

I). solid

$$\log_{10} P = -1286/T + 9.13061 - 0.0014038T$$

II). liquid

$$\log_{10} P = -893.56/T + 6.72158$$

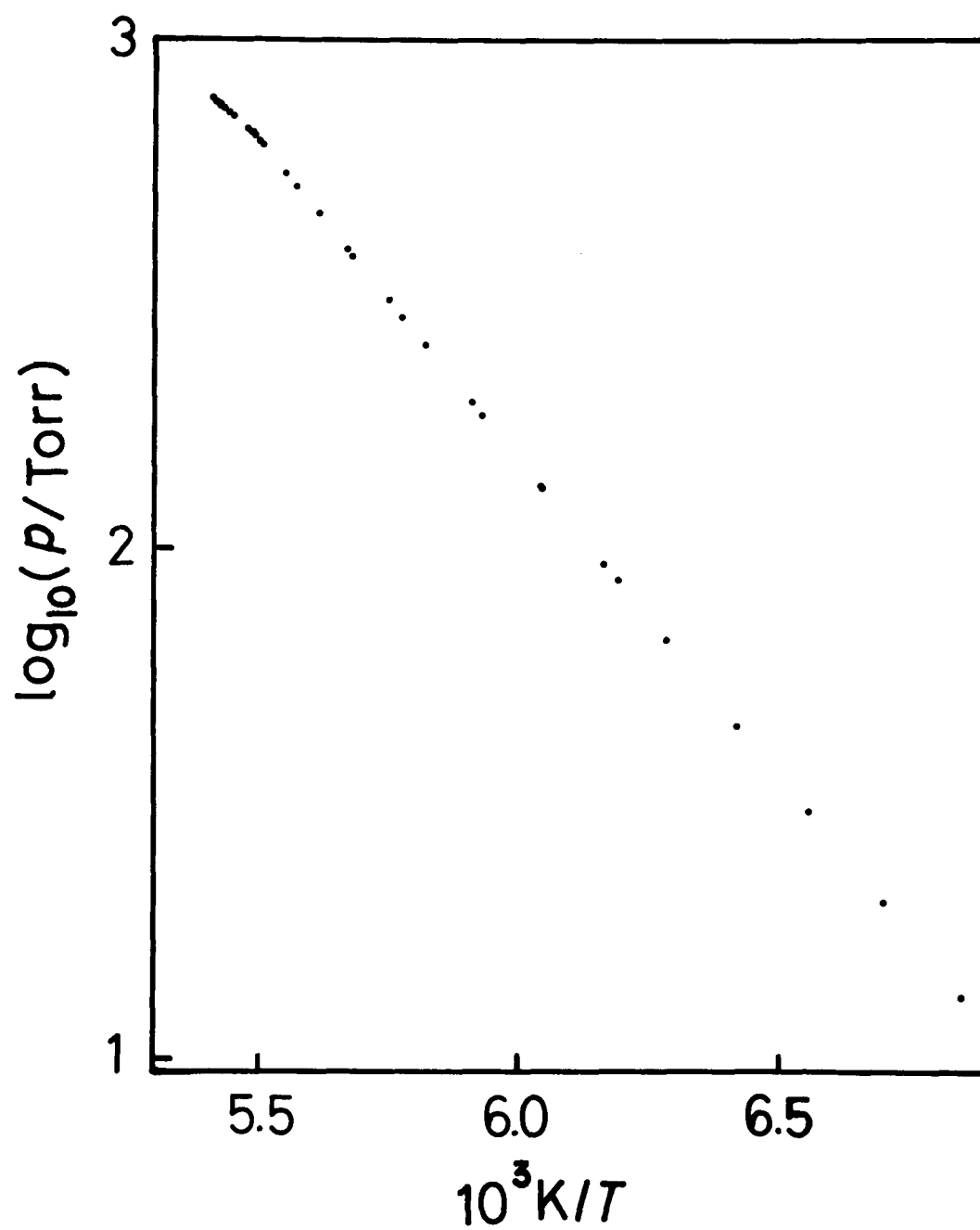


FIGURE 16. VAPOR PRESSURE OF DINITROGEN OXIDE.

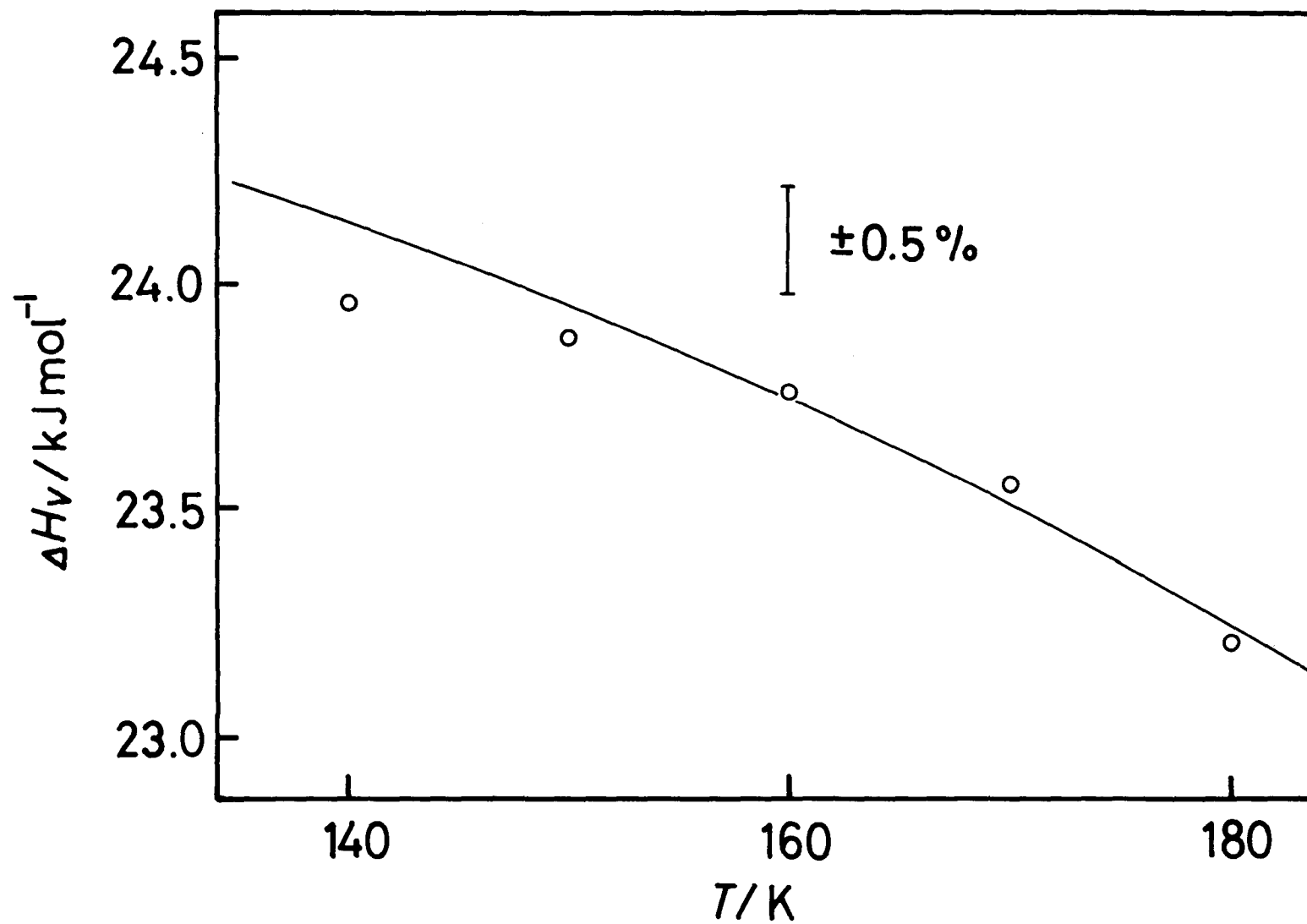


FIGURE 17. HEAT OF VAPORIZATION OF DINITROGEN OXIDE.
 —, FROM KIRCHHOFF'S LAW; O, FROM CLAPEYRON-CLAUSIUS EQUATION.

3.3.5. Thermodynamic functions

Thermodynamic functions of dinitrogen oxide are obtained from the smoothed heat capacity values and other data described above, being tabulated in Table 15, where S_0° and H_0° denote the residual entropy and the heat of sublimation at 0 K, respectively. The contribution of the heat capacities below the lowest temperature measured (1.9 K) was estimated by a smooth extrapolation, which was negligibly small.

TABLE 15. Thermodynamic functions of dinitrogen
oxide.

$\frac{T}{K}$	$\frac{(H^\circ - H_0^\circ)}{J_{mol}^{-1}}$	$\frac{(S^\circ - S_0^\circ)}{JK^{-1}mol^{-1}}$	$\frac{(H^\circ - H_0^\circ)/T}{JK^{-1}mol^{-1}}$	$\frac{-(G^\circ - H_0^\circ)/T}{JK^{-1}mol^{-1}}$
10	1.957	0.2556	0.1957	0.060
20	33.38	2.215	1.669	0.546
30	136.74	6.294	4.558	1.736
40	318.34	11.467	7.958	3.509
50	564.14	16.93	11.28	5.65
60	858.65	22.29	14.31	7.98
70	1189.94	27.39	17.00	10.39
80	1549.66	32.19	19.37	12.82
90	1933.13	36.70	21.48	15.22
100	2336.72	40.95	23.37	17.58
110	2758.52	44.97	25.08	19.89
120	3198.12	48.79	26.65	22.14
130	3655.84	52.46	28.12	24.34
140	4132.39	55.99	29.52	26.47
150	4628.93	59.41	30.86	28.55
160	5147.02	62.76	32.17	30.59
170	5688.92	66.04	33.46	32.58
180	6257.51	69.29	34.76	34.53
182.4	6398.23	70.07	35.08	34.99
182.4	12914.23	105.79	70.80	34.99
184.8	13099.00	106.80	70.88	35.92
184.8	29643.00	196.32	160.40	35.92

3.4. Analysis and discussion

3.4.1. Residual entropy

The third-law entropy of dinitrogen oxide was determined as $(196.3 \pm 1.0) \text{ J K}^{-1} \text{ mol}^{-1}$ at 184.81 K and 763 Torr for the actual gas, and as $(196.8 \pm 1.0) \text{ J K}^{-1} \text{ mol}^{-1}$ corrected to the ideal state at its normal boiling point (184.74 K). The calculation is summarized in Table 16, where the correction for gas imperfection was made by using the temperature dependence of second virial coefficient³¹⁾ and the relation:

$$\Delta S = R \ln P + \left(\frac{dB}{dT} \right) P + \left(\frac{dC}{dT} \right) \frac{P^2}{2} + \dots, \quad (12)$$

where B and C denote the second and third virial coefficients, respectively.

On the other hand, the spectroscopic entropy of dinitrogen oxide was calculated by the statistical thermodynamic relations:

$$S_{(\text{translational})} = R \left(\frac{5}{2} \ln T + \frac{3}{2} \ln M - \ln P + 12.664 \right), \quad (13)$$

$$S_{(\text{rotational})} = R (\ln IT + 89.408) , \quad (14)$$

$$S_{(\text{vibrational})} = R \left[\frac{x}{e^x - 1} - \ln (1 - e^{-x}) \right],$$

$$(x = hc\nu/kT) , \quad (15)$$

where M is the molecular weight of dinitrogen oxide ($44.0128 \text{ g mol}^{-1}$), P is the pressure in dyne cm^{-2} and I is the moment of inertia of dinitrogen oxide ($6.647 \times 10^{-39} \text{ g cm}^2$ derived from the distances of ~~11.257~~ 0.11257 nm for N-N and ~~11.863~~ 0.11863 nm for N-O). The wavenumbers of intramolecular vibrations of 1277 cm^{-1} for ν_1 , 589 cm^{-1} for ν_2 (doubly degenerate) and 2224 cm^{-1} for ν_3 were used for the calculation of vibrational contribution in the harmonic approximation (equation (15)). The spectroscopic entropy was determined as $202.8 \text{ J K}^{-1} \text{ mol}^{-1}$ at 184.74 K .

The residual entropy of dinitrogen oxide was derived from the difference between these two values of entropies, which is given in Table 16. Blue and Giauque¹⁾ obtained the residual entropy of $4.8 \text{ J K}^{-1} \text{ mol}^{-1}$, and explained the difference from $R \ln 2 = 5.8 \text{ J K}^{-1} \text{ mol}^{-1}$ as due to a partial ordering of the end-for-end orientational disorder before the orientational degrees of freedom is frozen in the solid state. The small amount of short-range order in the solid state has been suggested also by Hamilton and Petrie (from neutron diffraction pattern).³³⁾ However, the residual entropy of dinitrogen oxide $6.0 \text{ J K}^{-1} \text{ mol}^{-1}$ obtained in this investigation is very close to $R \ln 2$, which fact suggests freezing-in of the perfect disorder of end-for-end orientation in the solid state. The perfect disorder model is not incompatible with the results derived in the following discussion.

TABLE 16. THE THIRD LAW ENTROPY OF DINITROGEN OXIDE.

Contribution	$S^\circ/\text{JK}^{-1}\text{mol}^{-1}$
0 K — 2 K (smooth extrapolation)	0.002
2 K — 182.41 K (graphical)	70.07
Fusion (6516/182.41)	35.72
182.41 K — 184.81 K (graphical)	1.01
Vaporization (16544/184.81)	89.52
	<hr/>
The entropy of actual gas at 184.81 K	196.32 ± 1.0
The entropy of ideal gas at 184.74 K	196.8 ± 1.0
The spectroscopic entropy	
$S_{(\text{trans.})} = R[5/2\ln(T) + 3/2\ln(M) - \ln(P) + 12.664]$	145.99
$S_{(\text{rot.})} = R[\ln(IT) + 89.408]$	55.87
$S_{(\text{vib.})} = R[x/(e^x - 1) - \ln(1 - e^{-x})]$ ($x = h\nu/kT$)	0.96
	<hr/>
The spectroscopic entropy at 184.74 K	202.8
The residual entropy	
	6.0 ± 1.0
<hr/>	
Blue and Giauque (1935)	$S_0^\circ = 4.8$

3.4.2. Structure and librational motion in solid state

There are two possibilities for the discrepancy between the two values of entropies derived above; (a) anomaly of heat capacity below the lowest temperature measured, (b) non-equilibrium state frozen in solid state. In the first case, for example, there may be a lambda-type transition of end-for-end orientational order-disorder below the lowest temperature measured, and the orientational molecular motion may be significantly excited above the transition.

The motions in molecular crystals were first studied by L. Pauling.³⁴⁾ There are two extreme cases in the molecular motions; primarily rotating and oscillating states. Hydrogen and methane and their deuterated derivatives are primarily rotating in solid state. In this case, the intermolecular potential can be considered as a perturbation on the free rotational motion. Most other heavy molecular crystals belong to the second category. The moment of inertia of dinitrogen oxide is $I = 6.647 \times 10^{-39}$ g cm², and the free rotator energy levels are 1.2 K, 3.6 K and 7.3 K for $J = 1, 2$ and 3 , respectively. The maximum height of the barrier hindering the rotation is estimated to be 2900 cm^{-1} (4000 K) in the harmonic approximation by a small-angle expansion of the simplest potential form:

$$V(\theta) = V_0 (1 - \cos 2\theta) \quad ,$$

$$\nu = 1/\pi \cdot (V_0/I)^{1/2} \quad , \quad (16)$$

where ν is the librational frequency (70 cm^{-1}). It seems very likely that the molecule of dinitrogen oxide can not be reoriented in the crystal in the low~~x~~temperature region and there may be no transition below the lowest temperature measured.

The crystalline dinitrogen oxide has a cubic symmetry of T^4_1 ($P2_13$),^{32),33)} which is similar to the structure of CO_2 ($\text{Th}^6\text{-Pa}3$),³⁵⁾ and both of these two crystals have no solid phase transition. There are another pair of crystals, which have identical structures with those of this group; $\alpha\text{-CO}$ ³⁶⁾ and $\alpha\text{-N}_2$ ³⁷⁾ (their lower temperature phase below phase transitions). The crystal structure of dinitrogen oxide is illustrated in Figure 18, and the lattice parameters and molecular constants are listed in Table 17.

In 1964, Melhuish and Scott²⁹⁾ calculated electronic energies of these crystals by use of slightly different molecular constants, and obtained the Curie temperatures of 5 K and 11 K at which dipole ordering is to occur in solid CO and N_2O , respectively, if it should occur at all. The values of electrostatic contributions obtained by Melhuish and Scott are given in Table 18. Apparently, the effect of dipolar interactions is very small, and the principal contribution to the molecular orientation must come from the quadrupolar interactions.

In 1968, K.S.Pitzer, et al.³⁰⁾ considered another possibility;

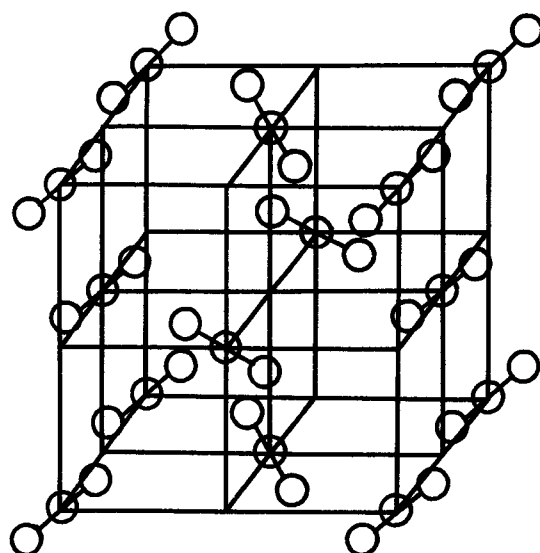


FIGURE 18. THE CRYSTAL STRUCTURE OF DINITROGEN OXIDE.

TABLE 17. THE LATTICE PARAMETERS AND MOLECULAR CONSTANTS OF SOME SIMPLE MOLECULES.^{32),33),35),36),37),38)} I , Moment of inertia; a , Lattice constant; $(x,x,x),(y,y,y)$, Positions of the terminal nuclei in units of a ; μ , Dipole moment; θ , Quadrupole moment.

	I 10^{-39} gcm^2	a 10^{-8} cm	x	y	μ 10^{-18} esucm	θ 10^{-26} esucm^2
N_2O	6.647	5.65 (83 K)	0.117	0.117	0.166	-3.0
CO_2	7.187	5.553(20 K)	0.117	0.117	0	-4.3
$\alpha\text{-CO}$	1.448	5.63 (20 K)	0.067	0.042	0.112	-2.5
$\alpha\text{-N}_2$	1.401	5.644(25 K)	0.070	0.039	0	-1.4

TABLE 18. THE LATTICE ENERGIES AND ELECTROSTATIC CONTRIBUTIONS
 PROVIDED BY MELHUISE AND SCOTT (1964). (in cal.mol⁻¹)

	$\alpha\text{-N}_2$	$\alpha\text{-CO}$	CO_2	N_2O
E_{lattice}	-1650	-1900	-6450	-5800
$E_{\text{dipole-dipole}}$	0	-4.39	0	-9.54
$E_{\text{dipole-octopole}}$	0	-0.12	0	-1.20
Total E_{dipoles}	0	-4.51	0	-10.72
$E_{\text{quadrupole-quadrupole}}$	(-160)	(-180)	-2800	(-940)
$E_{\text{quadrupole-hexadecapole}}$	(+6)	+7	+500	(+170)
Total $E_{\text{quadrupoles}}$	(-150)	(-170)	-2300	(-770)

the kinetics of the order-disorder transition in solid carbon monoxide by a tunneling mechanism. They obtained an approximate form of the probability that molecule number p originally in the torsional state 2 emits a phonon and falls to state 1 one per unit time as:

$$r_p = \frac{k T \omega_0^2 \omega_t^2}{8\pi \rho c_1^5} \left(\frac{\delta \ln V_2}{\delta \Delta} \right)^2 \left(\frac{\delta \ln \omega_t}{\delta \Delta} \right)^2 . \quad (17)$$

Using approximate values of the splitting between the two levels $\omega_0 = 1.2 \times 10^{12} \text{ rad s}^{-1}$, the density ρ (from the molar volume of about 40 cm^3), the longitudinal sound velocity $c_1 = 2 \times 10^5 \text{ cm s}^{-1}$, the derivative $\delta \ln V_2 / \delta \Delta = 10$ (V_2 is the barrier height of about 600 cm^{-1} and Δ is the cubical dilation), the tunneling frequency $\omega_t = 3.2 \text{ rad s}^{-1}$, and the quantity of $\delta \ln \omega_t / \delta \ln V_2 = 6.82$, they found that the rate of ordering in solid carbon monoxide would be unobservably slow; $r_p = 5.5 \times 10^{-7} \text{ year}^{-1}$. Applying their theory to a heavier molecule, N_2O , by using about the same values as for CO, it seems apparent that the orientation of dinitrogen oxide is frozen in solid state.

Raman and infrared spectroscopic studies of molecular motion in solid dinitrogen oxide have been carried out by several investigators.³⁹⁾ The correlation diagrams for dinitrogen oxide and carbon dioxide are shown in Figure 19. The lattice frequencies of $K = 0$ for some simple molecular crystals are listed in Table 19.³⁹⁾ The librational frequencies of $\alpha\text{-CO}$ and $\alpha\text{-N}_2$ compare

Mode	Molecular Symmetry	Site Symmetry	Unit Cell Symmetry
	$C_{\infty v}$	C_3	T
ν_1, ν_3, T_z	$\Sigma^+(R, ir)$	$A(R, ir)$	$A(R)$
ν_2, T_{xy}, R_{xy}	$\Pi(R, ir)$	$E(R, ir)$	$E(R)$
			$T(R, ir)$

(a). for N_2O

Mode	Molecular Symmetry	Site Symmetry	Unit Cell Symmetry
	$D_{\infty h}$	S_6	T_h
ν_1	$\Sigma_g^+(R)$	$A_g(R)$	$A_g(R)$
R_{xy}	$\Pi_g(R)$	$E_g(R)$	$E_g(R)$
ν_3, T_z	$\Sigma_u^+(ir)$	$A_u(ir)$	$A_u(-)$
ν_2, T_{xy}	$\Pi_u(ir)$	$E_u(ir)$	$E_u(-)$
			$T_u(ir)$

(b). for CO_2

FIGURE 19. THE CORRELATION DIAGRAMS FOR N_2O AND CO_2 .

TABLE 19. THE FREQUENCIES OF LATTICE MODES IN SIMPLE MOLECULAR CRYSTALS OBTAINED FROM RAMAN AND INFRARED SPECTRA. (in cm^{-1})
L: Librational, T: Translational (obtained by several investigators³⁹⁾)

	CO_2			$\alpha\text{-N}_2$	
	15 K	18 K	79 K	16 K	18 K
L(E _g)	73.5	75.5	73.5	33.5	32
L(T _g)	91.5	94	91	37.5	36.5
L(T _g)	132	134	131		60
T(A _u)					
T(E _u)					
T(T _u)			68		
T(T _u)			114		

	N_2O			$\alpha\text{-CO}$	
	15 K	18 K	79 K	12 K	18 K
L(E)	68	70.5	67.5		44
L(T)	82	83	80	47.5	52
L(T)	124.5	126.5	121.5		90.5
T(A)					64.5
T(E)					58
T(T)		66.5			
T(T)			113		

favorably with those given by the formula,

$$\nu_n = C_n Q (I a_0^5)^{-1/2} \quad , \quad (18)$$

where the C_n are coefficients deduced from lattice sums including the second and more distant neighbour interactions in the point quadrupole model, Q is the quadrupole moment, I the molecular moment of inertia, a_0 the lattice constant. In the case of larger rod-like molecules N_2O and CO_2 , this formula does not give so good agreement, where assumed Q values of 6.05×10^{-26} and 6.4×10^{-26} esu cm² are needed to get the best agreement with the observed librational frequencies, whereas the recommended values are 3.0×10^{-26} and 4.3×10^{-26} esu cm², respectively, and therefore the point model for molecular interactions is invalid. The librational contributions calculated for N_2O from the values of 70 cm^{-1} (E), 83 cm^{-1} (T) and 126 cm^{-1} (T) were subtracted from the total heat capacity of dinitrogen oxide, and the remains, lattice heat capacity, is analyzed in Section 3.4.4.

The vapor pressures also provide some informations about molecular motion in crystalline solids.^{40),41)} In 1963, L.Salter⁴⁰⁾ derived a vapor pressure equation for monatomic crystals, which has been extended by H.Chihara and N.Nakamura⁴¹⁾ to some simple molecular crystals. The Gibbs energy of a molecular crystal may be expressed as a sum of contributions of several types of molecular motion:

$$G^c = G_{\text{trans}}^c + G_{\text{vib}}^c + G_{\text{rot}}^c + G_{\text{exp}}^c \quad , \quad (19)$$

where the superscript c denotes 'crystal' and the terms represent the contributions from translational, vibrational (intramolecular), and rotational (librational) motions and from thermal expansion. By using the high temperature Thirring expansion,⁴²⁾ the translational contribution in high temperature region ($T > \theta_D/10$) may be expressed as:

$$G_{\text{trans}}^c = E'_0 + 3NkT \left[\ln(h\nu_g/kT) + \sum_{n=1}^{\infty} (-1)^{n-1} B_{2n} / 2n(2n)! \right. \\ \left. \times \mu_{2n} (h/2\pi kT)^{2n} \right] \quad , \quad (20)$$

where ν_g is the geometric mean frequency for the translational lattice modes, B_{2n} the Bernoulli number, μ_{2n} the 2nth moment of the translational lattice frequency spectrum, and E'_0 the pseudo-static lattice energy, which is related to the static lattice energy E_0 by

$$E_0 = E'_0 - E_{z,lib} \quad , \quad (21)$$

because the translationally static lattice may still possess the zero point kinetic energy $E_{z,lib}$ of molecular libration. The

contribution of intramolecular vibrations in the harmonic approximation is given in standard textbooks as:

$$G_{vib}^C = NkT \sum_i \left[\ln(h\nu_i^C/kT) - h\nu_i^C/2kT + \left(\frac{1}{24}\right)(h\nu_i^C/kT)^2 + \dots \right] + \sum_i Nh\nu_i^C/2, \quad (22)$$

where ν_i^C is the frequency of the i th intramolecular vibration mode and the last term is the vibrational zero point energy. The rotational contribution may be expressed in two extreme cases, primarily oscillating and rotating states, which are given by the equation (22) and the equation,

$$G_{rot}^C = -NkT \sum_j \ln[(1/n_j)(8\pi^2 I_j kT/h^2)^{1/2}] \quad , \quad (23)$$

respectively, where I_j is the moment of inertia and n_j is the symmetry number of the rotational potential. The following analysis is made in this approximation. The contribution from thermal expansion is given by

$$G_{exp}^C = NP V_C \quad , \quad (24)$$

where P and V_C are the pressure and the molar volume, respectively. The corresponding Gibbs energy of vapor is given by

$$G^v = G_{trans}^v + G_{vib}^v + G_{rot}^v + G_{exp}^v \quad , \quad (25)$$

where v denotes 'vapor' and the terms on the right-hand side are given in standard textbooks. From the condition of $G^C = G^v$ for vapor-solid equilibrium, the following relation is obtained:

$$\ln (PT^{n/2}) = a/T + b \quad , \quad (26)$$

where the exponent n is 3 for a linear molecule oscillating about two axes in solid state and a is given by

$$a = E'_0/Nk \quad . \quad (27)$$

b is related to the geometric mean frequency ν_g as:

$$b = \ln[8\pi^2(2\pi m/k)^{3/2} \cdot 1/\sigma \cdot I_v^3 \nu_g^2 \nu_l^2 \nu_c^{intra} / \nu_v^{intra}] \quad , \quad (28)$$

where it has been assumed that

$$h\nu_i/kT < 1 \quad ,$$

$$h\nu_{2n}^{1/2n}/2\pi kT \ll 1 \quad ,$$

$$B(T)/V_v \ll 1 \quad . \quad (29)$$

A linear plot of $\ln(PT^{n/2})$ against $1/T$ gives the static lattice energy from its slope, and its intercept b should give the geometric mean frequency. The good linearity of $\ln(PT^{3/2})$ against $1/T$ for dinitrogen oxide is shown in Figure 20. The static lattice energy (25913 J mol^{-1}) and geometric mean frequency ($6.9 \times 10^{12} \text{ s}^{-1}$) derived from this analysis are used in the following analyses.

3.4.3. Zero point properties

The molar heat of sublimation at 0 K can be obtained from calorimetric quantities by the relation:

$$H_0^O = \Delta H_T^O - \int_0^T C_{p(gas)} dT + \int_0^T C_{p(solid)} dT + RPT^2 \left(\frac{dB}{dT} \right), \quad (30)$$

The heat of sublimation of dinitrogen oxide at 0 K was determined as 24214 J mol^{-1} ($5787 \text{ cal mol}^{-1}$). From the slope a in the analysis of vapor pressure described above, the pseudo-static lattice energy E_0^O was obtained as 25913 J mol^{-1} . The translational zero point energy of crystal of dinitrogen oxide is derived as 1699 J mol^{-1} from the difference between these two values:

$$E_{z,trans} = E_0^O - H_0^O \quad . \quad (31)$$

The approximate value of librational zero point energy is calcu-

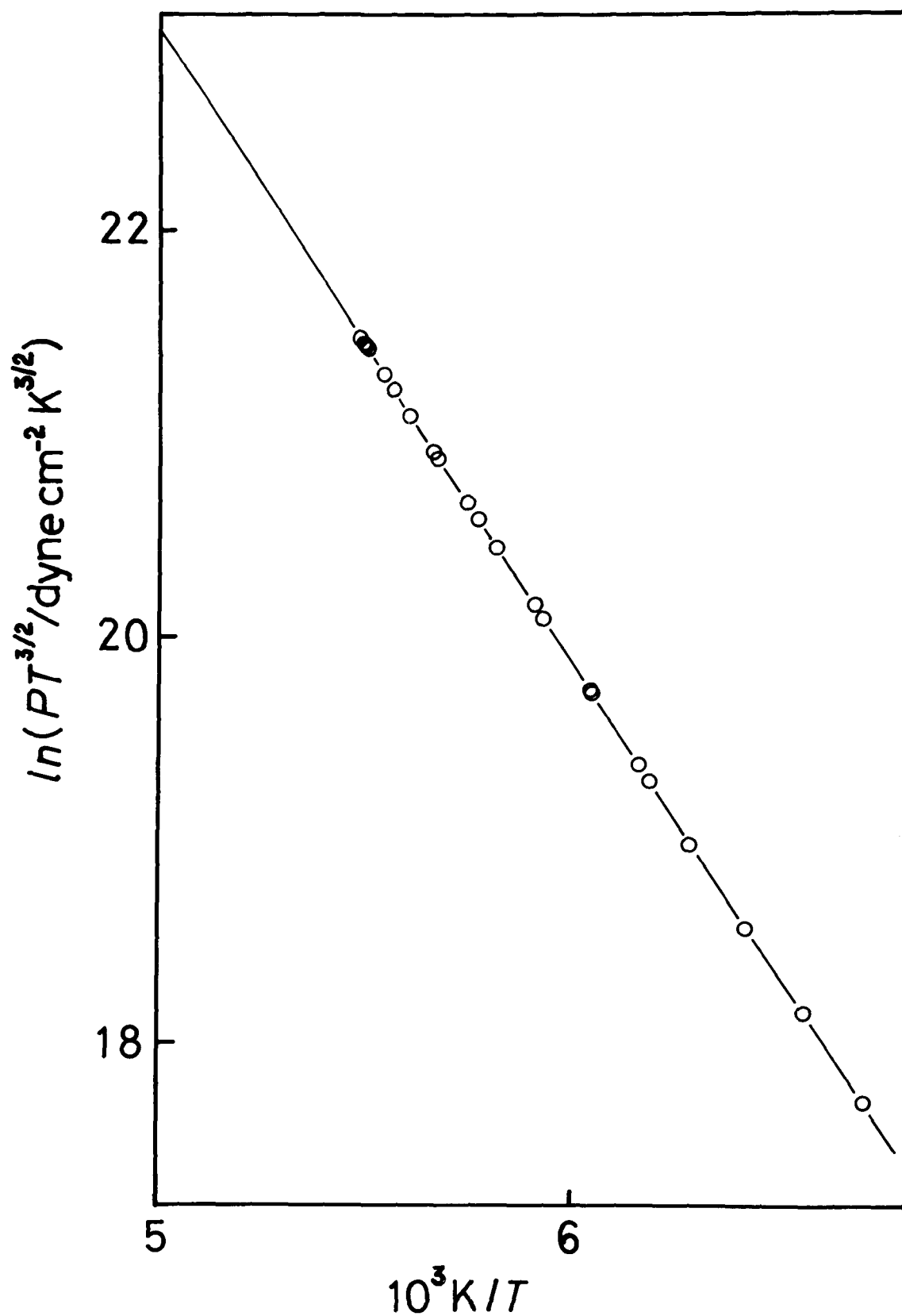


FIGURE 20. PLOT OF $\ln(P T^{3/2})$ AGAINST T^{-1} FOR FOR SOLID DINITROGEN OXIDE.

lated as 1150 J mol^{-1} from the librational frequencies mentioned in Section 3.4.2., and the total zero point energy of solid dinitrogen oxide is estimated as 2849 J mol^{-1} . On the other hand, from the analysis of low temperature lattice mode, which will be described in the following section, the translational zero point energy of crystal of dinitrogen oxide is determined as 1338 J mol^{-1} and the total zero point energy is derived as 2488 J mol^{-1} .

The Debye characteristic temperatures of dinitrogen oxide derived from measured heat capacities are shown in Figure 11, and the limiting value at 0 K can be obtained by the method of smooth extrapolation. The more sensitive derivation is carried out by using the low temperature expansion of heat capacity:

$$C = aT^3 + bT^5 + cT^7 + \dots \quad . \quad (32)$$

The intercept of the curve of C_p/T^3 against T^2 gives the value of a (Figure 21), and θ_D can be obtained by the relation:

$$\theta_D = \left(\frac{1943.7}{a} \right)^{1/3} \quad . \quad (33)$$

Assuming $5N$ degrees of freedom, of which $3N$ degrees of freedom correspond to the translational lattice modes and the remaining $2N$ to the librational modes, the Debye characteristic temperature at 0 K is determined as $(167.4 \pm 1.0) \text{ K}$. Assuming $3N$ degrees of freedom, the Debye characteristic temperature of dinitrogen

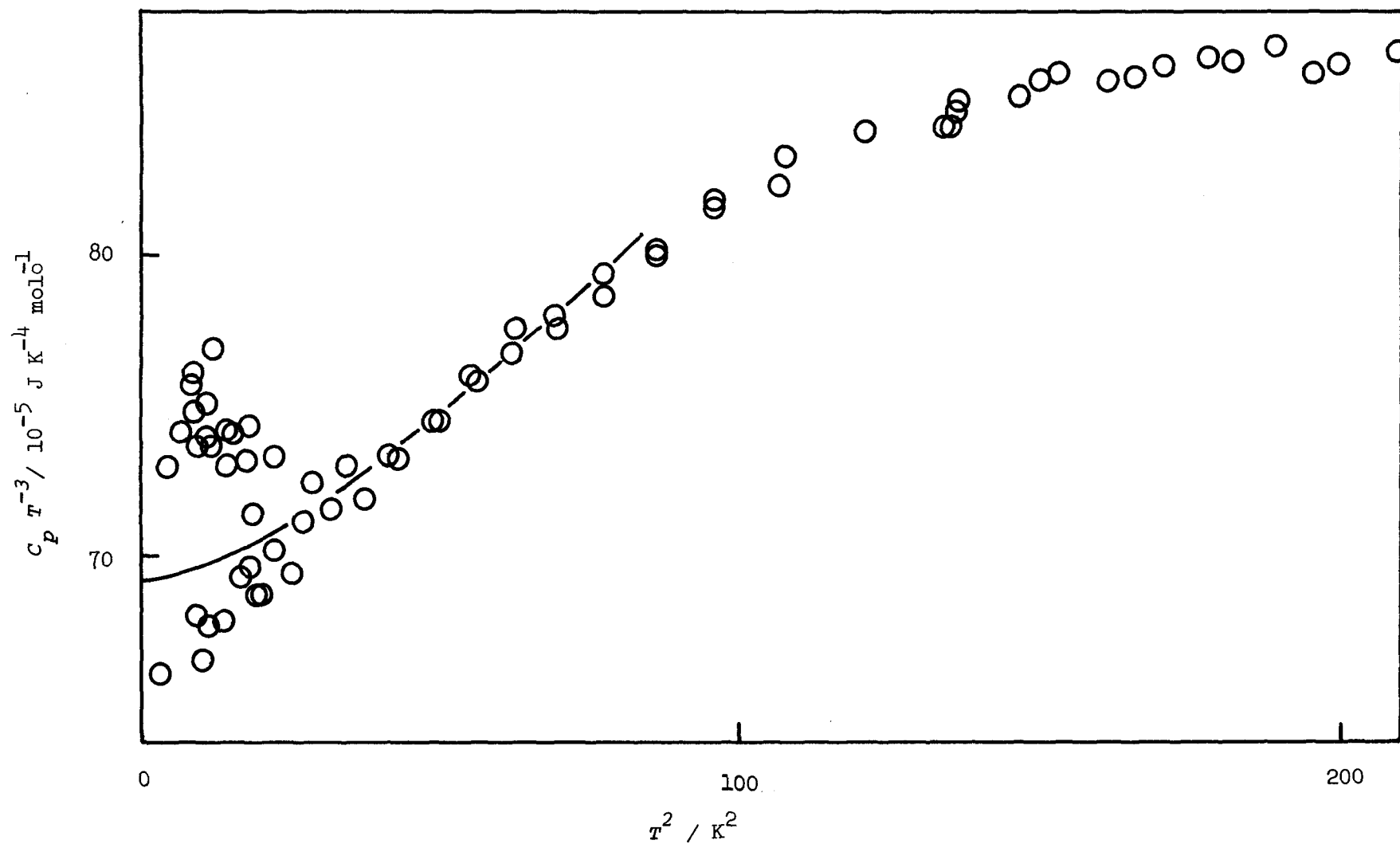


FIGURE 21. A GRAPH OF C_p/T^3 AGAINST T^2 FOR DINITROGEN OXIDE.

oxide at 0 K is determined as (141.0 ± 1.0) K. In the latter case, the curve of $(C_p - C_{lib})/T^3$ against T^2 , where the librational contribution has been subtracted from the total heat capacity, also gives the same value of θ_D as from the curve of C_p/T^3 against T^2 , because the librational contribution calculated by the Einstein model is negligibly small in the lowest temperature region. The temperature dependences of the Debye characteristic temperatures of dinitrogen oxide assuming these two values of degrees of freedom are shown in Figure 22. The zero point properties of dinitrogen oxide are summarized in Table 20, together with those of some other simple molecular crystals calculated from previous data of several investigators.^{1), 9), 12), 17), 41)}

3.4.4. Lattice modes in the low temperature region

The lattice dynamics dealing with the relation between the macroscopic-thermodynamic properties and the molecular or atomic behaviors in crystals has been improved, especially for monatomic crystals and simple ionic crystals. In the case of molecular crystals, inert^ygas crystals have been widely investigated, and recently, the investigation has been extended to diatomic molecular crystals, especially by far-infrared and Raman spectroscopy.^{39), 43)} Dinitrogen oxide is a molecule of interest for extending such studies.

In the first approximation, the heat capacity C_p may be divided into various contributions:

TABLE 20. THE ZERO POINT PROPERTIES OF SOME SIMPLE MOLECULAR CRYSTALS.

	a	b	$\Theta_{D(3N)}$	$\Theta_{D(5N)}$	H_0°	H_z	$H_{z(\text{trans})}$	$H_{z(\text{lib})}$
	$\text{Jmol}^{-1}\text{K}^{-4}$	$\text{Jmol}^{-1}\text{K}^{-6}$	K	K	J mol^{-1}	J mol^{-1}	J mol^{-1}	J mol^{-1}
N_2O	6.93×10^{-4}	5.7×10^{-7}	141.0	167.4	24200	2650	1500	1150
CO_2	5.23×10^{-4}		154.9	183.7	27000	2750	1500	1250
CO	17.7×10^{-4}		103.1	122.3	8000	941	171	770
N_2	36.6×10^{-4}		81.4	96.5	6900	891	361	530

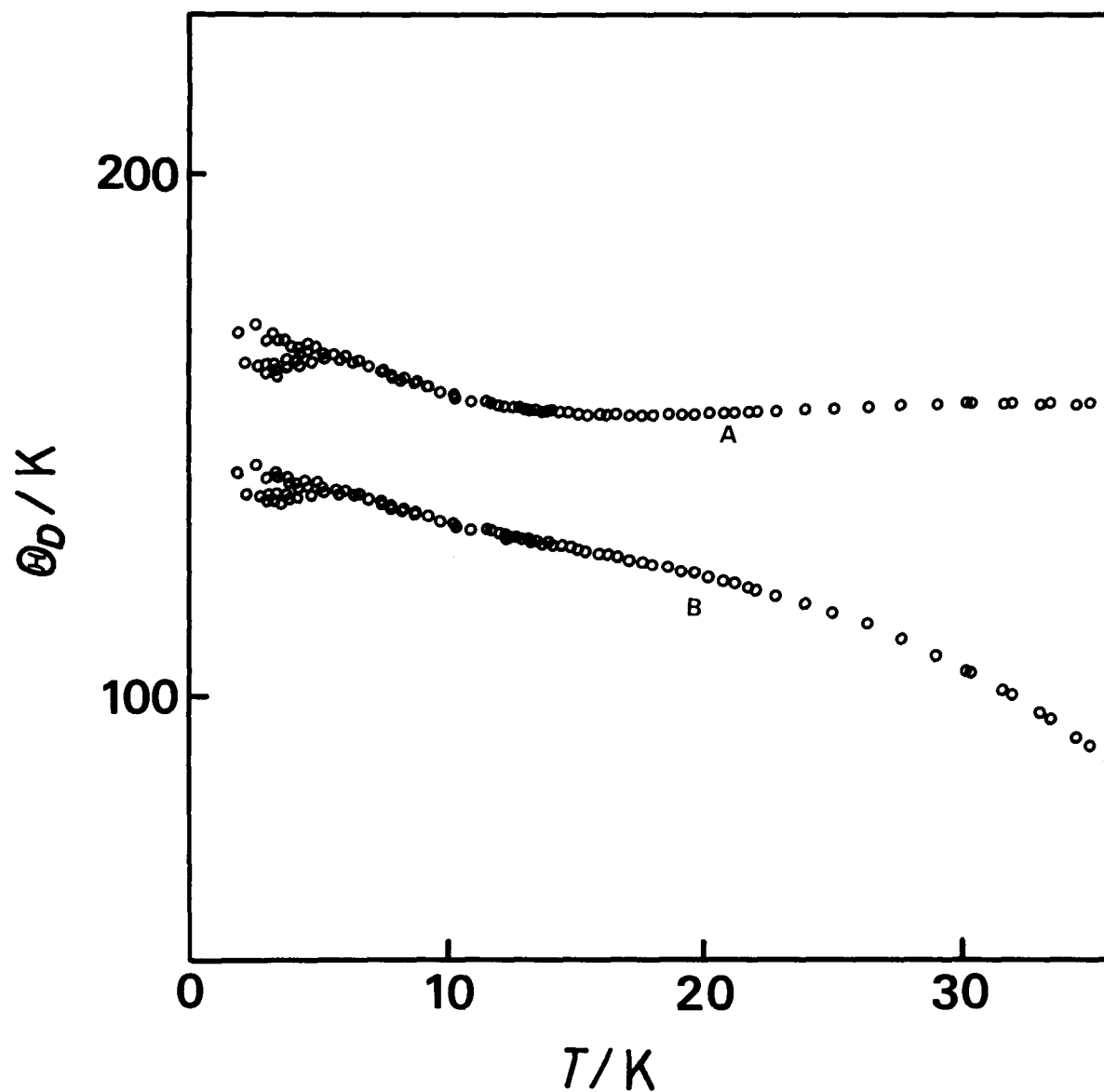


FIGURE 22. THE DEBYE CHARACTERISTIC TEMPERATURE OF DINITROGEN OXIDE. A, assuming 5N degrees of freedom; B, assuming 3N degrees of freedom.

$$C_p = C_{trans} + C_{lib} + C_{intra} + (C_p - C_v) \quad , \quad (34)$$

where the terms represent the contributions from translational lattice modes, molecular librational motions and intramolecular vibrations and the correction for $C_p - C_v$. The same method as for monatomic crystals may be applied to the analysis of the contribution of translational lattice heat capacity separated.

The intramolecular contribution C_{intra} was calculated on the assumption that the vibrations were harmonic and were not coupled to other modes of oscillations, because of their high frequencies; $\nu_1 = 1293 \text{ cm}^{-1}$, $\nu_2 = 590 \text{ cm}^{-1}$ (doubly degenerate), and $\nu_3 = 2240 \text{ cm}^{-1}$.³⁹⁾

The $(C_p - C_v)$ contribution was estimated at 20 K as in the following. The thermal expansivity β was estimated as 0.000176 K^{-1} from the lattice constant and the density of dinitrogen oxide at -190°C and 20 K, respectively.³²⁾ Assuming the Gruneisen constant γ being 2.0, the $(C_p - C_v)$ contribution was estimated as $0.043 \text{ J K}^{-1} \text{ mol}^{-1}$ by using the thermodynamic relations:

$$\begin{aligned} \gamma &= \frac{\beta V}{\chi_s C_p} \quad , \\ \chi_T &= \chi_s + \frac{\beta^2 V}{C_p} T \quad , \\ C_p - C_v &= \frac{\beta^2 V}{\chi_T} T \quad . \end{aligned} \quad (35)$$

The ($C_p - C_v$) contribution is negligibly small below about 25 K, and the following analysis (below about 25 K) was made without this correction.

The lattice heat capacity of molecular crystals have been studied by many investigators.^{39),43),44)} A large number of studies of molecular crystals have been made by using the Debye⁴⁾ and Einstein models.⁴⁵⁾ On the other hand, there are several numerical methods for lattice dynamics based on the microscopic model which was first studied by Born and von Karman.⁴⁶⁾ The moment trace method has been developed by Thirring,⁴²⁾ Montroll,⁴⁷⁾ and others.⁴⁸⁾ In this methods, the distribution function $g(\nu)$ of the frequencies ν of the crystal lattice is given by a series expansion in Legendre polynomials of which the coefficients are linear combinations of the moments, and this is not so good method for obtaining the map of $g(\nu)$. However, this moment method is a most convenient one for calculating thermodynamic quantities.

In the first approximation, the librational contribution may be subtracted from the total lattice heat capacity on the assumption that the vibrations are harmonic and independent of other modes of oscillations. The librational contribution C_{lib} in solid dinitrogen oxide was estimated from the frequencies of 70 cm^{-1} (E), 83 cm^{-1} (T), and 126 cm^{-1} (T) for $2N$ degrees of freedom. From the translational lattice heat capacity thus separated, corresponding to which the Debye characteristic temperature is shown in Figure 23, the values of moments of the

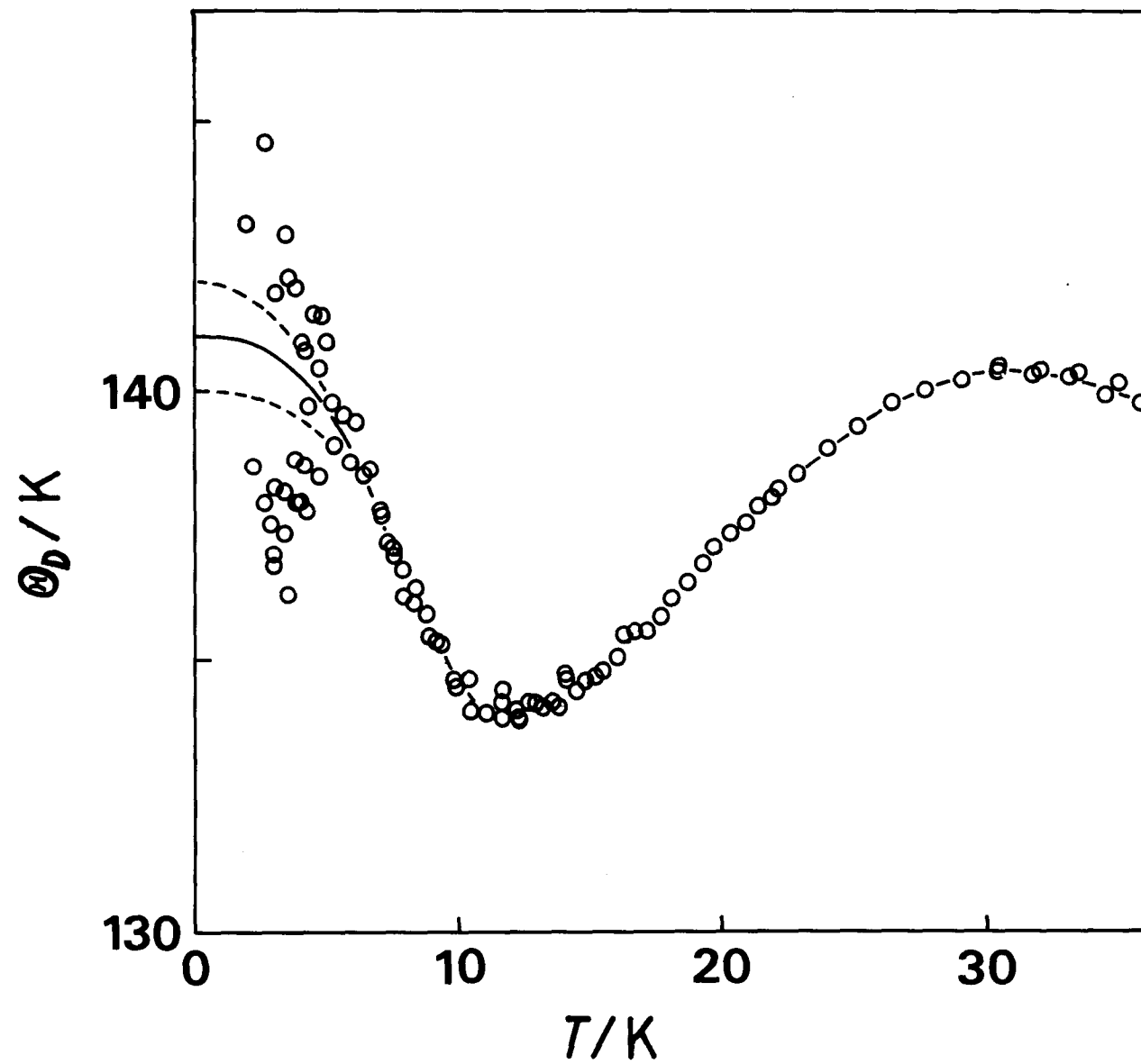


FIGURE 23. THE DEBYE CHARACTERISTIC TEMPERATURE CORRESPONDING TO THE LATTICE HEAT CAPACITY OF DINITROGEN OXIDE.

frequency spectrum were obtained by using the relations derived in the moment method. The n th moment of the frequency spectrum is defined by the expression:

$$\mu_n = \frac{1}{3N} \int_0^\infty \nu^n g(\nu) d\nu \quad . \quad (36)$$

The high temperature expansion of lattice heat capacity derived by Thirring⁴²⁾ was converted into the form of the corresponding Debye characteristic temperature by Domb and Salter:⁴⁹⁾

$$\begin{aligned} \theta_D^2 &= \theta_\infty^2 \left[1 - A \left(\frac{\theta_\infty}{T} \right)^2 + B \left(\frac{\theta_\infty}{T} \right)^4 - \dots \right] , \\ \theta_\infty &= \frac{h}{k} \left(\frac{5\mu_2}{3} \right)^{1/2} , \\ A &= \frac{3}{100} \left(\frac{\mu_4}{\mu_2^2} - \frac{25}{21} \right) , \\ B &= \frac{1}{1400} \left[\left(\frac{\mu_6}{\mu_2^3} - \frac{125}{81} \right) - 100A \right] , \end{aligned} \quad (37)$$

which converges more rapidly than that obtained by Thirring.⁴²⁾ The plot of θ_D^2 against $1/T^2$, which is shown in Figure 24, gives the value of θ_∞ from the extrapolation to $1/T^2 = 0$, and the coefficients A and B are determined from the intercept and slope of the plot of $[1 - (\theta_D/\theta_\infty)^2]/(\theta_\infty/T)^2$ against $(\theta_\infty/T)^2$ as shown in Figure 25. From these values, the moments μ_2 , μ_4 and μ_6 of the frequency spectrum of the translational lattice modes of solid

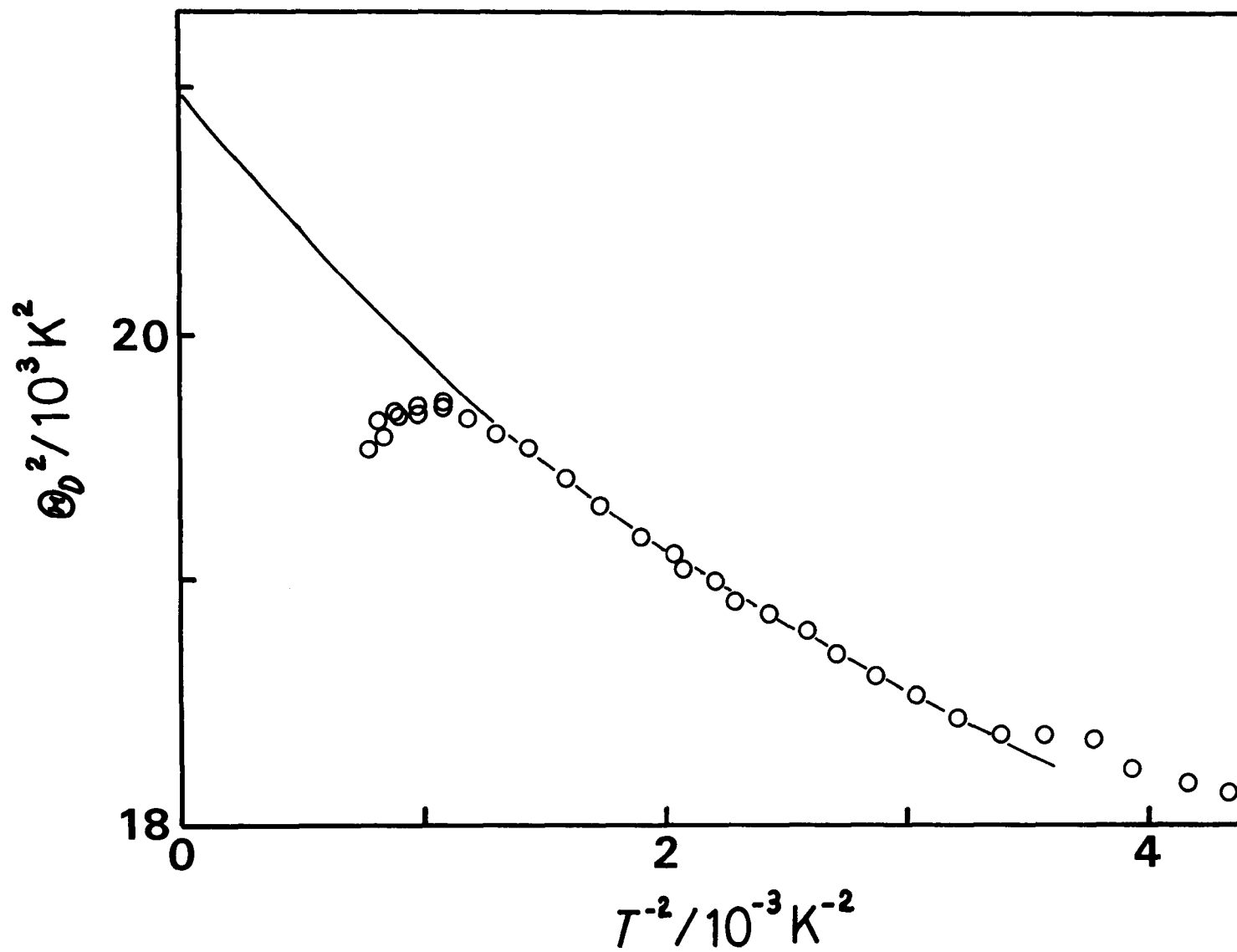


FIGURE 24. DETERMINATION OF θ_∞ FOR DINITROGEN OXIDE.

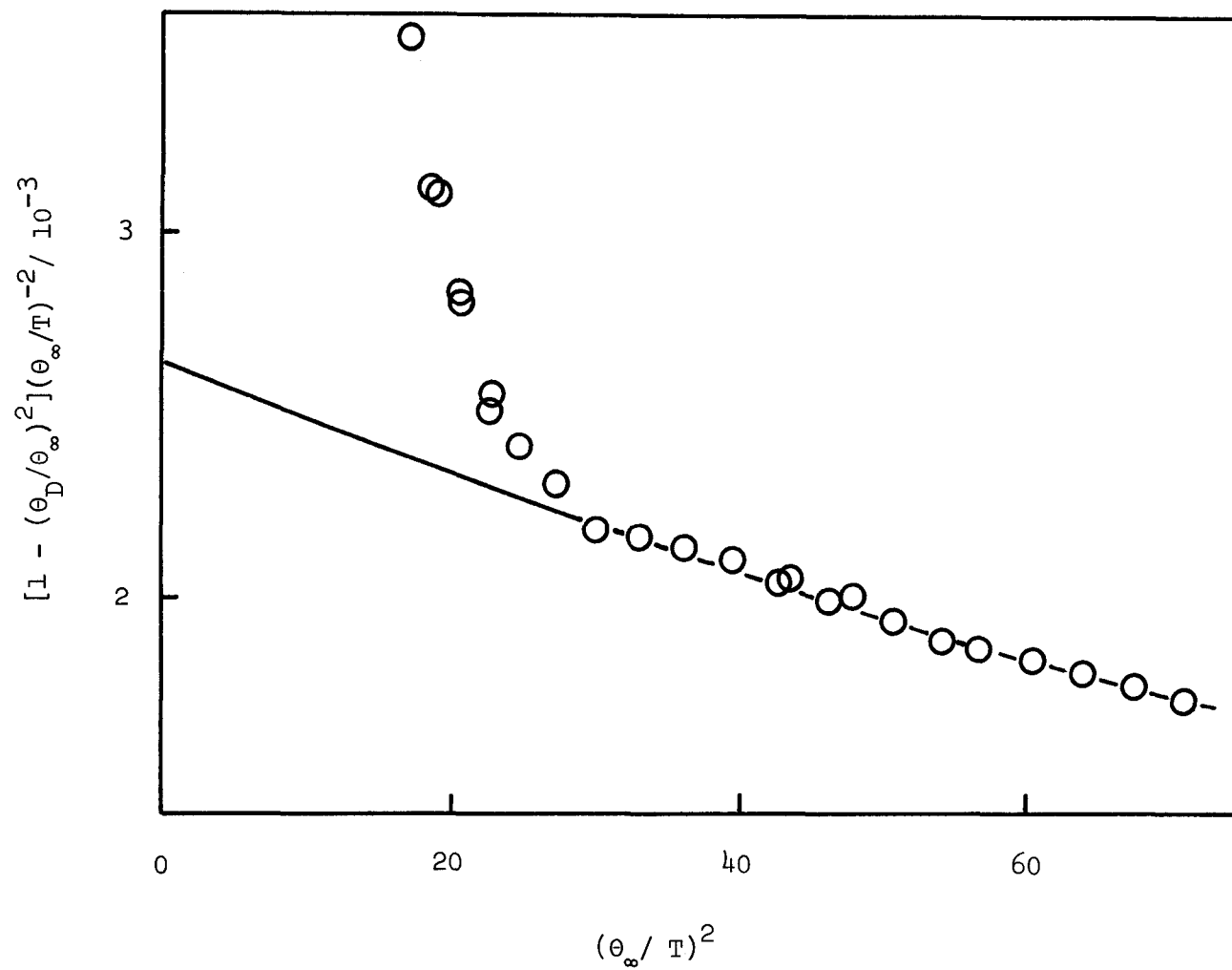


FIGURE 25. DETERMINATION OF THE COEFFICIENTS OF THE THIRRING EXPANSION FOR DINITROGEN OXIDE.

dinitrogen oxide were obtained as $(5.45 \pm 0.06) 10^{24} \text{ s}^{-2}$;
 $(37.9 \pm 1.1) \times 10^{48} \text{ s}^{-4}$ and $(295 \pm 15) \times 10^{78} \text{ s}^{-6}$, respectively.
Different moments are conveniently compared by using the ν_D
function:

$$\nu_D(n) = \left[\frac{1}{3} (n+3) \mu_n \right]^{1/n} ; \quad (n > -3) \quad . \quad (38)$$

This is equivalent to the cut-off frequency of the hypothetical
Debye spectrum which would give the same n th moment of the actual
spectrum in question. In Figure 26, $\nu_D(n)$ is plotted against n
for n up to 6. Here $\nu_D(-3)$ was calculated from $\theta_0 = (141.0 \pm$
 $1.0) \text{ K}$ obtained from a plot of C/T^3 against T^2 by the relation:

$$\nu_D(-3) = k\theta_0/h \quad , \quad (39)$$

and $\nu_D(2)$ was calculated from $\theta_\infty = (144.6 \pm 1.0) \text{ K}$ by the relation:

$$\nu_D(2) = k\theta_\infty/h \quad . \quad (40)$$

The $\nu_D(4)$ and $\nu_D(6)$ were calculated from the values of μ_4 and μ_6
mentioned above. The $\nu_D(0)$ and $\nu_D(1)$ were obtained from the
approximate value of $\theta_\infty^S = 141 \text{ K}$ and from the approximate relation
of $E_z = \frac{9}{8} Nk\theta_\infty^S$, respectively, by the relations:

$$\nu_D(0) = \frac{k}{h} \theta_\infty^S = e^{1/3} \nu_g \quad , \quad (41)$$

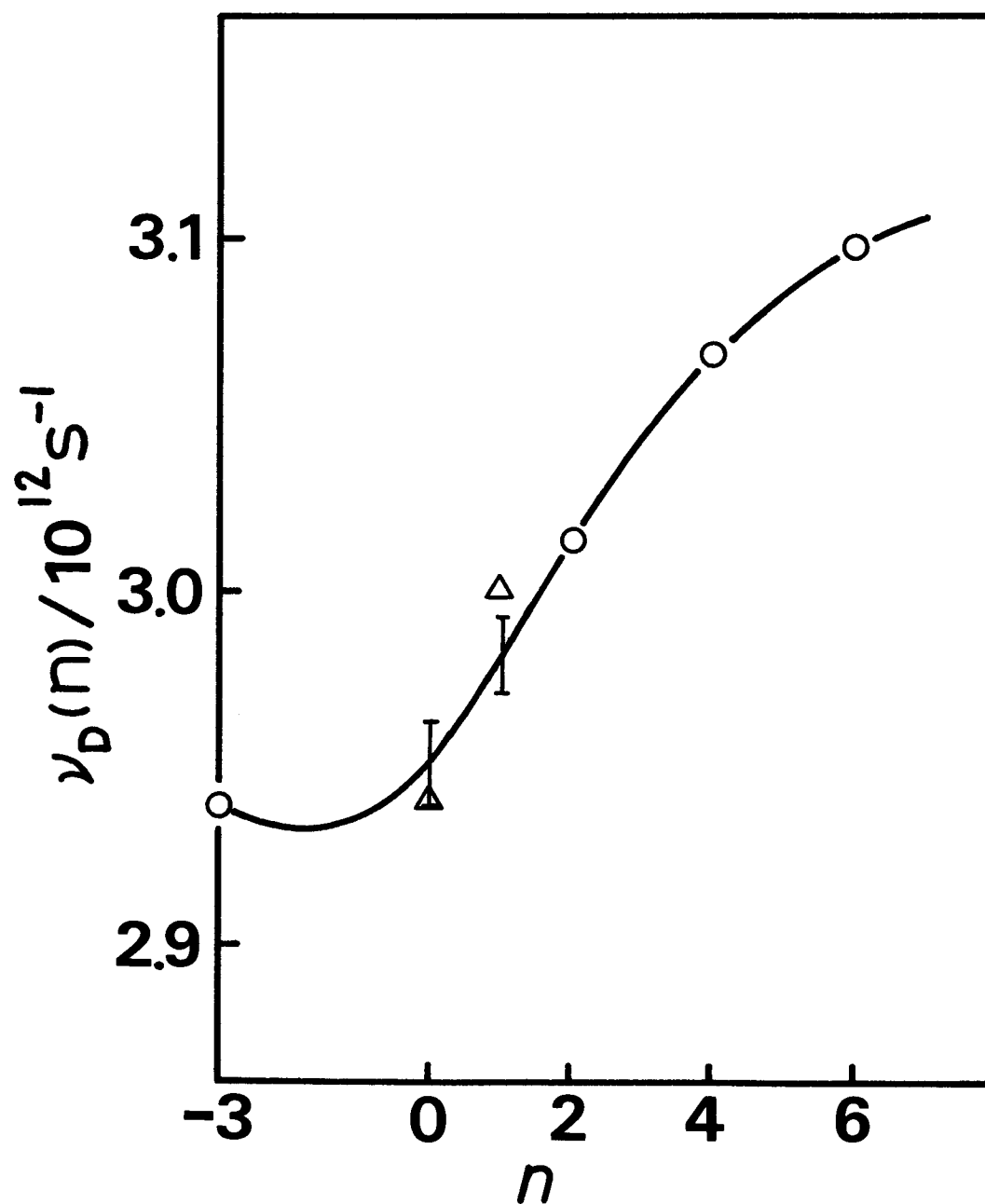


FIGURE 26. PLOT OF $\nu_D(n)$ AGAINST n FOR SOLID DINITROGEN OXIDE.
 Δ , from approximate calculation.

$$\nu_D(1) = \frac{8}{9} \frac{E_z}{Nh} \quad . \quad (42)$$

$\nu_D(n)$ for other values of n could not be obtained, because of the poor convergence of the expansion equations where some corrections for anharmonicity, which have been neglected in this analysis for low temperature region, are necessary.

As shown in Figure 26, a most plausible curve can be drawn by smooth interpolation, and the translational zero point energy was determined as 1338 J mol^{-1} by the equation (42). This value agrees very closely with the translational zero point energy 1699 J mol^{-1} obtained from the analysis of vapor pressure of solid dinitrogen oxide (in Section 3.4.3.). The discrepancy of 361 J mol^{-1} may be mainly due to the rather uncertain value of the pseudo-static lattice energy determined by the analysis of vapor pressure in higher temperature region in the harmonic approximation, where the anharmonicity of vibrations seems significant. This is suggested also by the fact that the ν_g obtained concurrently with the determination of the pseudo-static lattice energy (from the b and a , respectively, described in Section 3.4.2) gives the $\nu_D(0)$ of about 3 times larger value than the value of about $2.95 \times 10^{12} \text{ s}^{-1}$ as shown in Figure 26. The anomalous behavior in the higher temperature region is described in the following section.

To obtain the frequency spectrum of the crystal vibration, an attempt of the direct inversion of the heat capacity curve was

made by using a digital computer, which was not successful because of the insufficient precision of the calorimetry and the limited number of the significant figures in the computer.

On the other hand, the self-consistent phonon approximation may be a logical starting point for the calculation of the lattice dynamics of molecular crystals, which is unavailable for the present time.

3.4.5. Premelting

In the higher temperature region below the triple point (from about 120 K to 182.4 K), the solid dinitrogen oxide shows anomalous increase of heat capacity, which is shown in Figure 27. Such anomaly as this type of increase of heat capacity below the thermodynamic first-order transition has been called 'premelting' and not been taken notice for a long time. In 1961, however, J.A.Morrison, et al. reported the precise thermodynamic properties of argon and krypton,^{5),6)} which showed anomalous increases of heat capacity below the triple points. They concluded that the major cause of the rise in heat capacity is the thermal creation of imperfections, in particular the creation of lattice vacancies of Schottky type, and calculated the enthalpies of formation; $(1280 \pm 130) \text{ cal mol}^{-1}$ for argon and $(1770 \pm 200) \text{ cal mol}^{-1}$ for krypton. In 1969, T.Shinoda, et al.⁵⁰⁾ measured the heat capacity of high purity neopentane $\text{C}(\text{CH}_3)_4$, which showed anomalous increase below the triple point, and they also attributed the anomaly to

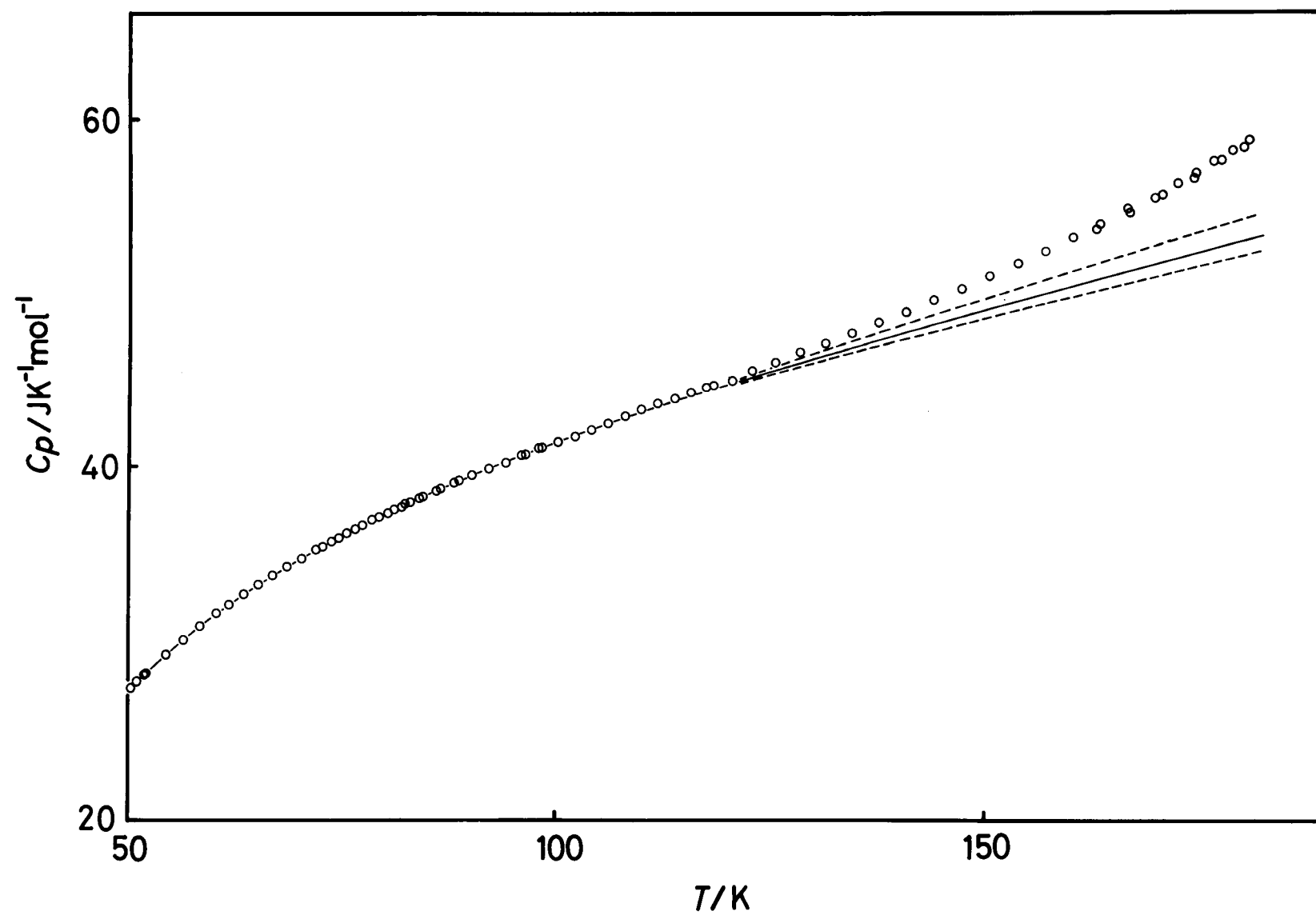


FIGURE 27. THE HEAT CAPACITY OF DINITROGEN OXIDE IN THE PREMELTING REGION.

the formation of lattice vacancies. It seems very likely that the anomalous increases of heat capacities of molecular crystals below the melting points are not only caused by the impurity effect, but also due to the intrinsic characteristics of the materials; the thermal creation of lattice vacancies. In the case of dinitrogen oxide, however, there is another possibility; the creation of orientational defects. Because of the fact that there is no phase transition in solid dinitrogen oxide, it seems that the rotational phase transition may exist above the melting point. The thermal creation of orientational disorders in the crystal field of cubic symmetry may occur below the melting point. In this investigation, in fact, it has been found that the heat capacity of tetramethylstannane also showed anomalous behavior below the triple point, implying two kinds of mechanism for creations of imperfections, which will be described in the next chapter.

The normal heat capacity $C_{p(\text{normal})}$ of solid dinitrogen oxide shown by a solid line in Figure 27 was obtained by the method of smooth extrapolation of the heat capacity from the lower temperature region. The excess heat capacity ΔC_p was obtained from the difference between the $C_{p(\text{normal})}$ and the measured heat capacity C_p ; $\Delta C_p = C_p - C_{p(\text{normal})}$. Besides the two potential minima (most stable end-for-end orientations), it seems that there is no other such deep minimum in the site symmetry C_3 in the crystal of dinitrogen oxide. However, there may be

several very shallow minima in between these two minima. As the temperature increases, the orientational disorder may occur. It costs an enthalpy ΔH_{or} to make a orientational defect but gains entropy S due to the disorder associated with the entropy of mixing of defects with the normal orientations. By applying the equation of Schottky defect, the slope of the plot of $\log(\Delta C_p T^2)$ against T^{-1} (shown in Figure 28) gives the enthalpy of the formation of orientational defect; $\Delta H_{or} = (10800 \pm 500) \text{ J mol}^{-1}$ ($900 \text{ cm}^{-1} = 1300 \text{ K}$). This value may be compared with the height of the barrier hindering the rotation obtained from the simplest model in Section 3.4.2.; ($2900 \text{ cm}^{-1} = 4000 \text{ K}$). Therefore, it may be assumed that the metastable orientations do not exist at about the top of the potential barrier and the ΔH_{or} is very close to one-third of the height of the barrier hindering the molecular reorientation.

Solid carbon dioxide also has no phase transition, and shows the similar rise in heat capacity, which was measured by W.F. Giaque and C.J.Egan.¹⁾ From the same analysis applied to the anomaly in the heat capacity measured by Giaque and Egan, the approximate value of the energy of the formation of orientational defect in solid carbon dioxide is obtained as about 20000 J mol^{-1} .

Carbon monoxide has two thermodynamic first-order transitions; the solid phase transition from the α to β phase at 61.57 K and the fusion from the β to liquid phase at the triple point 68.15 K .¹⁰⁾ The disorder of molecular end-for-end orientation of carbon monoxide

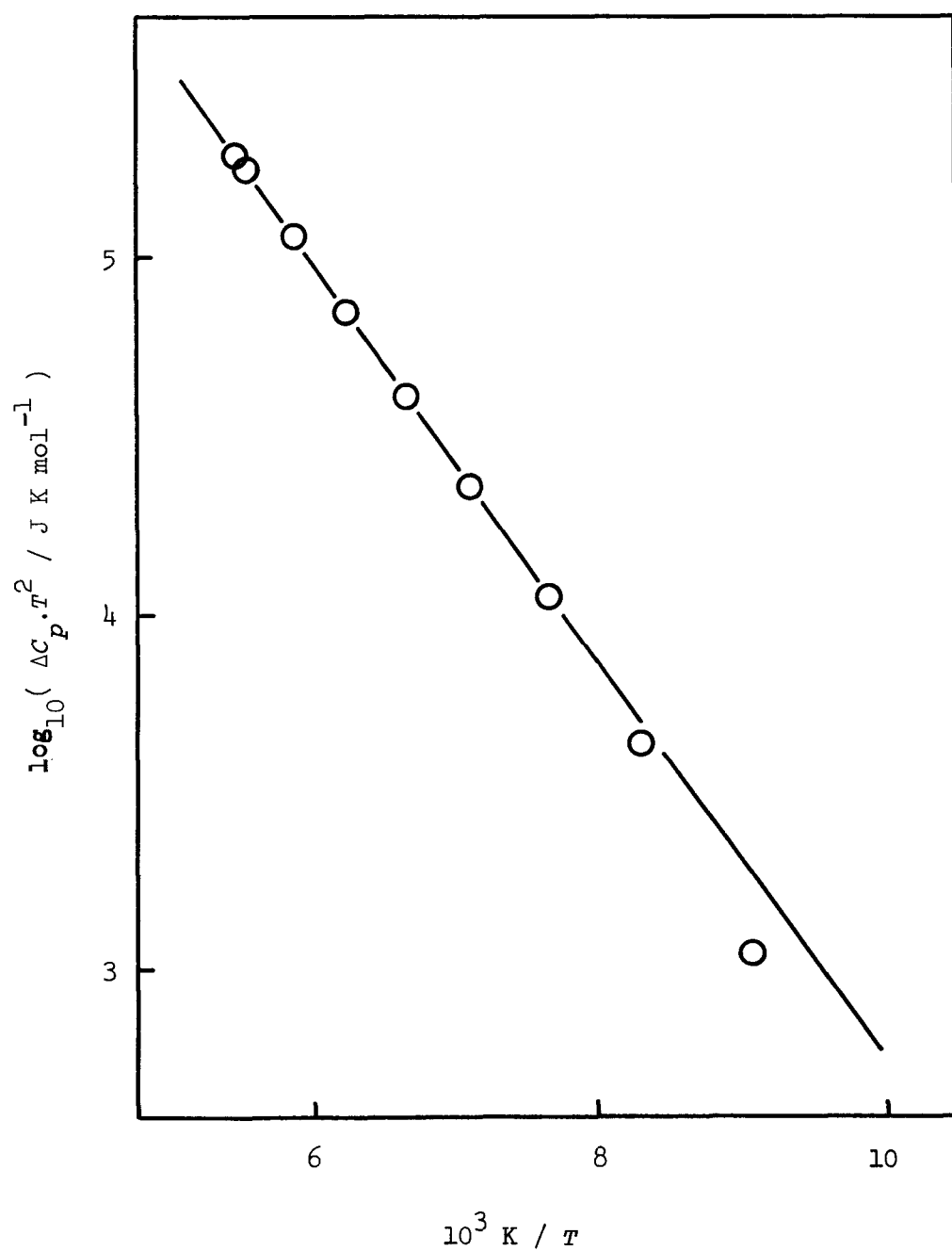


FIGURE 28. PLOT OF $\log_{10}(\Delta C_p \cdot T^2)$ AGAINST $1/T$ FOR DINITROGEN OXIDE.

is also frozen in the α phase, but the rotational motion is significantly excited above the solid phase transition and the entropy of fusion is small; $12.30 \text{ J K}^{-1} \text{ mol}^{-1}$.¹⁰⁾ In this case, also there are anomalous increases in heat capacity below the solid phase transition and the triple point, which correspond to the formation of orientational defect and the formation of lattice vacancy, respectively. From the same analysis applied to the anomaly below the solid~~x~~ phase transition, the energy of the formation of orientational defect in α -CO is obtained as about 3000 J mol^{-1} .

Nitrogen has similar aspects to carbon monoxide, and the approximate value of ΔH_{or} is obtained as about 2000 J mol^{-1} from the heat capacity data of W.F.Giauque and J.O.Clayton.¹⁾

From the data of $\text{C}(\text{CH}_3)_4$ of T.Shinoda, et al.,⁵⁰⁾ which shows anomalous increase in heat capacity below the solid phase transition, the value of ΔH_{or} is obtained as 9700 J mol^{-1} .

These are summarized in Table 21. It seems that the values of $\Delta H_{\text{or}}/H_0^\circ$ and $\Delta H_{\text{or}}/T_f$ are convenient parameters: In the case of the substances which have no rotational solid phase transition, the values of $\Delta H_{\text{or}}/H_0^\circ$ and $\Delta H_{\text{or}}/T_f$ are larger than the values of about 0.4 and $59 \text{ J K}^{-1} \text{ mol}^{-1}$, respectively.

3.4.6. General discussion

The calorimetry on dinitrogen oxide was carried out from 1.9 K to 184 K. The temperature dependences of the heat capacity,

TABLE 21. COMPARISON OF ENTHALPIES OF FORMATION OF ORIENTATIONAL DEFECTS IN SOME SIMPLE MOLECULAR CRYSTALS.

	N_2O	CO_2	CO	N_2	$\text{C}(\text{CH}_3)_4$
T_b/K	184.74	194.67	81.61	77.32	282.61
T_f/K	182.408		68.15	63.14	256.750
T_t/K			61.57	35.61	140.498
$H_0^\circ/\text{Jmol}^{-1}$	24200	27000	8000	6900	
$\Delta H_{\text{or}}/\text{Jmol}^{-1}$	10800	20000	3000	2000	9700
$\Delta H_{\text{or}}/H_0^\circ$	0.45	0.74	0.38	0.29	
$\Delta H_{\text{or}}/T_f$	59.2	103	44	32	38

vapor pressure and other thermodynamic functions of dinitrogen oxide were obtained and tabulated in Tables 8, 13 and 15. The triple point and heat of fusion were determined as (182.408 ± 0.002) K and (6516 ± 20) J mol⁻¹, respectively. The heat of vaporization was obtained as (16544 ± 20) J mol⁻¹ at 184.181 K and 763 Torr, and the normal boiling point was determined as 184.74 K from the vapor pressure-temperature equation, which was obtained from the vapor pressure data by the method of least squares. The rather large uncertainties of the data are caused by the large corrections for the manometry with the mercury manometer used in the first series of the calorimetry.

The third-law entropy was obtained as 196.8 J K⁻¹mol⁻¹ corrected to the ideal state at the boiling point, and the spectroscopic entropy was calculated as 202.8 J K⁻¹mol⁻¹ by using the recent values of molecular constants. The residual entropy of dinitrogen oxide was determined as (6.0 ± 1.0) J K⁻¹mol⁻¹, which agrees very closely with the value of $R \ln 2 = 5.8$ J K⁻¹mol⁻¹ and suggests the perfect disorder of end-for-end orientation frozen in solid state. Although the uncertainty of the value of the residual entropy is rather large, it may be concluded that dinitrogen oxide does not show the same phenomenon (abnormal value of residual entropy) as for carbon monoxide of which the residual entropy is (3.3 ± 0.8) J K⁻¹mol⁻¹. In the case of carbon monoxide, the discrepancy between the measured residual entropy (3.3 J K⁻¹mol⁻¹) and the expected value ($R \ln 2 = 5.8$ J K⁻¹mol⁻¹)

has not been explained as yet. Such 'abnormal' values of the residual entropies have been found also in some other simple molecular substances; $S_0^\circ = 5.6 \text{ J K}^{-1} \text{ mol}^{-1}$ for POF_3 (the expected value = $R \ln 4 = 11.5 \text{ J K}^{-1} \text{ mol}^{-1}$),⁷⁷⁾ $S_0^\circ = 6.2 \text{ J K}^{-1} \text{ mol}^{-1}$ for SO_2F_2 (the expected value = $R \ln 6 = 14.9 \text{ J K}^{-1} \text{ mol}^{-1}$)⁷⁸⁾ and $S_0^\circ = 10.1 \text{ J K}^{-1} \text{ mol}^{-1}$ for ClO_3F (the expected value = $R \ln 4 = 11.5 \text{ J K}^{-1} \text{ mol}^{-1}$),¹⁾ etc. In these cases, however, the calorimetric measurements, which were less precise, have been carried out only above about 15 K. Therefore, it seems desirable that more precise data of thermodynamic properties are obtained down to lower temperature region for these substances.

The molecular motion in solid dinitrogen oxide is analyzed successfully in the harmonic approximation. The translational zero point energy obtained from the analysis of the contribution of lattice modes of the heat capacity in the lowest temperature region is 1338 J mol^{-1} , which compares favorably with the value of 1699 J mol^{-1} derived from the difference between the heat of sublimation at 0 K (24214 J mol^{-1}) and the pseudo-static lattice energy (25913 J mol^{-1}) obtained from the analysis of vapor pressure of solid dinitrogen oxide in the higher temperature region. The temperature dependence of the Debye characteristic temperatures derived from the measured heat capacity values also implies the characteristics of the vibrations of lattice modes. In general, the anharmonicity of the lattice vibrations causes the Debye characteristic temperature to drop down rapidly in the higher

temperature region. The rather little temperature dependence of the Debye characteristic temperatures corresponding to the measured heat capacity values of dinitrogen oxide maintained in the higher temperature region (given partly in Figure 22) shows also this situation of good approximation of the harmonic analyses.

The discrepancy of about 361 J mol^{-1} between these two values of translational zero point energies may be mainly due to the rather uncertain value of the pseudo-static lattice energy determined by the analysis of vapor pressure in the higher temperature region in the harmonic approximation, where the anharmonicity of vibrations is probably significant. On the other hand, however, the uncertainty of the value of translational zero point energy obtained from the analysis of the lattice modes in the lowest temperature region principally come from two causes. One is the approximate estimation of librational contribution calculated from the frequencies of 70 cm^{-1} (E), 83 cm^{-1} (T) and 126 cm^{-1} (T) for 2N degrees of freedom, of which the uncertainty can not be estimated because their dispersion relations are not known. Another cause is the assumption that the same method as for monatomic crystals may be applied to the analysis of the contribution of translational lattice heat capacity thus separated. As described in Section 3.4.2., the lattice frequencies of $k = 0$ in the crystal of dinitrogen oxide can not be explained by the point model and the atom-atom interactions should be taken into account, whereas the point model is applied successfully to the

smaller molecules α -CO and α -N₂. The uncertainty coming from this cause also can not be estimated. Therefore the value of the translational zero point energy may be adopted as (1500 ± 200) J mol⁻¹. The librational zero point energy of 1150 J mol⁻¹ calculated from the frequencies of 70 cm⁻¹ (E), 83 cm⁻¹ (T) and 126 cm⁻¹ (T) for 2N degrees of freedom is rather good approximate value, because the librational contribution to the zero point energy obtained from simple summation of the frequency distribution is dependent only on the average frequencies.

The zero point properties of a series of simple molecular crystals (N₂O, CO₂, CO and N₂) tabulated in Table 20 show good internal consistency. The Debye characteristic temperatures, heats of sublimation at 0 K and zero point energies show the same tendency as for the melting temperatures given in Table 21. These substances have also similar aspects as given in Tables 17 and 18. Therefore the comparative study of these substances are very interesting. For CO₂,¹⁷⁾ N₂,^{11),12)} and CO,^{9),10),11)} however, no complete data of heat capacity and related thermodynamic properties in the entire temperature region other than the data of W.F.Giauque, et al.¹⁾ have been available. For example, therefore, the heats of sublimation at 0 K for these substances can not be estimated precisely.

The lattice modes of solid dinitrogen oxide was analyzed by the moment trace method, which is a most convenient one for obtaining the thermodynamic quantities, and the $v_D(n)$ function gives

the relation of the moments of the frequency spectrum from which the feature of the frequency spectrum may be suggested. The graph of Figure 26 shows a shallow minimum. This minimum corresponds to the shallow minimum in the graph of the Debye characteristic temperatures given in Figure 23. The minima suggest a hump deviating from the frequency spectrum $g(\nu)$ expected by the Debye model. The features of $\nu_D(n)$ for CO_2 , N_2 and CO , which have not been obtained, can not be calculated from the previous data^{1),9),10),11),12),17)} because of their insufficient precision. However, the shallow well feature may be very common in the case of simple molecular crystals because of the weak intermolecular forces such as van der Waals force. In the cases of ionic crystals and covalent bonded crystals, deeper and sharper minima have been found, which correspond to the sharp peaks in the frequency spectra.

It seems very likely that the anomalous increases of heat capacities of molecular crystals below their thermodynamic first order phase transitions are not only caused by the impurity effect, but also due to the intrinsic characteristics of the substances; such as thermal creation of lattice defects. As shown in Table 21, the values of $\Delta H_{\text{or}}/H_0^0$ and $\Delta H_{\text{or}}/T_f$ may be convenient parameters. In the case of the substances which have rotational solid phase transitions, $\Delta H_{\text{or}}/H_0^0$ and $\Delta H_{\text{or}}/T_f$ are smaller than the values of about 0.4 and $59 \text{ J K}^{-1} \text{ mol}^{-1}$, respectively. These values for CO , N_2 and $\text{C}(\text{CH}_3)_4$ show the same tendency as their

temperatures of the rotational phase transitions. In the case of N_2O , the values of $\Delta H_{\text{or}}/H_0^\circ$ and $\Delta H_{\text{or}}/T_f$ are 0.45 and $59.2 \text{ J K}^{-1} \text{ mol}^{-1}$, which are very close to the values for carbon monoxide. Therefore, it seems that the rotational phase transition of dinitrogen oxide may exist just above the melting point. In the case of carbon dioxide, the rotational phase transition may exist at more or less higher temperature than for dinitrogen oxide.

Chapter 4

The heat capacity, vapor pressure and related thermodynamic properties of tetramethylstannane

4.1. Introduction

4.2. Experimental

4.2.1. Material

4.2.2. Calorimetry

4.2.3. Vapor pressure measurement

4.2.4. Raman spectra

4.3. Results

4.3.1. Heat capacity

4.3.2. Fusion

4.3.3. Vapor pressure and heat of vaporization

4.3.4. Thermodynamic functions

4.3.5. Raman spectra

4.4. Analysis and discussion

4.4.1. The third-law entropy and internal rotation of methyl groups

4.4.2. Zero point properties

4.4.3. Premelting

Chapter 4

The heat capacity, vapor pressure and related thermodynamic properties of tetramethylstannane

4.1. Introduction

The simple molecular crystals are grouped into two classes according to their molecular structure; (a) rod-like molecules, (b) spherical molecules. Dinitrogen oxide belongs to the first group. A molecule of the tetrahedral type MX_4 is the simplest in the second group. The molecules of the type $M(CH_3)_4$, where $M = C, Si, Ge$ and Sn , also belong to the simplest type in the second group, and have another degree of internal freedom; the internal rotation of the methyl groups. The heat capacities and related thermodynamic properties of $C(CH_3)_4$ and $Si(CH_3)_4$ were measured by J.G.Aston, et al.⁵¹⁾ in 1936 and 1941, respectively, and recently T.Shinoda, et al.^{50),52)} reported the more precise data of both of them but in the limited temperature regions; 4.1 - 20 K and 62 - 260 K for $C(CH_3)_4$, and 2.2 - 26 K and 106 - 177 K for $Si(CH_3)_4$. From their data, the barriers to reorientation of the methyl groups have been determined as $4300 \text{ cal mol}^{-1}$ and $1300 \text{ cal mol}^{-1}$ for $C(CH_3)_4$ and $Si(CH_3)_4$, respectively. In the case of $C(CH_3)_4$, the value of the barrier is compared favorably with those of the series $C(CH_3)_n H_{4-n}$; 2930,⁵³⁾ 3575,⁵⁴⁾ 3900⁵⁵⁾ and 4300⁵⁶⁾ cal mol^{-1} for ethane, propane, isobutane and

neopentane, respectively, obtained by the microwave techniques. As the number of methyl groups increases the barrier increases, which is explained as the intramolecular interaction of methyl groups with one another. In the case of $\text{Si}(\text{CH}_3)_n\text{H}_{4-n}$, however, the potential barriers in methylsilane,⁵⁷⁾ dimethylsilane,⁵⁸⁾ trimethylsilane⁵⁹⁾ and tetramethylsilane⁵⁶⁾ have been determined as 1670, 1647, 1830 and 2000 cal mol⁻¹ from the microwave spectra. In this case, although the value of 1300 cal mol⁻¹ for tetramethylsilane determined by J.G.Aston, et al.⁵¹⁾ is rather less precise, it seems that the number of methyl groups exerts less influence on the barrier height than for $\text{C}(\text{CH}_3)_n\text{H}_{4-n}$, because of the longer Si - C bond. More recently, A.J.Valerga and J.E. Kilpatrick⁶⁰⁾ measured the heat capacity and related thermodynamic properties of $\text{Ge}(\text{CH}_3)_4$, and obtained the barrier height of 750 cal mol⁻¹. The barrier heights for methylgermane,⁶¹⁾ dimethylgermane⁶²⁾ and tetramethylgermane⁵⁶⁾ have been obtained as 1240, 1180 and 1300 cal mol⁻¹, respectively, from the microwave spectra. In this case, also the value of 750 cal mol⁻¹ for tetramethylgermane derived from the thermodynamic measurements is smaller than the value derived from the microwave techniques. It seems that there is no relation between the number of methyl groups and the barrier height.

On the other hand, the crystal of $\text{C}(\text{CH}_3)_4$ has a phase transition below its melting point, and the crystal of $\text{Si}(\text{CH}_3)_4$ has no phase transition but has two metastable forms.⁶³⁾ Neither

phase transition nor metastable polymorphs have been found in the crystals of $\text{Ge}(\text{CH}_3)_4$ and $\text{Sn}(\text{CH}_3)_4$.⁶⁴⁾ In the cases of $\text{C}(\text{CH}_3)_4$ and $\text{Si}(\text{CH}_3)_4$, T. Shinoda, et al. analyzed the premelting phenomena and obtained the enthalpies of formation of lattice vacancies as $3240 \text{ cal mol}^{-1}$ and 28 kcal mol^{-1} , respectively. In the case of the metastable form of $\text{Si}(\text{CH}_3)_4$, they found two values of 30 and 47 kcal mol^{-1} . They considered that the values for $\text{Si}(\text{CH}_3)_4$ were extremely large than the value of the enthalpy of formation of lattice vacancies for $\text{C}(\text{CH}_3)_4$, which might be due to simultaneous positional and orientational transitions at melting point. The heat capacity data by A.J. Valerga and J.E. Kilpatrick are rather less precise and can not be analyzed in detail.

Tetra methylstannane is a molecule of interest for extending such studies described above. In this chapter, the measurements of heat capacity and related thermodynamic properties of tetra-methylstannane are described, and analyzed in detail.

4.2. Experimental

4.2.1. Material

Commercial reagent grade tetramethylstannane purchased from Nakarai Chemicals, Ltd. contained a few percent of impurities such as methyl iodide, and was purified by fractional distillation several times. The resultant purity, which was monitored by gas-chromatography, was higher than 99.9 mol per cent. It was then deaerated in vacuum by a freeze-and-thaw technique and re-purified by distillation in vacuum and ^atransferred directly into the calorimeter vessel α , which is similar to the method described in the earlier paper of carbon tetrachloride.²²⁾ The final purity was higher than 99.9 mol per cent determined by the gas-chromatographic analysis. The fractional melting method in the calorimetry gave the rather approximate value of purity of about 99.85 mol per cent, because the crystal of tetramethyl stannane showed an abnormally large premelting phenomenon, which is described in the following section. The 60 MHz NMR spectrum of the sample of tetramethylstannane showed the existence of a trace of water (less than about 0.05 mol per cent). The purity of the sample of tetramethylstannane used in the calorimetry may be higher than 99.85 mol per cent. The examination of the purity of the sample after the measurements indicated that no contamination had occurred during the experiment.

The tetramethylstannane in the calorimeter had a mass of 43.182 g (0.24147 mol).

4.2.2. Calorimetry

The boiling point of tetramethylstannane is 78°C ,⁶⁵⁾ and therefore the specimen can be treated easily in condensed phase (liquid) at room temperature and the heat capacity was measured by using the solid calorimeter constructed by Minoru Nakamura⁶⁶⁾ as described in the earlier paper,²²⁾ because it gave more precise data than the condensed gas calorimeter which needed several kinds of corrections. The system for measurements was the same as that for dinitrogen oxide. The vapor pressure measurement was made by using the condensed gas calorimeter, which will be described in the next section.

The gold calorimeter vessel α (internal volume = 47.65 cm^3 at 14°C) was used, which was equipped with the platinum resistance thermometer α and the germanium resistance thermometer β , which were of the same type as those of the condensed gas calorimeter. The temperature scale of the germanium resistance thermometer β was determined by the comparison with the germanium resistance thermometer γ in the temperature~~x~~ region from 1.7 K to 15 K, which is summarized in Table 22. The temperature scale of the platinum resistance thermometer α was determined by Minoru Nakamura⁶⁶⁾ on the IPTS-48 for the temperature region from 90 K to 45°C and on the NBS-55 temperature scale for the temperature region from 11 K to 90 K. Because the difference between the IPTS-68 and IPTS-48 (and NBS-55) is negligibly small for calculating the heat capacity, the temperature scale of the platinum resistance thermometer α

TABLE 22.a) THE CALIBRATION POINTS FOR THE GERMANIUM RESISTANCE THERMOMETER β .

T	R	T	R
K	Ω	K	Ω
1.79076	6449.454	6.77193	329.188
1.8965	5577.158	7.05550	298.981
2.16427	4017.172	7.46814	261.996
2.25125	3648.435	8.16630	212.437
2.41241	3108.526	8.99824	169.459
2.55975	2704.858	9.65017	144.000
2.84193	2151.294	9.94215	135.032
3.35994	1507.045	10.12307	129.677
3.79032	1168.237	10.96859	109.064
4.07869	1003.370	11.56410	97.681
4.16789	955.297	11.73769	94.722
4.21011	938.852	12.73857	80.556
4.43446	840.936	13.66156	70.397
4.60515	773.940	14.66193	61.700
5.31238	567.942	15.01161	59.156
6.02028	430.642		

b) THE CALIBRATION FORMULA~~X~~ FOR THE GERMANIUM RESISTANCE THERMOMETER β BETWEEN 1.7 K AND 15 K.

$$\log_{10}(R/\Omega) = \sum_{i=1}^{10} A_i T^{i-4}$$

$$A_1 = -11.4030435969$$

$$A_2 = 22.3998407504$$

$$A_3 = -16.6095584460$$

$$A_4 = 11.2519494473$$

$$A_5 = -2.3223689174$$

$$A_6 = 0.3736948964$$

$$A_7 = -0.0404475737$$

$$A_8 = 0.0027027561$$

$$A_9 = -0.0000992990$$

$$A_{10} = 0.0000015254$$

$$\sum_{i=1}^{31} (\log_{10} R_i(\text{calc.}) - \log_{10} R_i(\text{obs.}))^2 = 0.00000477$$

was not converted to the IPTS-68.

The calorimeter did~~n~~ot contain any helium gas for heat exchange. The corrections for vaporization caused by the vapor pressure increase during heat input were estimated approximately from the data of vapor pressure, heat of vaporization, density of liquid tetramethylstannane and the volume of the calorimeter vessel, which were negligibly small. The correction of ($C_s - C_p$) was also neglected. The sample contributed about 80 per cent at 5 K, 70 percent at 30 K, 60 per cent at 100 K, and 70 per cent at 250 K of the total heat capacity.

4.2.3. Vapor pressure measurement

The vapor pressure and heat of vaporization of tetramethylstannane were measured by using the condensed gas calorimeter. After the heat capacity measurement, the sample of tetramethylstannane was re-distilled in the system of the condensed gas calorimeter and transfer~~r~~ed into the calorimeter vessel by the same method as for dinitrogen oxide. In this case, therefore, the temperature scale was on the IPTS-68.

The vapor pressure of tetramethylstannane was measured with the quartz Bourdon gauge in the temperature region from 222 K to 280 K. The heats of vaporization were measured at 276.56 K and at 278.37 K by the same method as for dinitrogen oxide, but the amount of tetramethylstannane evaporated from the calorimeter vessel was determined by measuring the weight of the sample,

which was condensed in a small pyrex glass tube connected to the system shown in Figure 6 and fused off from the system.

4.2.4. Raman spectra

After the vapor pressure measurement, the sample of tetramethylstannane was deaerated and distilled in the system of the vacuum line, and the center portion was taken in a small thin-wall glass tube (2 mm in outer diameter, 40 mm in length), and then it was fused off from the system by using liquid nitrogen as the refrigerant.

Raman spectra of liquid and solid tetramethylstannane (at room temperature, at 158 K and at 95 K) were obtained with the laser excitation of argon ion; 514.5 nm. The Laser Raman Spectrophotometer Model R750 of Japan Spectroscopic Co., Ltd. was used.

4.3. Results

4.3.1. Heat capacity

The heat capacity of solid and liquid tetramethylstannane was measured in the temperature region from 3.8 K to 299 K. The measured values of heat capacity without curvature corrections are tabulated in Table 23. The data are shown graphically in Figure 29. The scatter of the measured points of heat capacity is at most 0.5 per cent at 15 K and 0.1 per cent above 25 K. The smooth values at rounded temperatures are given in Table 24, together with the deviations derived from the comparison with the values obtained by L.A.K.Staveley, et al.⁶⁴⁾ In spite of the less precise measurements by L.A.K.Staveley, et al., the data of the smoothed values of heat capacity show rather good agreement.

4.3.2. Fusion

The solid tetramethylstannane shows anomalous increase of heat capacity below its melting point and the heat of fusion can not be determined in the usual manner illustrated schematically in Figure 14; An approximate value of about 7750 J mol^{-1} was obtained in this method. Taking account of the enthalpy of premelting due to impurity⁶⁷⁾ assumed as 0.15 mol per cent, the heat of fusion of tetramethylstannane was obtained as 8030 J mol^{-1} . On the other hand, including the total enthalpy of premelting below the triple point, the enthalpy of fusion was 9240 J mol^{-1} ,

TABLE 23. Measured heat capacity values of
tetramethylstannane.

1 mol $\text{Sn}(\text{CH}_3)_4 = 178.8288\text{g}$, $0^\circ\text{C} = 273.15\text{ K}$

$\frac{T}{\text{K}}$	$\frac{C_p}{\text{JK}^{-1}\text{mol}^{-1}}$	$\frac{T}{\text{K}}$	$\frac{C_p}{\text{JK}^{-1}\text{mol}^{-1}}$
(Run 1)		(Run 4)	
182.137	137.37	221.638	179.19
184.541	138.53	248.245	184.44
186.940	139.64	251.639	185.78
189.384	141.12	255.014	186.63
191.860	142.53	258.376	187.21
194.315	143.97	261.726	187.89
196.747	145.71	265.064	188.60
199.226	147.21	268.392	189.77
201.738	150.31	271.693	190.52
204.251	153.67	274.980	191.29
206.784	159.39	278.250	192.06
(Run 2)		281.507	193.39
209.347	169.61	284.744	193.87
211.810	191.25	(Run 5)	
213.965	246.97	11.712	8.061
215.580	418.74	12.325	9.168
216.552	877.57	12.989	10.102
(fusion)		13.679	11.238
221.360	179.14	14.377	12.382
(Run 3)		15.100	13.527
220.224	179.19	15.942	14.924

TABLE 23.(continued)

$\frac{T}{K}$	$\frac{C_p}{JK^{-1}mol^{-1}}$	$\frac{T}{K}$	$\frac{C_p}{JK^{-1}mol^{-1}}$
16.874	16.491	33.079	43.86
17.784	17.960	35.176	47.33
18.682	19.417	37.181	50.53
19.579	20.987	39.119	53.57
(Run 6)		41.008	56.40
11.632	7.983	42.975	59.22
12.297	9.057	45.000	62.16
13.029	10.148	46.956	64.86
13.779	11.420	48.862	67.36
14.541	12.685	50.728	69.71
15.419	14.113	52.561	71.81
16.384	15.692	54.370	73.88
17.319	17.243	(Run 8)	
18.238	18.674	51.253	70.48
19.151	20.256	53.067	72.51
20.067	21.726	54.859	74.49
20.997	23.306	56.633	76.41
21.944	24.950	58.394	78.27
(Run 7)		60.268	80.17
21.585	24.377	62.254	82.09
22.731	26.278	64.231	83.93
23.916	28.309	66.204	85.60
25.118	30.427	68.176	87.11
26.353	32.48	70.151	88.53
27.668	34.69	72.136	89.93
29.082	37.09	74.254	91.39
30.910	40.18	76.505	92.92

TABLE 23.(continued)

$\frac{T}{K}$	$\frac{C_p}{JK^{-1}mol^{-1}}$	$\frac{T}{K}$	$\frac{C_p}{JK^{-1}mol^{-1}}$
78.765	94.49	107.679	108.16
81.035	95.94	110.147	109.12
83.324	97.39	112.621	110.09
85.630	98.73	115.103	111.08
87.930	100.02	117.593	111.95
90.228	101.09	120.078	112.94
92.553	102.19	122.556	113.84
94.907	103.19	125.049	114.49
97.262	104.17	126.956	115.48
99.626	105.06	(Run 11)	
(Run 9)		126.769	115.32
3.898	0.295	129.390	116.25
4.380	0.454	132.111	117.24
4.884	0.668	134.843	118.33
5.393	0.937	137.494	119.63
5.966	1.302	140.158	120.34
6.645	1.829	142.838	121.42
7.325	2.452	145.533	122.40
7.926	3.074	148.244	123.43
8.502	3.733	150.969	124.47
9.074	4.433	153.709	125.47
9.660	5.184	156.467	126.66
(Run 10)		159.242	127.75
97.967	104.24	162.034	128.91
100.365	105.19	164.842	129.87
102.795	106.16	167.668	130.97
105.232	107.20	170.502	131.82
		173.310	133.47

TABLE 23.(continued)

$\frac{T}{K}$	$\frac{C_p}{JK^{-1}mol^{-1}}$	$\frac{T}{K}$	$\frac{C_p}{JK^{-1}mol^{-1}}$
(Run 12)			
173.000	133.10	233.045	181.15
175.167	134.24	236.093	182.05
177.524	135.20	239.128	182.81
180.149	136.63	242.146	183.58
182.919	137.58	245.153	184.03
185.751	138.90	248.151	184.53
188.590	140.49	251.438	185.41
191.453	142.13	255.154	186.36
194.319	143.84	259.003	187.24
197.145	145.93	262.832	188.12
(Run 13)		266.790	189.21
191.756	142.00	270.880	190.04
195.005	144.06	274.949	191.10
198.212	146.57	278.998	192.13
201.374	149.57	283.028	193.16
204.528	154.08	287.034	194.33
207.647	161.64	291.007	195.73
210.621	176.71	294.966	195.71
213.294	218.87	298.930	197.37
215.311	366.25	(Run 15)	
(fusion)		205.316	155.45
220.815	178.89	207.649	161.17
233.744	179.77	209.902	171.03
(Run 14)		212.018	191.99
227.048	179.91	213.889	242.15
230.030	180.69	215.348	372.93

TABLE 23. (continued)

$\frac{T}{K}$	$\frac{C_p}{JK^{-1}mol^{-1}}$	$\frac{T}{K}$	$\frac{C_p}{JK^{-1}mol^{-1}}$
216.312	690.03		
(fusion)			
220.668	178.74		

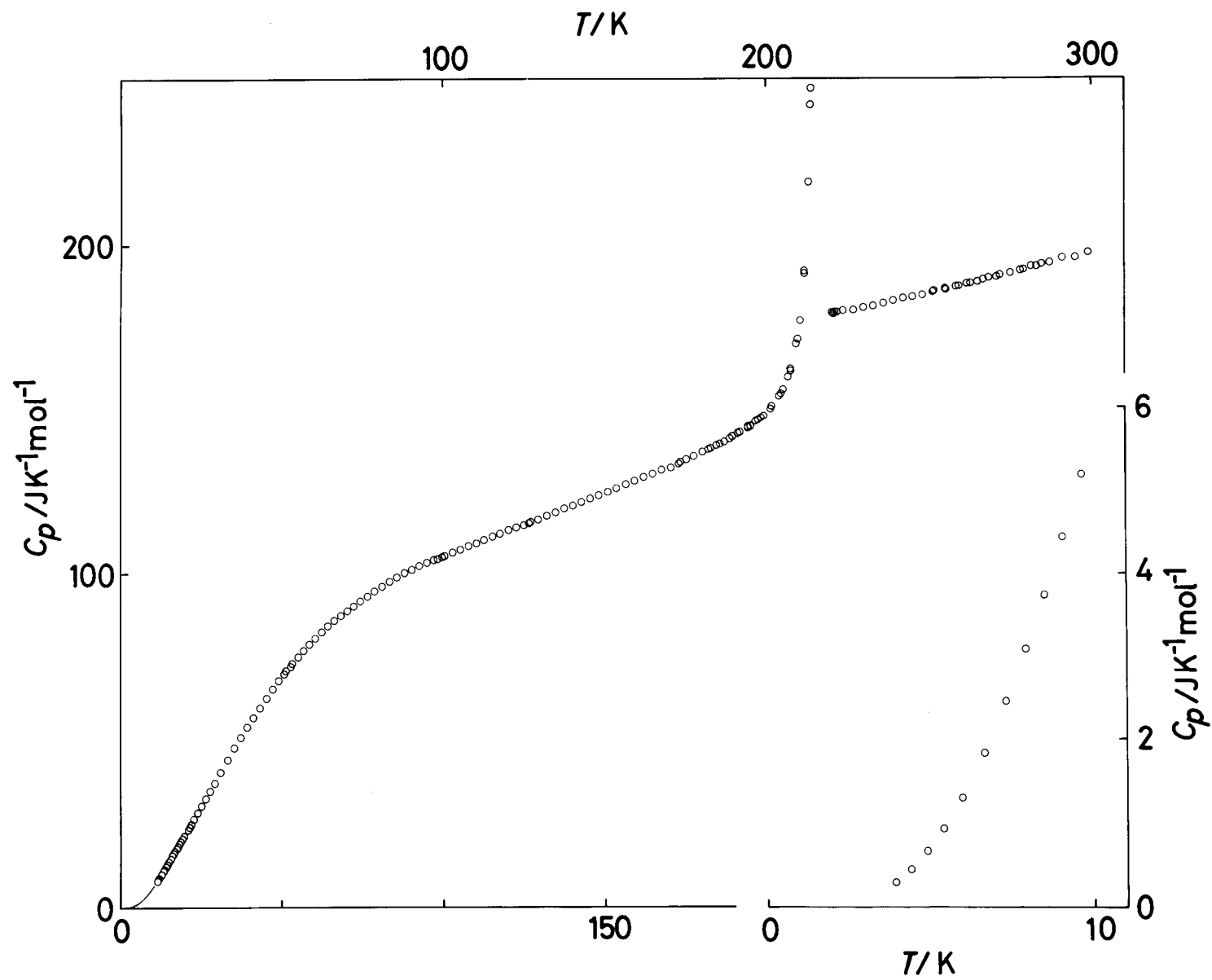


FIGURE 29. HEAT CAPACITY OF TETRAMETHYLSTANNANE.

TABLE 24. Smoothed values of heat capacity of tetramethylstannane.

1 mol $\text{Sn}(\text{CH}_3)_4$ = 178.8288 g,
 0°C = 273.15 K

T K	C_p^o $\text{JK}^{-1}\text{mol}^{-1}$	Deviation* %
(Solid)		
5	0.723	
10	5.647	
15	13.40	
20	21.61	
30	38.64	
40	54.90	
50	68.82	
60	79.92	
70	88.44	
80	95.22	
90	100.99	
100	105.13	+ 0.7
110	109.09	- 0.1
120	112.85	- 0.5
130	116.55	- 0.4
140	120.30	+ 0.2
150	124.10	+ 1.3

$$* \text{ Deviation} = \left[C_p(\text{Staveley, et al.}) - C_p(\text{This}) \right] \\ \times \frac{100}{C_p(\text{This})}$$

TABLE 24 (continued)

<u>T</u>	<u>C_p^o</u>	<u>Deviation*</u>
K	JK ⁻¹ mol ⁻¹	%
160	128.00	+ 1.3
170	132.01	+ 0.5
180	136.33	- 1.5
190	141.27	
200	148.28	
210	171.80	
(Liquid)		
220	178.80	+ 2.3
230	180.71	+ 2.3
240	182.81	
250	185.10	
260	187.50	
270	190.00	
280	192.45	
290	194.93	
300	197.43	

which compares favorably with the value 9439 J mol^{-1} obtained by L.A.K.Staveley, et al.⁶⁴⁾ in the temperature interval from about 190 K to about 223 K. The value of $(9240 \pm 50) \text{ J mol}^{-1}$ was adopted as the enthalpy of fusion of tetramethylstannane.

The triple point of pure tetramethylstannane was determined as $(218.13 \pm 0.08) \text{ K}$ from the fractional melting curve assuming the melting~~x~~ region from 217.20 K to 218.03 K, which is shown in Figure 30. The triple point of the tetramethylstannane used in this calorimetry which was given as the value at $1/f = 1$ in Figure 30 was 218.03 K. The amount of impurity was estimated as 0.15 mol per cent from this curve. L.A.K.Staveley, et al.⁶⁴⁾ obtained the triple point of pure tetramethylstannane as 218.18 K from their measurements of the sample containing the impurity of about 0.26 mol percent. The data of the fusion of tetramethylstannane are summarized in Table 25.

4.3.3. Vapor pressure and heat of vaporization

The vapor pressure of the liquid tetramethylstannane of higher purity was measured in the system of the condensed gas calorimeter on the IPTS-68. The measured values of vapor pressure are tabulated in Table 26, together with the deviations from the empirical equation:

$$\log (P/\text{dyne cm}^{-2}) = -2304.27/T + 15.02058 - 0.00715727 \quad , (43)$$

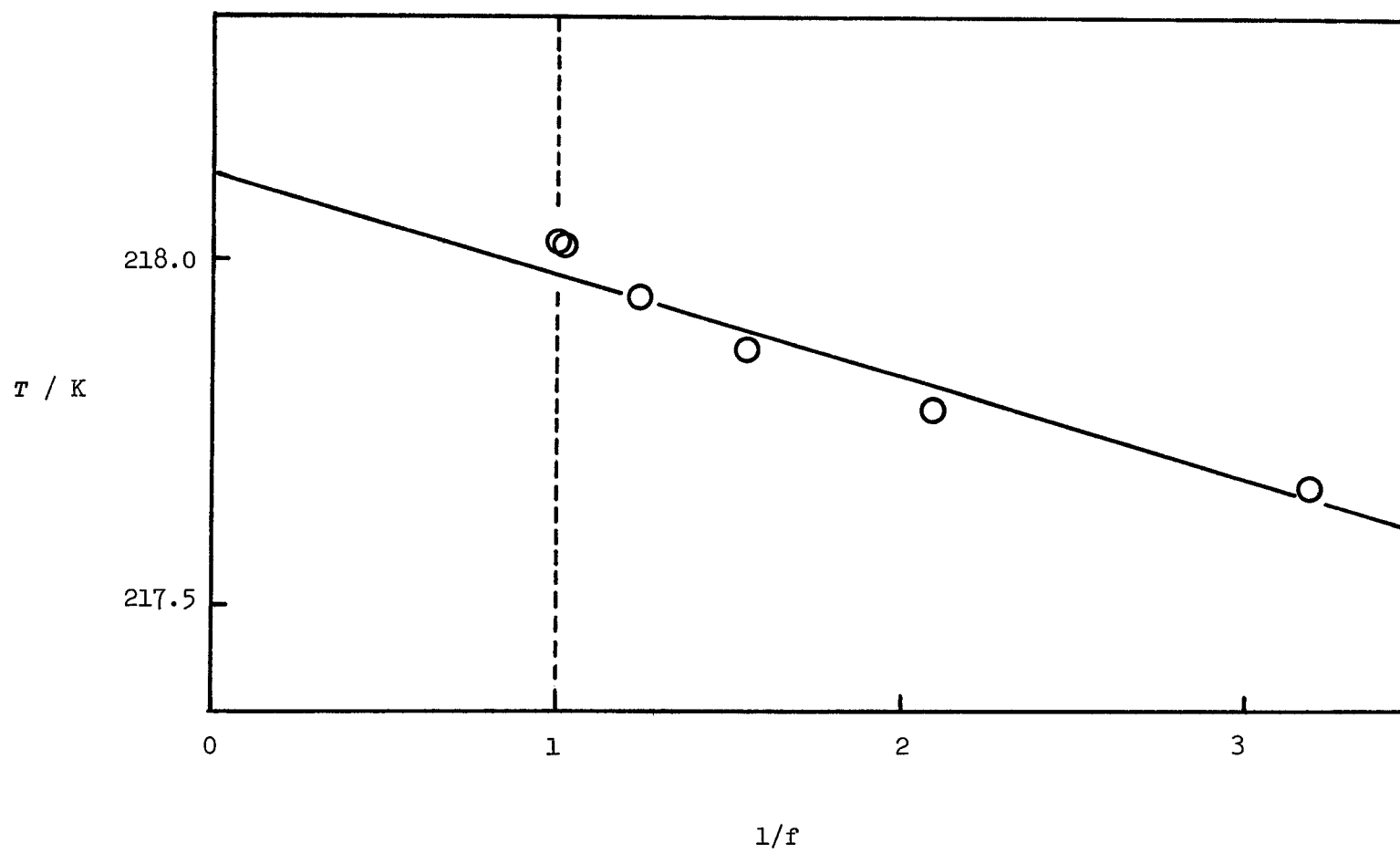


FIGURE 30. MELTING CURVE OF TETRAMETHYLSTANNANE.

TABLE 25. FUSION OF TETRAMETHYLSTANNANE.

a). THE HEAT OF FUSION OF TETRAMETHYLSTANNANE

TEMPERATURE INTERVAL:	216.0942 K — 219.3467 K
HEAT INPUT:	2171.69 J
$\int C_{p(\text{normal})} dT$:	129.63 J
$\int C_{p(\text{impurity})} dT$:	82.34 J
$\int C_{p(\text{anomaly})} dT$:	170.96 J
<hr/>	
(0 K — 216.0942 K)	
$\int C_{p(\text{impurity})} dT$:	67.37 J
$\int C_{p(\text{anomaly})} dT$:	121.46 J
<hr/>	
$\Delta H_f = 9240 \pm 50 \text{ J mol}^{-1}$	

L.A.K.Staveley, et al. (1954)

$$\Delta H_f = 9439 \text{ J mol}^{-1}$$

b). THE TRIPLE POINT OF TETRAMETHYLSTANNANE

Fraction melted	T
	K
0.158	217.478
0.320	217.669
0.484	217.781
0.648	217.867
0.813	217.947
0.979	218.0135
(1.000)	218.03

The triple point of tetramethylstannane = $218.13 \pm 0.08 \text{ K}$

L.A.K.Staveley, et al. (1954)

$$T_f = 218.18 \text{ K}$$

TABLE 26. VAPOR PRESSURE OF TETRAMETHYLSTANNANE.

T	P	Deviation
K	dyne cm ⁻²	$\log_{10}(P_{\text{Obs.}} - P_{\text{smoothed}})$
222.7610	1200	
228.8204	2080	
236.3669	3746	0.00650
244.9026	7160	0.00391
254.2553	13773	-0.00105
264.2397	25759	-0.00197
275.0765	47477	-0.00155
225.5356	1573	
232.5503	2840	-0.00585
239.5669	4880	-0.00086
246.8728	8333	-0.00100
254.6274	14079	-0.00003
262.2351	22732	-0.00000
269.4025	34585	0.00023
274.5631	46144	-0.00117
274.6816	46464	-0.00140
274.7604	46598	-0.00080
276.6466	51544	-0.00094
276.4663	50744	0.00171
278.4234	56344	0.00083
278.3138	55864	0.00207
280.3553	62157	0.00139

which was determined by the method of least squares. The data are shown graphically in Figure 31, which shows good agreement with the previous data in the higher temperature region above 0 °C obtained by R.H.Bullard and A.C.Hausmann.⁶⁵⁾ The smoothed values of vapor pressure at rounded temperatures derived from the equation (43) are given in Table 27.

The heat of vaporization of tetramethylstannane also was measured in the system of the condensed gas calorimeter, on the IPTS-68, and in the same manner as for dinitrogen oxide. The measurements of heat of vaporization are summarized in Table 28. The value of the heat of vaporization of tetramethylstannane is $(3.416 \pm 0.014) \times 10^4 \text{ J mol}^{-1}$ at 277.46 K and at 40.27 Torr. The approximate value of heat of vaporization calculated by the Clapeyron-Clausius equation was about 5 per cent smaller than this value obtained by direct measurements.

4.3.4. Thermodynamic functions

Thermodynamic functions of tetramethylstannane were obtained from the data described above, being tabulated in Table 29, where S_0° and H_0° denote the residual entropy and the heat of sublimation at 0 K, respectively. The contribution of the heat capacity below the lowest temperature measured (3.8 K) was estimated by a method of smooth extrapolation.

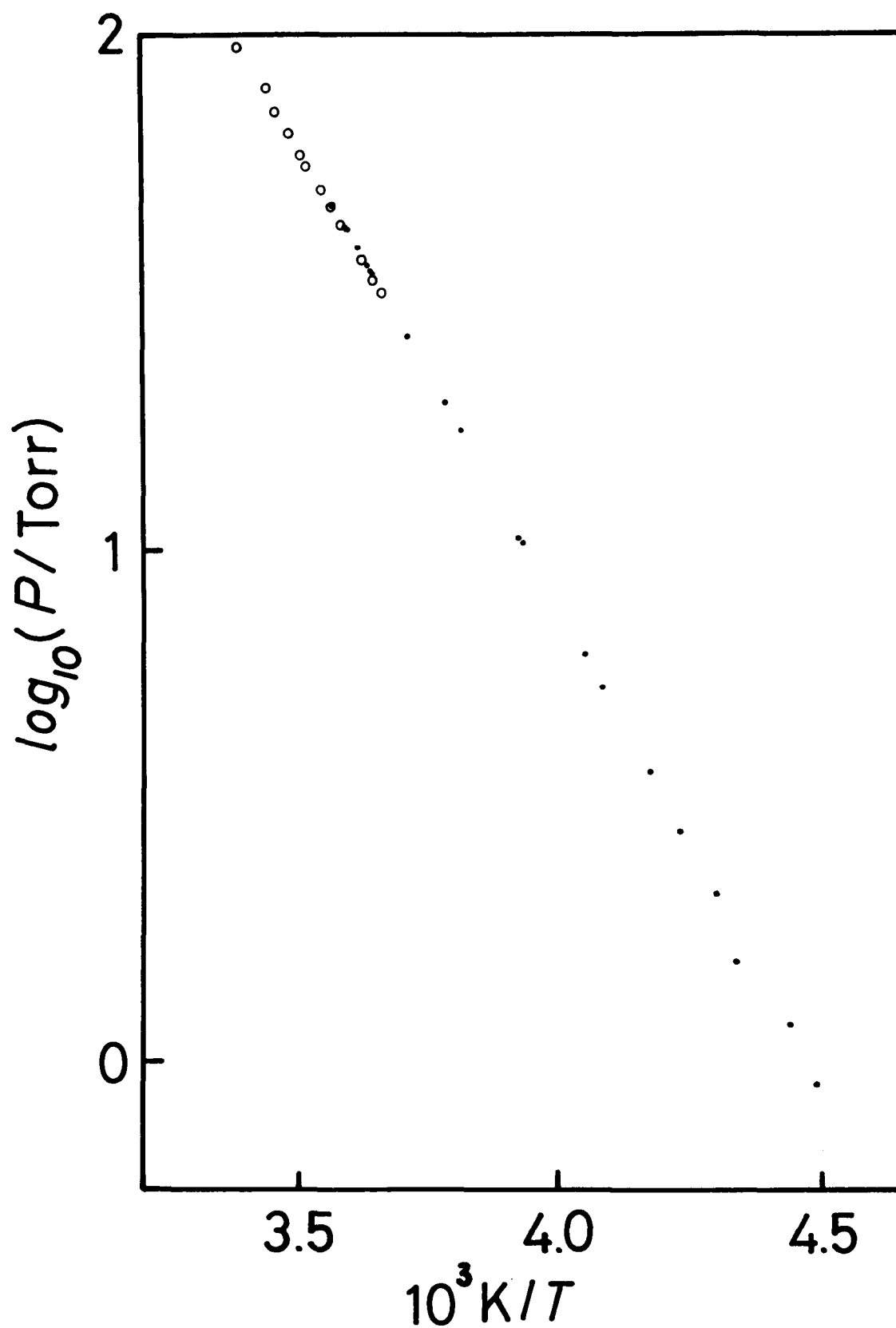


FIGURE 31. VAPOR PRESSURE OF TETRAMETHYLSTANNANE.
●, THIS RESEARCH; ○, R.H.BULLARD AND A.C.HAUSSMANN.⁽⁶⁵⁾

TABLE 27. Smoothed values of vapor pressure of tetramethylstannane at rounded temperatures.

$$\log(P/\text{dyne cm}^{-2}) = -230.427/T + 15.02058 - 0.00715727T$$

$\frac{T}{K}$	$\frac{P}{\text{dyne cm}^{-2}}$	$\frac{T}{K}$	$\frac{P}{\text{dyne cm}^{-2}}$
230	2269	260	19820
235	3413	265	26824
240	5031	270	35790
245	7275	275	47114
250	10332	280	61234
255	14425		

TABLE 28. The heat of vaporization of tetramethylstannane.

Starting point (T/K, P/dyne cm ⁻²)	Final point (T/K, P/dyne cm ⁻²)	Heat Input (ΔE/J)	Amount of Evaporated Sn(CH ₃) ₄ (Δn/mol)
i) T_1 276.6466	T_2 276.4657		
P_1 38.66	P_2 38.05	212.949	0.0062054
ii) T_1 278.4234	T_2 278.3133		
P_1 42.25	P_2 41.89	210.549	0.0061908

$$\text{Average } \Delta H_V = (3.416 \pm 0.014) \times 10^4 \text{ J mol}^{-1} \\ \text{at } 277.46 \text{ K} \\ 40.27 \text{ Torr}$$

TABLE 29. THERMODYNAMIC FUNCTIONS OF TETRAMETHYLSTANNANE.

T	$(H^\circ - H_0^\circ)$	$(S^\circ - S_0^\circ)$	$(H^\circ - H_0^\circ)/T$	$-(G^\circ - H_0^\circ)/T$
K	J mol ⁻¹	J K ⁻¹ mol ⁻¹	J K ⁻¹ mol ⁻¹	J K ⁻¹ mol ⁻¹
10	15	2.0	1.5	0.5
20	150	10.8	7.5	3.3
30	451	22.7	15.0	7.7
40	920	36.1	23.0	13.1
50	1540	50.0	30.8	19.2
60	2286	63.4	38.1	25.3
70	3131	76.4	44.7	31.7
80	4050	88.6	50.6	38.0
90	5032	100.2	55.9	44.3
100	6063	111.1	60.6	50.5
110	7134	121.3	64.9	56.4
120	8244	130.9	68.7	62.2
130	9391	140.1	72.2	67.9
140	10575	148.8	75.5	73.3
150	11797	157.3	78.6	78.7
160	13058	165.4	81.6	83.8
170	14355	173.3	84.4	88.9
180	15699	180.9	87.2	93.7
190	17086	188.3	89.9	98.4
200	18529	195.7	92.6	103.1
210	20096	203.2	95.7	107.5
218.03	30378	250.5	139.3	111.2
220	30723	252.1	139.6	112.5
230	32528	260.1	141.4	118.7
240	34333	267.8	143.0	124.8
250	36185	275.3	144.7	130.6
260	38048	282.6	146.3	136.3
270	39936	289.7	147.9	141.8
280	41846	296.7	149.4	147.3
290	43775	303.4	150.9	152.5

4.3.5. Raman spectra

The Raman spectra obtained on liquid and solid tetramethylstannane (at room temperature, at 158 K and at 95 K) are shown in Figure 32. The assignments which are given in Table 30 are those of E.R.Lipincott and M.C.Tobin,⁶⁸⁾ and these values of frequencies were used for evaluating the intramolecular contribution to the thermodynamic quantities. However, an additional band at 2840 cm^{-1} was found in this experiment on liquid tetramethylstannane at room temperature, of which the assignment still remains to be a problem. In the crystalline state, some Davydov splittings are found. The lattice frequencies are found at about 39 cm^{-1} and at about 80 cm^{-1} in the crystalline state, which shift to higher frequencies as the sample is cooled. The crystal structure has not been known, and therefore the lattice modes can not be analyzed in detail.

FIGURE 32. a) Raman spectra of tetramethylstannane at room temperature (liquid) and at 158 K (solid).

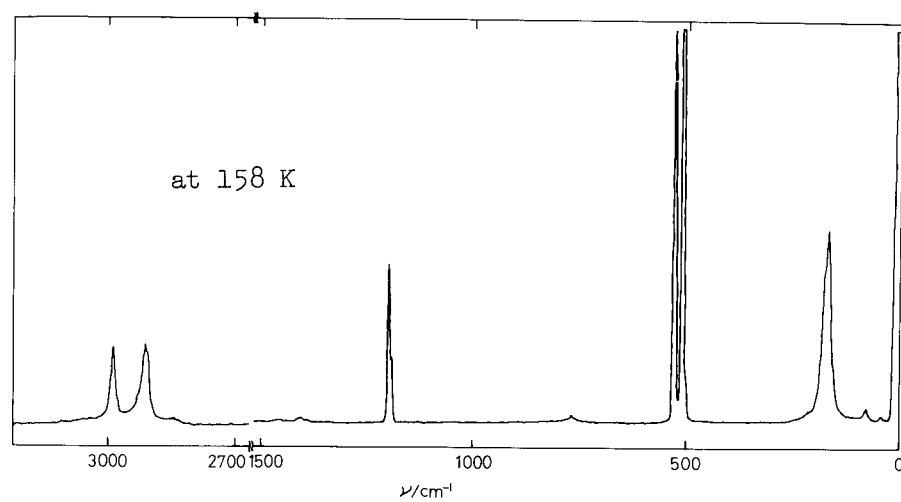
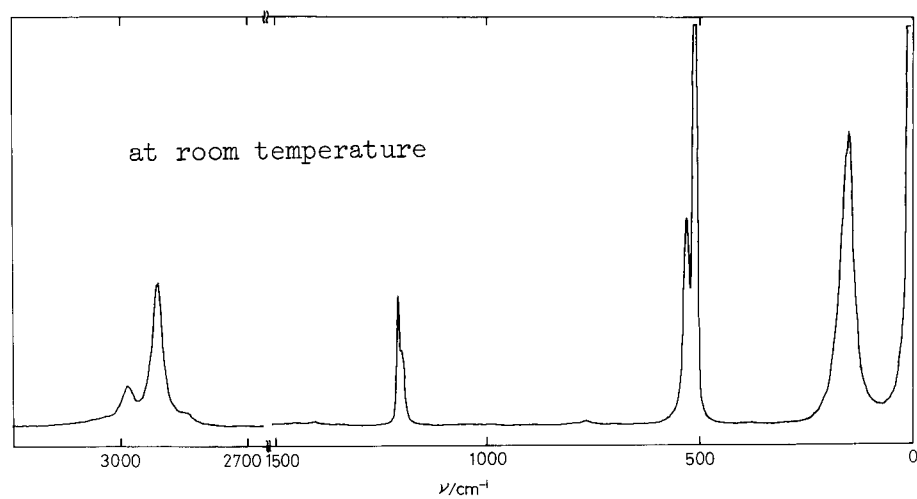


FIGURE 32. b) Comparison of the Raman spectra of liquid and solid tetramethylstannane.

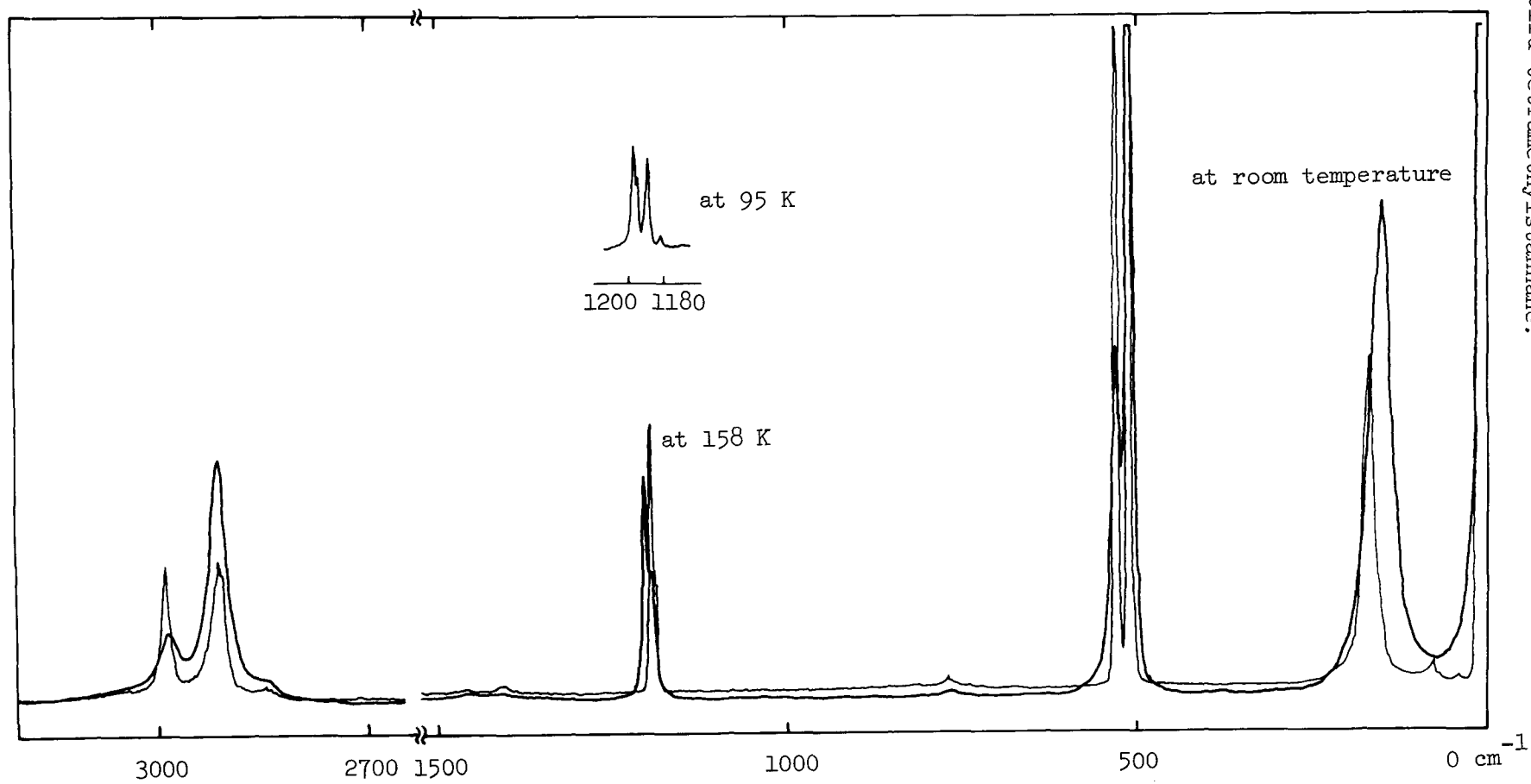


FIGURE 32. c) Raman spectra of tetramethylstannane at 95 K.

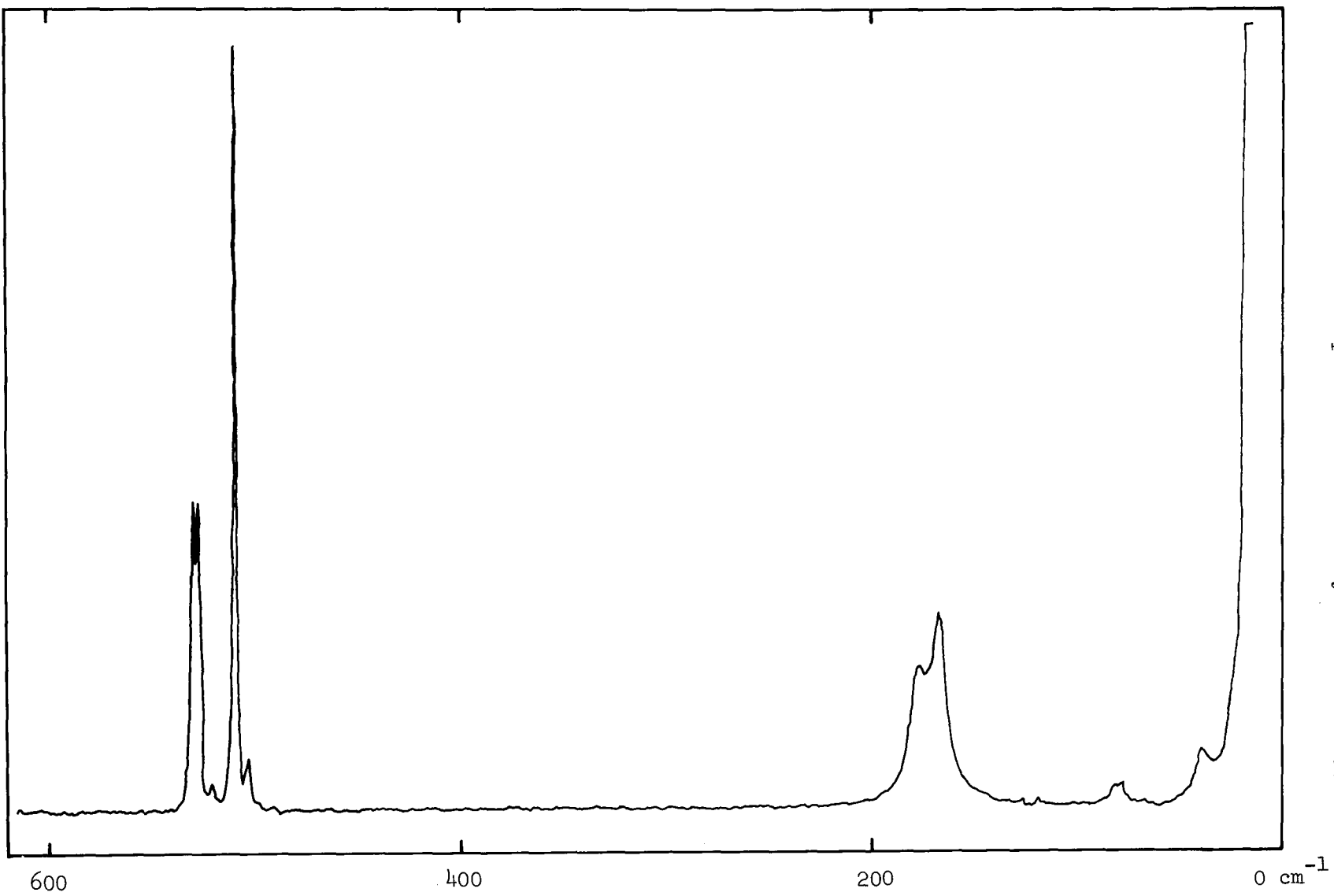


TABLE 30. RAMAN SPECTRA OF TETRAMETHYLSTANNANE. (in cm^{-1})

		Previous results ⁶⁸⁾	This results		
			Room temp.	158 K	95 K
ν_1	(A ₁)	2912	2913	2912	2911
ν_2	(A ₁)	1205	1206	1197	1197
ν_3	(A ₁)	507	512	512	512
ν_4	(A ₂)	(CH ₃ rotation)			
ν_5	(E)	2988	2985	2989	2989
ν_6	(E)	1400	1405	1405	1405
ν_7	(E)	772	770	770	770
ν_8	(E)	145	150	168	169
ν_9	(F ₁)	(2988)			
ν_{10}	(F ₁)	(1451)			
ν_{11}	(F ₁)	(772)	770	770	770
ν_{12}	(F ₁)	(CH ₃ rotation)			
ν_{13}	(F ₂)	2988	2985	2989	2989
ν_{14}	(F ₂)	2912	2913	2912	2911
ν_{15}	(F ₂)	1451	1455	1460	1460
ν_{16}	(F ₂)	1194	1196	1189	1188
ν_{17}	(F ₂)	772	770	770	770
ν_{18}	(F ₂)	532	531	531	531
ν_{19}	(F ₂)	160	150	176	178
			2840	2845	2845
				77	81
				38	39

4.4. Analysis and discussion

4.4.1. The third-law entropy and internal rotation of methyl groups

The third-law entropy of tetramethylstannane was determined as $(418.0 \pm 0.8) \text{ J K}^{-1} \text{ mol}^{-1}$ at 277.46 K and at 40.27 Torr, and as $(418.1 \pm 0.9) \text{ J K}^{-1} \text{ mol}^{-1}$ corrected to ideal state at this point. The correction for gas imperfection was made by using the Berthelot's relation:

$$S_{ideal} - S_{real} = 27RT_c^3 P / 32T_c^3 P_c, \quad (44)$$

where the critical constants T_c and P_c were estimated as 524 K and as 29 atm, respectively, by the method of R.F.Curl and K.S. Pitzer.⁶⁹⁾

The spectroscopic entropy of tetramethylstannane was calculated at 277.46 K and at 40.27 Torr, in the same manner as for dinitrogen oxide. The molecular moment of inertia of $373.1 \times 10^{-40} \text{ g cm}^2$ was used for the calculation of the rotational contribution by the equation:

$$S_{(rotational)} = \frac{3}{2}R + R \ln \frac{8\pi^2 (8\pi^3 I^3)^{1/2} (kT)^{3/2}}{\sigma h^3}, \quad (45)$$

and the symmetry number was taken as 12, assuming the free internal rotation of methyl groups. The contribution of free internal rotation of methyl groups was calculated by using the equation:

$$S_{(\text{internal rotation})} = \frac{1}{2}R + R \ln \frac{2.7930}{\sigma} (10^{38} I_r T)^{1/2}, \quad (46)$$

where the reduced moment of inertia I_r of methyl group was taken as $5.45 \times 10^{-40} \text{ g cm}^2$. For calculating the contribution of other modes of intramolecular vibrations, the frequencies tabulated in Table 30 were used in the harmonic approximation (equation (15)). The spectroscopic entropy of tetramethylstannane was determined as $418.0 \text{ J K}^{-1} \text{ mol}^{-1}$ at 277.46 K and at 40.27 Torr , on the assumption of free internal rotation of methyl groups.

The calculations of the third-law entropy and the spectroscopic entropy are summarized in Table 31. The difference between these two values of entropies is zero within the error of measurements. It seems that the model of free internal rotation of methyl groups is valid, and the barrier height to reorientation of methyl groups is very low. Assuming the difference to be $\Delta S \leq 0.8 \text{ J K}^{-1} \text{ mol}^{-1}$, the barrier height to reorientation of methyl groups in tetramethylstannane is estimated as $V \leq 400 \text{ cal mol}^{-1}$ from the table of K.S.Pitzer and W.D.Gwinn.⁷⁰⁾

The barrier heights in the molecules of the series $M(\text{CH}_3)_n\text{H}_{4-n}$, where $M = \text{C, Si, Ge and Sn}$, are summarized in Table 32. In the case of $\text{C}(\text{CH}_3)_n\text{H}_{4-n}$, as the number of methyl groups increases the barrier increases, which is explained as the intramolecular interaction of methyl groups with one another. In the case of $\text{Si}(\text{CH}_3)_n\text{H}_{4-n}$, the number of methyl groups exerts less influence

TABLE 31. THE ENTROPY OF TETRAMETHYLSTANNANE.

a). Calorimetric entropy

contribution	$S / J K^{-1} mol^{-1}$
0 K — 217.20 K	216.0
217.2 K — 218.03 K(Fusion)	34.2
218.03 K — 277.46 K	44.7
Vaporization(34160/277.46)	123.1
<hr/>	
The entropy of actual gas at 277.46 K	418.0 ± 0.8
The entropy of ideal gas at 277.47 K	418.1 ± 0.9

b). Spectroscopic entropy

contribution	
$S_{(translational)}$	196.36
$S_{(rotational)}$	94.49
$S_{(vibrational)}$	67.66
$S_{(internal\ rotation)}$	59.46
<hr/>	
The spectroscopic entropy at 277.46 K	
40.27 Torr	418.0
<hr/>	
The residual entropy	$S_0 = -0.1 \pm 0.9$

TABLE 32. TORSIONAL BARRIERS FOR SOME $(\text{CH}_3)_n\text{MH}_{4-n}$ MOLECULES.
(in kcal mol⁻¹)

Molecule	M			
	C	Si	Ge	Sn
CH_3MH_3	2.93 ⁵³⁾	1.70 ⁷¹⁾ 1.67 ⁵⁷⁾	1.24 ⁶¹⁾	0.65 ⁷²⁾
$(\text{CH}_3)_2\text{MH}_2$	3.33 ⁷³⁾ 3.57 ⁵⁴⁾	1.65 ⁵⁸⁾	1.18 ⁶²⁾	
$(\text{CH}_3)_3\text{MH}$	3.9 ⁵⁵⁾	1.83 ⁵⁹⁾		
$(\text{CH}_3)_4\text{M}$	4.3 ⁵⁶⁾	2.0 ⁵⁶⁾	1.3 ⁵⁶⁾	0.8 ⁵⁶⁾
	4.3 ⁵¹⁾	1.3 ⁵¹⁾	0.75 ⁶⁰⁾	0.46 ⁷⁴⁾
			0.65 ⁷⁴⁾	<0.4 ^{This)}

C - C = 0.154 nm

C - Si = 0.19 nm

C - Ge = 0.198 nm

C - Sn = 0.218 nm

on the barrier height than for $C(CH_3)_nH_{4-n}$. In the case of $Ge(CH_3)_nH_{4-n}$ and $Sn(CH_3)_nH_{4-n}$, it seems that there is no relation between the number of methyl groups and the barrier height.

In all the cases, however, there is significant relation between the distance of M-C and the barrier height to reorientation of methyl groups. The barrier height is smaller for the larger central atom M. In the case of $Sn(CH_3)_4$, therefore, each methyl group may reorient independently and freely. Assuming that the rotational motion of methyl groups in the molecule of tetramethylstannane is not coupled to other modes of oscillations, the heat capacity curve should show a hump due to the change from torsional oscillation of methyl groups to hindered rotation, which in fact is shown in Figure 33. The more sensitive curve $C_p - C_{(intra)}$ was obtained by subtracting the contribution of intramolecular vibrations given in Table 30 from the total heat capacity.

There is a small hump at about 40 - 70 K, the temperature which corresponds to a value of about 200 - 400 cal mol⁻¹ of barrier height to ~~h~~ⁿdering uniaxial rotation of methyl groups if one uses the table of K.S.Pitzer and W.D.Gwinn.⁷⁰⁾ This value of barrier height is consistent with the value (< 400 cal mol⁻¹) derived from the analysis of the entropy of tetramethylstannane described above. No hump has been reported in the heat capacity of neopentane,^{50),51)} tetramethylsilane^{51),52)} and tetramethylgermane⁶⁰⁾.

In the case of neopentane, it is reasonable that no hump was discernible in the heat capacity curve because ^{the} barrier height

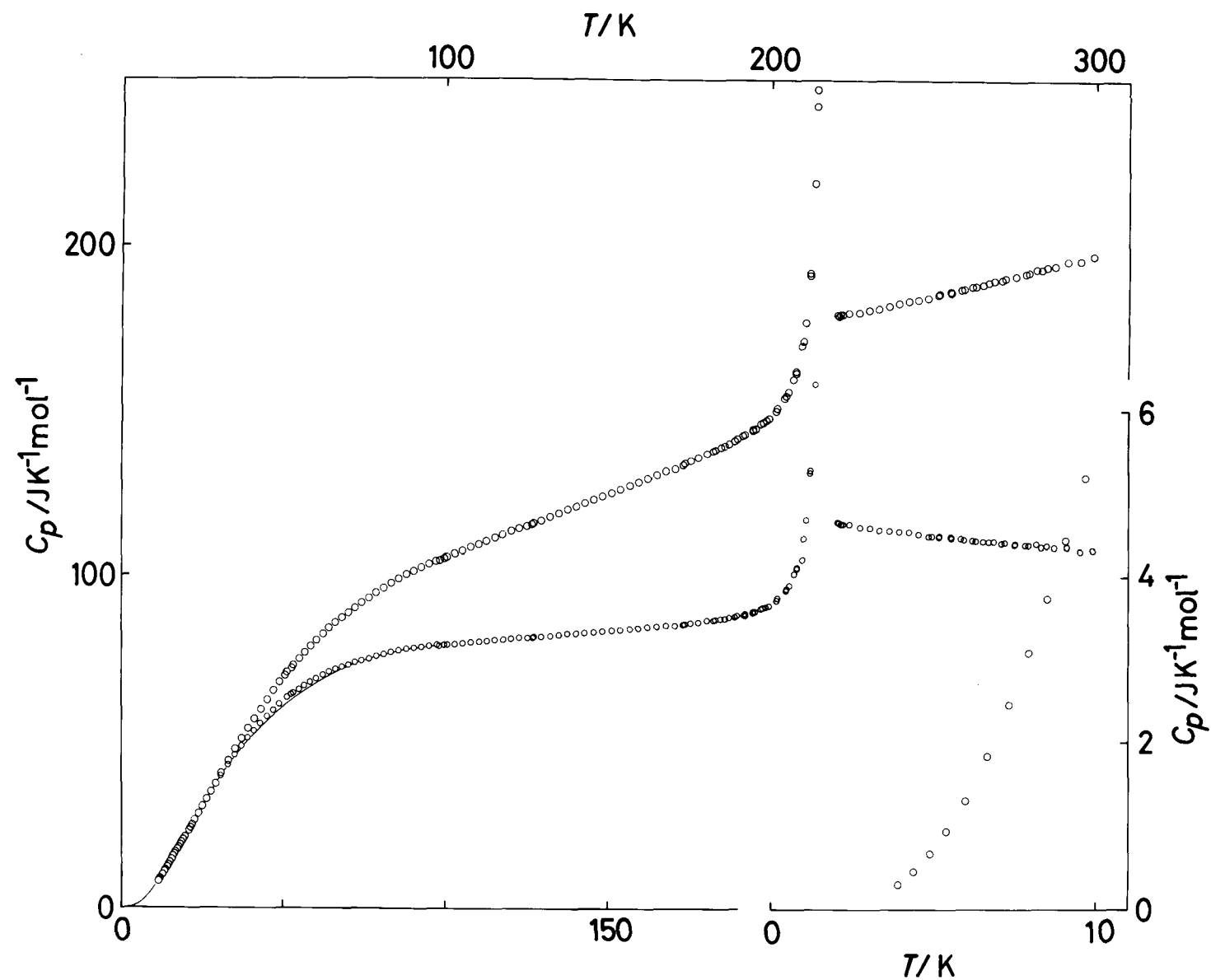


FIGURE 33. HEAT CAPACITY OF TETRAMETHYLSTANNANE.
THE SMALLER VALUES, $C_{p(obs.)} - C_{p(intra.)}$.

will be higher and also because the methyl rotations are not independent. In the case of tetramethylgermane, a hump could have been found in the heat capacity curve, if the heat capacity measurements had been of greater precision of A.J.Valerga and J.E.Kilpatrick. Tetramethylsilane is situated~~in~~^x the intermediate condition, which can not be analyzed in the less precise data of J.G.Aston, et al.⁵¹⁾ or the data in the limited temperature region by T.Shinoda, et al.⁵²⁾

4.4.2. Zero point properties

The molar heat of sublimation of tetramethylstannane at 0 K was calculated in the same way as for dinitrogen oxide. For the enthalpy of the gas, however, the rotational contribution of methyl groups is dependent on the barrier height to reorientation of methyl groups. Assuming the barrier height to reorientation of methyl groups as 400 cal mol^{-1} or 0 cal mol^{-1} , the value H_0° was obtained as 51000 J mol^{-1} or 54000 J mol^{-1} , respectively.

The Debye characteristic temperatures derived from the measured heat capacities are shown in Figure 34, and the limiting value at 0 K was determined from the plot of C_p/T^3 against T^2 by the same method as for dinitrogen oxide. Assuming $6N$ degrees of freedom, where $3N$ degrees of freedom correspond to the translational lattice modes and another $3N$ to the librational modes, the Debye characteristic temperature at 0 K was determined as $(99.0 \pm 1.0) \text{ K}$. Assuming only $3N$ degrees of freedom, the limiting

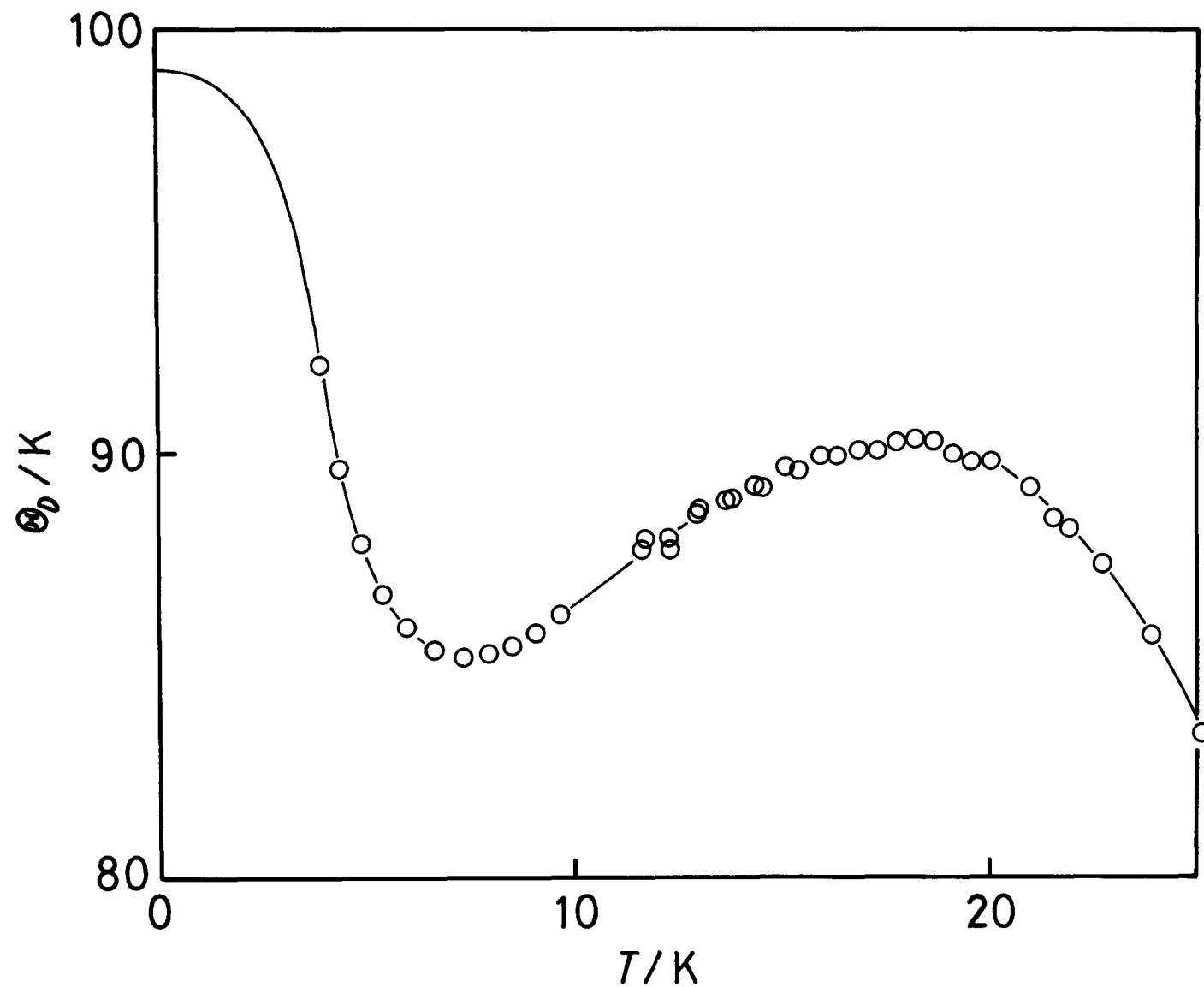


FIGURE 34. THE DEBYE CHARACTERISTIC TEMPERATURES OF TETRAMETHYLSTANNANE DERIVED FROM THE MEASURED HEAT CAPACITIES, ASSUMING 6N DEGREES OF FREEDOM.

value at 0 K of tetramethylstannane was determined as (78.5 ± 1.0) K.

These are summarized in Table 33, together with the data of other substances of the series of $M(\text{CH}_3)_4$. The Debye characteristic temperature of tetramethylgermane is an approximate value, because the data of heat capacity has been reported only above 15 K and the curve of the temperature dependence of the Debye characteristic temperature must show a shallow minimum below 15 K, and therefore the limiting value at 0 K can not be estimated from the data above 15 K. However, it is interesting to note that the Debye characteristic temperature of neopentane at 0 K is abnormally low as compared with those other substances in the series of $M(\text{CH}_3)_4$, none the less the triple point of neopentane is the highest in the series. The peculiarity of the properties of neopentane is found also in Tables 21, 32 and 34. It is apparent that neopentane has peculiar properties, while the other substances $M(\text{CH}_3)_4$ ($M = \text{Si}, \text{Ge}$ and Sn) form a group, in which the properties show good internal consistency. The normal boiling point of neopentane is the lowest in the series of $M(\text{CH}_3)_4$, while the triple point is the highest. The very narrow temperature region of liquid phase is common in the very simple molecular substances such as N_2O , CO_2 , CO and N_2 , etc., and the properties of neopentane (concerning intermolecular motion) are comparable with those of substances of this group, which are found in Tables 21 and 34.

TABLE 33. DEBYE CHARACTERISTIC TEMPERATURES AT 0 K OF SOME $M(\text{CH}_3)_4$ MOLECULES.

	$\frac{\theta_D(6N)}{\text{K}}$	$\frac{\theta_D(3N)}{\text{K}}$	$\frac{T_b}{\text{K}}$	$\frac{T_f}{\text{K}}$	$\frac{T_t}{\text{K}}$
$\text{C}(\text{CH}_3)_4$	129	102	282.61	256.750	140.498
$\text{Si}(\text{CH}_3)_4$	137	109	299.80	174.049	
$\text{Ge}(\text{CH}_3)_4$	(106)		316.6	184.37	
$\text{Sn}(\text{CH}_3)_4$	99.0	78.5	351.2	218.13	

4.4.3. Premelting

In the temperature region from about 100 K to about 160 K, the heat capacity of solid tetramethylstannane can be expressed satisfactorily by $C_p = A + BT$. By fitting the measured values of heat capacity (from 100 K to 160 K) into this formula, the constants were determined:

$$C_{p(normal)} = 0.3806T + 67.14 \quad , \quad (47)$$

and it may be extended to the higher temperature region (from 165 K to 218 K), where the total heat capacity may be expressed as:

$$C_p = C_{p(normal)} + \Delta C_p \quad . \quad (48)$$

The solid tetramethylstannane shows anomalous increase of heat capacity in the high temperature region below the triple point (from 165 K to 218 K), which is shown in Figure 35, and the excess heat capacity ΔC_p was estimated from the equations (47) and (48). However, the sample of tetramethylstannane contained significant amount of impurity, and the contribution of the impurity (0.15 mol per cent), which is shown by the dashed curve in Figure 35, was calculated by the equation:⁶⁷⁾

$$\Delta C_{pm} = xRT_0^2 / (T_0 - T)^2 \quad , \quad (49)$$

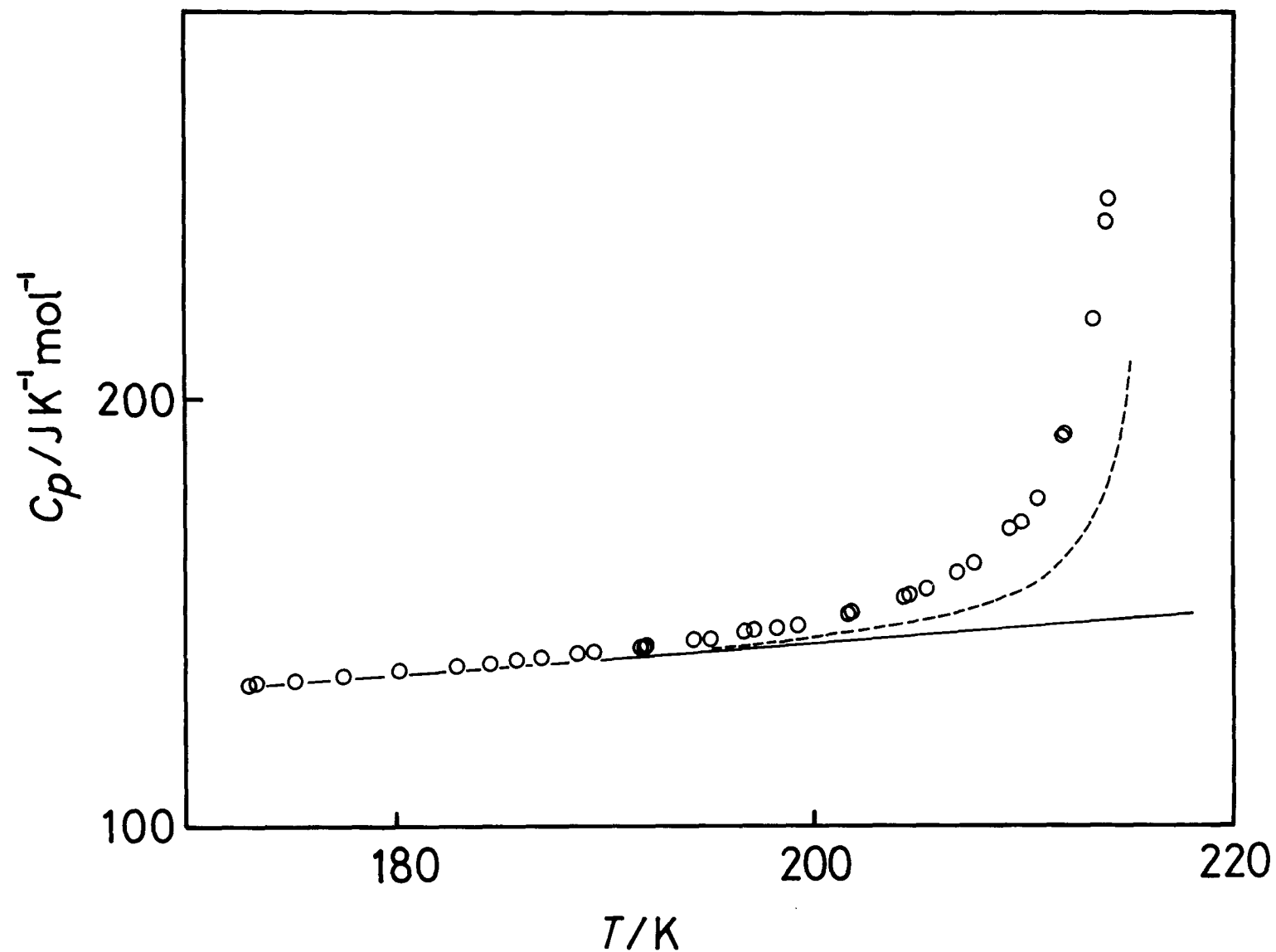


FIGURE 35. THE HEAT CAPACITY OF TETRAMETHYLSTANNANE IN THE PREMELTING REGION. —, $C_{p(\text{normal})}$; ----, $C_{p(\text{normal})} + C_{p(\text{impurity})}$.

where x denotes the mole fraction of the impurity and T_0 is the melting point of pure tetramethylstannane. This contribution was subtracted from the excess heat capacity obtained above, and the rest ($\Delta C_p' = \Delta C_p - \Delta C_{pm}$) was analyzed in the same manner as for dinitrogen oxide. The plot of $\log(\Delta C_p' T^2)$ against T^{-1} is shown in Figure 36, where two slopes can be drawn and two values of enthalpy of formation of imperfections can be obtained; $3.48 \times 10^4 \text{ J mol}^{-1}$ and $1.5 \times 10^5 \text{ J mol}^{-1}$. (By neglecting the impurity effect, the plot of $\log(\Delta C_p T^2)$ against T^{-1} gives also two values; $2.53 \times 10^4 \text{ J mol}^{-1}$ and $1.0 \times 10^5 \text{ J mol}^{-1}$.) This implies that there are two kinds of mechanism of thermal creation of imperfections in solid tetramethylstannane just below its melting point. It seems very likely that the two values correspond to the enthalpy of formation of orientational defects and of lattice vacancies, respectively. The value of the former may be smaller than that of the latter.

The crystal of neopentane has a phase transition (at 140.498 K) below its melting point (256.750 K). The molecular rotational motion is significantly excited above the phase transition, and therefore the entropy change at the melting point is small ($2.88 \text{ cal K}^{-1} \text{ mol}^{-1}$). In this case, there are anomalous increases of heat capacity below each thermodynamic first order transitions (solid phase transition and melting point). T. Shinoda, et al.⁵⁰⁾ analyzed only the premelting phenomenon below the melting point and obtained the value of enthalpy of formation of lattice vacan-

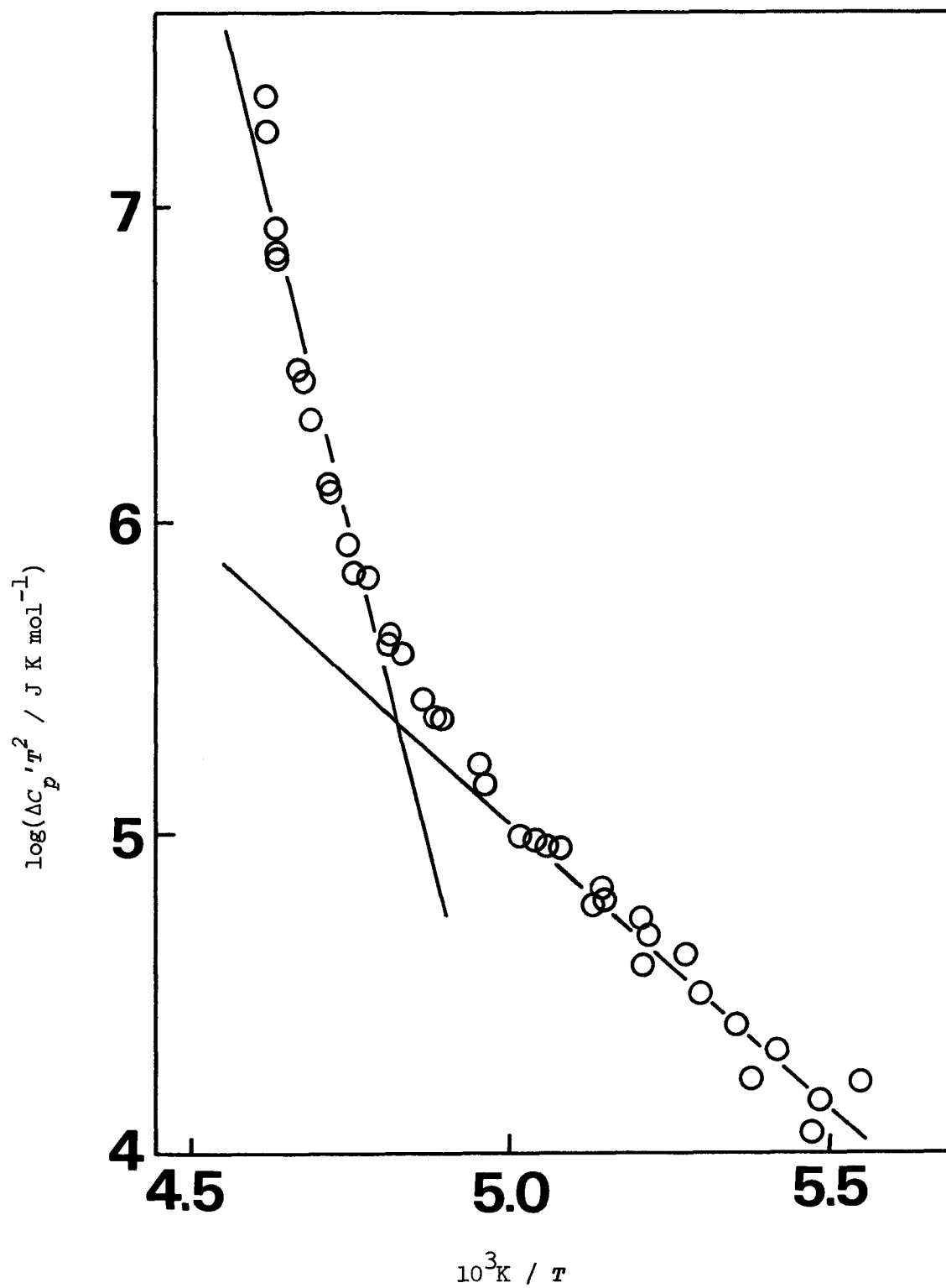


FIGURE 36. PLOT OF $\log(\Delta C_p T^2)$ AGAINST $1/T$ FOR TETRAMETHYL-STANNANE.

cies; $3240 \pm 220 \text{ cal mol}^{-1}$. In this investigation, however, the anomalous increase of heat capacity below the phase transition of neopentane was analyzed and the enthalpy of formation of orientational defects was obtained as 9700 J mol^{-1} . The crystal of tetramethylstannane has no phase transition below its melting point, and it seems that the rotational ^{phase transition} may exist just above the triple point, and therefore the thermal creations of imperfections of the two kinds of mechanism may occur simultaneously.

In the case of tetramethylsilane, T. Shinoda, et al. obtained only one value for the enthalpy of formation of lattice vacancies in the stable form; 28 kcal mol^{-1} . They considered this value ($1.17 \times 10^5 \text{ J mol}^{-1}$) to be extremely large compared with the value of $1.36 \times 10^4 \text{ J mol}^{-1}$ for neopentane. However, this value compares favorably with that of tetramethylstannane (Table 34). They reported also two values for the metastable form of tetramethylsilane; 30 kcal mol^{-1} and 47 kcal mol^{-1} . In this case, however, the scatter of the plot of $\log(\Delta C_p T^2)$ against T^{-1} is rather large, and therefore only one value also can be derived as $1.5 \times 10^5 \text{ J mol}^{-1}$ from their data.

Tetramethylgermane is a molecule of interest for extending such studies. However, the data by A.J. Valerga and J.E. Kilpatrick are rather less precise and can not be analyzed in detail.

These are summarized in Table 34, where the parentheses denote the values which can not be calculated ^{from} the ~~published~~ ^{published} data but should be obtained from the more precise data.

TABLE 34. COMPARISON OF PREMELTING PHENOMENA OF SOME SIMPLE MOLECULAR CRYSTALS.

	N_2O	CO_2	CO	N_2	$C(CH_3)_4$	$Si(CH_3)_4$	$Ge(CH_3)_4$	$Sn(CH_3)_4$
T_b/K	184.74		81.61	77.32	282.61	299.80	316.6	351.2
T_f/K	182.408	194.67	68.15	63.14	256.750	174.049	184.37	218.13
T_t/K	-----	-----	61.57	35.61	140.498	-----	-----	-----
$H_0^\circ/Jmol^{-1}$	24200	27000	8000	6900	()	()	()	(⁵¹⁰⁰⁰ 54000)
$\Delta H_{or}/Jmol^{-1}$	10800	20000	3000	2000	9700	()	()	(³⁴⁸⁰⁰ 25300)
$\Delta H_{vac}/Jmol^{-1}$	-----	-----	()	()	13600	117000	()	(¹⁵⁰⁰⁰⁰ 104000)
$\Delta H_{or}/H_0^\circ$	0.45	0.74	0.38	0.29	()	()	()	(^{0.68} 0.47)
$\Delta H_{or}/T_f$	59.2	103.	44.	32.	38.	()	()	(¹⁵⁹ 116)

REFERENCES

- 1). W.F.Giauque and his coworkers, HCl: J. Am. Chem. Soc., 50, 101 (1928), HBr: ibid., 50, 2193 (1928), HI: ibid., 51, 1441 (1929), O₂: ibid., 51, 2300 (1929), NO: ibid., 51, 3194 (1929), I₂: ibid., 53, 507 (1931), CO: ibid., 54, 2610 (1932), N₂: ibid., 55, 4875 (1933), N₂O: ibid., 57, 991 (1935), H₂S: ibid., 58, 831 (1936), H₂O: ibid., 58, 1144 (1936), COS: ibid., 59, 79 (1937), NH₃: ibid., 59, 254 (1937), CO₂: J. Chem. Phys., 5, 45 (1937), PH₃: ibid., 5, 149 (1937), SO₂: J. Am. Chem. Soc., 60, 1389 (1938), N₂O₄: J. Chem. Phys., 6, 40 (1938), Cl₂: J. Am. Chem. Soc., 61, 1970 (1939), CH₂=CH-CH₃: ibid., 61, 2366 (1939), HCN: ibid., 61, 2626 (1939), C₂N₂: ibid., 61, 2940 (1939), CH₃NO₂: ibid., 69, 983 (1947), COCl₂: ibid., 70, 120 (1948) and 82, 2689 (1960), C₂H₅Cl: ibid., 70, 1506 (1948), AsH₃: ibid., 77, 2154 (1955), ClO₃F: ibid., 80, 2659 (1958), etc.
- 2). K.Clusius and his coworkers, N₂, O₂, CO: Z. physik. Chem., B 3, 41 (1929), CH₄, CH_nD_{4-n}: Z. physik. Chem., B 3, 41 (1929) and Physica, 4, 1105 (1937), N₂O: Z. physik. Chem., B 8, 427 (1930), NH₃: Z. physik. Chem., B 8, 427 (1930), PH₃: Z. f. Elektrochem., 39, 598 (1933), H₂S, D₂S, H₂Se, D₂Se: Z. physik. Chem., B 38, 156 (1937), HX, DX: Z. Naturforsch., 2a, 495 (1947), etc.
- 3). a). F.E.Simon and his coworkers,

- b). A.Eucken and his coworkers,
- c). J.G.Aston and his coworkers,
- d). L.A.K.Staveley and his coworkers,
- e). E.L.Pace and his coworkers, et al.
- 4). P.P.Debye, Ann. Phys., Lpz. 39, 789 (1912).
- 5). P.Flubacher, A.J.Leadbetter and J.A.Morrison, Proc. Phys. Soc., 78, 1449 (1961).
- 6). R.H.Beaumont, H.Chihara and J.A.Morrison, Proc. Phys. Soc., 78, 1462 (1961).
- 7). J.H.Colwell, E.K.Gill and J.A.Morrison, J. Chem. Phys., 36, 2223 (1962), 39, 635 (1963), 42, 3144 (1965).
- 8). H.Fenichel and B.Serin, Phys. Rev., 142, 490 (1966).
- 9). E.K.Gill and J.A.Morrison, J. Chem. Phys., 45, 1585 (1966).
- 10). T.Shinoda, T.Atake, H.Chihara, Y.Mashiko and S.Seki, Kogyo Kagaku Zasshi, 69, 1619 (1966).
- 11). J.C.Burford and G.M.Graham, Canadian J. Phys., 47, 23 (1969).
- 12). M.I.Bagatskii, V.A.Kucheryavy, V.G.Manzhelii and V.A.Popov, Phys. Stat. Sol., 26, 453 (1968).
- 13). C.-H.Fagerstroem and A.C.Hollis Hallett, J. Low Temp. Phys., 1, 3 (1969).
- 14). M.L.Klein, J.A.Morrison and R.D.Weir, Discuss. Faraday Soc., 48, 93 (1969).
- 15). H.Enokido, T.Shinoda and Y.Mashiko, Bull. Chem. Soc. Japan, 42, 3415 (1969).
- 16). M.I.Bagatskii, V.G.Manzhelii and V.A.Popov, Phys. Stat. Sol.,

- 37, 65 (1970).
- 17). V.G.Manzhelii, A.M.Tolkachev, M.I.Bagatskii and E.I.Voitovich,
Phys. Stat. Sol., (b)44, 39 (1971).
 - 18). V.A.Popov, V.G.Manzhelii and M.I.Bagatskii, J. Low Temp.
Phys., 5, 427 (1971).
 - 19). J.H.Colwell, J. Chem. Phys., 51, 3820 (1969).
 - 20). J.A.Morrison and P.R.Norton, J. Chem. Phys., 56, 1457 (1972).
 - 21). T.Shinoda, H.Chihara and S.Seki, J. Phys. Soc. Japan, 19,
1637 (1964).
 - 22). T. Atake and H.Chihara, J. Chem. Thermodynamics, 3, 51
(1971).
 - 23). a). The International Practical Temperature Scale of 1968.
Comptes Rendus de la 13me Coference Generale des Poids et
Mesures 1967-68, Annex 2. Metrologia, 5, 35 (1969),
b). R.E.Bedford, H.Preston-Thomas, M.Durieux and R.Muijlwijk,
Metrologia, 5, 45 (1969),
c). R.E.Bedford, M.Durieux, R.Muijlwijk and C.R.Barber,
Metrologia, 5, 47 (1969).
 - 24). a). J.T.Schriempf, Cryogenics, 6, 362 (1966),
b). D.W.Osborne, H.E.Floto and F.Schreiner, Ann. Acad.
Sci. Fennicae AVI, No. 210, 35 (1966),
c). G.Ahlers and J.F.Macre, Rev. Sci. Instruments, 37, 962
(1966),
d). L.T.Claiborne, W.R.Hardin and N.G.Einspruch, Rev. Sci.
Instruments, 37, 1422 (1966),

- e). D.W.Osborne, H.E.Floto and F.Schreiner, Rev. Sci. Instruments, 38, 159 (1967),
- f). J.S.Blakemore, J.Winstel and R.V.Edwards, Rev. Sci. Instruments, 41, 835 (1970),
- g). E.Catalano, B.L.Shroyer and J.C.English, Rev. Sci. Instruments, 41, 1663 (1970).
- 25). F.G.Brickwedde, H.van Dijk, M.Durieux, J.R.Clement and J.K. Logan, J. Res. Natl. Bur. Std. 64A, 1 (1960).
- 26). F.C.Nix and D.MacNair, Phys. Rev., 60, 597 (1941).
- 27). a). J.E.Kilpatrick, W.E.Keller, E.F.Hammel and N.Metropolis, Phys. Rev., 94, 1103 (1954), 97, 9 (1955),
b). D.White, T.Rubin, P.Camky and H.L.Johnston, J. Phys. Chem., 64, 1607 (1960),
c). M.E.Boyd, S.Y.Larsen and H.Plumb, J. Res. Natl. Bur. Std. 72A, 155 (1968),
d). J.Brewer and G.W.Vaughn, J. Chem. Phys., 50, 2960 (1969),
e). M.E.Boyd, S.Y.Larsen and J.E.Kilpatrick, J. Chem. Phys., 50, 4034 (1969).
- 28). a). F.E.Simon, Zeit. f. Phys., 41, 806 (1927),
b). F.E.Simon, Physica, 4, 1089 (1937).
- 29). M.W.Melhuish and R.L.Scott, J. Phys. Chem., 68, 2301 (1964).
- 30). R.F.Curl, Jr., H.P.Hopkins, Jr. and K.S.Pitzer, J. Chem. Phys., 48, 4064 (1968).
- 31). a). H.L.Johnston and H.R.Weimer, J. AM. Chem. Soc., 56, 625 (1934).

- b). E.J.Couch and K.A.Kobe, J. Chem. Eng. Data, 6, 229 (1961).
- 32). a). J.deSmedt and W.H.Keesom, Koninkl. Ned. Akad. Wetenschap. Proc., 27, 839 (1924),
 b). W.Heuse, Z. physik. Chem., A147, 266 (1930),
 c). L.Vegard, Z. Physik., 71, 465 (1931),
 d). A.J.Leadbetter, D.J.Taylor and B.Vincent, Canad. J. Chem., 42, 2930 (1964).
- 33). W.C.Hamilton and M.Petrie, J. Phys. Chem., 65, 1453 (1961).
- 34). L.Pauling, Phys. Rev., 36, 430 (1930).
- 35). W.H.Keesom and J.W.L.Kohler, Physica, 1, 655 (1934).
- 36). L.Vegard, Z. Phys., 61, 185 (1930).
- 37). a). T.H.Jordan, H.W.Smith, W.E.Streib and W.N.Libscumb, J. Chem. Phys., 41, 756 (1964),
 b). E.J.Wachtel, J. Chem. Phys., 57, 5620 (1972).
- 38). D.E.Stogryn and A.P.Stogryn, Mol. Phys., 11, 371 (1966).
- 39). a). A.Anderson and S.H.Walmsley, Mol. Phys., 7, 583 (1964),
 b). A.Anderson and H.A.Gebbie, Spectrochim. Acta, 21, 883 (1965),
 c). J.E.Cahill, K.L.Treuil, R.E.Miller and G.E.Leroi, J. Chem. Phys., 47, 3678 (1967),
 d). J.E.Cahill, K.L.Treuil, R.E.Miller and G.E.Leroi, J. Chem. Phys., 49, 3320 (1968),
 e). J.E.Cahill and G.E.Leroi, J. Chem. Phys., 51, 1324 (1969),

- f). A.Anderson and T.S.Sun, Chem. Phys. Lett., 8, 537 (1971),
- g). P.F.Krause and H.B.Friedrich, Chem. Phys. Lett., 18,
186 (1973).
- 40). a). L.Salter, Trans. Faraday Soc., 59, 657 (1963),
b). A.J.Leadbetter and D.M.T.Newsham, Trans. Faraday Soc.,
61, 1646 (1965).
- 41). H.Chihara and N.Nakamura, Bull. Chem. Soc. Japan, 41, 1787
(1968).
- 42). H.Thirring, Phys. Z., 14, 867 (1913); 15, 127, 180 (1914).
- 43). a). B.C.Kohin, J. Chem. Phys., 33, 882 (1960),
b). A.Anderson and G.E.Leroi, J.Chem. Phys., 45, 4359 (1966),
c). O.Schnepp and A.Ron, J.Chem. Phys., 46, 3893, 3991 (1967),
d). J.E.Cahill and G.E.Leroi, J.Chem. Phys., 51, 97 (1969),
e). M.Brith, A.Ron and O.Schnepp, J. Chem. Phys., 51,
1318 (1969),
f). J.E.Cahill and G.E.Leroi, J. Chem. Phys., 51, 4514
(1969),
g). O.Schnepp and A.Ron, Discuss. Faraday Soc., 48, 26
(1969),
h). T.-S.Kuan, A.Warshel and O.Schnepp, J. Chem. Phys.,
52, 3012 (1970),
i). A.Anderson, T.S.Sun and M.C.A.Donkersloot, Canadian
J. Phys., 48, 2265 (1970),
j). N.Jacobi and O.Schnepp, J. Chem. Phys., 57, 2505, 2516
(1972); Chem. Phys. Letters, 13, 344 (1972),

- k). P.V.Dunmore, J. Chem. Phys., 57, 3348 (1972).
- 44). a). H.Chihara and T.Shinoda, J. Phys. Soc. Japan, 17, 1395 (1962),
- b). T.Shinoda and H.Enokido, J. Phys. Soc. Japan, 26, 1353 (1969),
- c). J.C.Raich and R.D.Etters, J. Chem. Phys., 55, 3901 (1971).
- 45). A.Einstein, Ann. Phys., 22, 180 (1907).
- 46). M.Born and Th. von Karman, Phys. Z., 13, 297 (1912); 14, 15 (1913).
- 47). E.W.Montroll, J. Chem. Phys., 10, 218 (1942); 11, 15 (1943).
- 48). a). V.I.Peresada and V.N.Afanasev, Soviet Physics JETP 26, 389 (1968); 31, 78 (1970),
- b). E.L.Pollock, J.Chem. Phys., 58, 1966 (1973).
- 49). C.Domb and L.Salter, Phil. Mag., 43, 1083 (1952).
- 50). H.Enokido, T.Shinoda and Y.Mashiko, Bull. Chem. Soc. Japan, 42, 84 (1969).
- 51). a). J.G.Aston and G.H.Messerly, J. Am. Chem. Soc., 58, 2354 (1936),
- b). J.G.Aston, R.M.Kennedy and G.H.Messerly, J. Am. Chem. Soc., 63, 2343 (1941).
- 52). T.Shinoda, H.Enokido, Y.Maeda, H.Tomita and Y.Mashiko, Bull. Chem. Soc. Japan, 46, 48 (1973).
- 53). S.Weiss and G.E.Leroi, J. Chem. Phys., 48, 962 (1968).
- 54). J.R.Hoyland, J. Chem. Phys., 49, 1908 (1968).
- 55). D.R.Lide,Jr. and D.E.Mann, J.Chem. Phys., 28, 572 (1958).

- 56). J.R.Durig, S.M.Craven and J.Bragin, J. Chem. Phys., 52, 2046 (1970).
- 57). D.R.Hirschenbach, J. Chem. Phys., 31, 91 (1959).
- 58). L.Pierce, J. Chem. Phys., 34, 498 (1961).
- 59). L.Pierce and D.H.Peterson, J. Chem. Phys., 33, 907 (1960).
- 60). A.J.Valerga and J.E.Kilpatrick, J. Chem. Phys., 52, 4545 (1970).
- 61). V.W.Laurie, J. Chem. Phys., 30, 1210 (1959).
- 62). E.C.Thomas and V.W.Laurie, J. Chem. Phys., 50, 3512 (1969).
- 63). M.Harada, et al. (to be published).
- 64). L.A.K.Staveley, J.B.Warren, H.P.Paget and D.J.Dowrick, J. Chem. Soc., 1954, 1992
- 65). R.H.Bullard and A.C.Haussmann, J. Phys. Chem., 34, 743 (1930).
- 66). M. Nakamura, thesis (Osaka University; 1967).
- 67). a). E.L.Skau, J. Am. Chem. Soc., 57, 243 (1935),
b). J.G.Aston, M.R.Cines and H.L.Fink, J. Am. Chem. Soc., 69, 1532 (1947),
c). S.V.R.Mastrangelo and R.W.Dornste, J. Am. Chem. Soc., 77, 6200 (1955),
d). D.D.Tunnicliff and H.Stone, Anal. Chem., 27, 73 (1955),
e). A.R.Ubbelohde, Anal. Chim. Acta, 17, 1 (1957),
f). Y.Mashiko, Japan Analyst, 15, 1151 (1966).
- 68). a). E.R.Lippincott and M.C.Tobin, J. Am. Chem. Soc., 75, 4141 (1953),
b). W.F.Edgeall and C.H.Ward, J. Am. Chem. Soc., 77, 6486(1955),

- c). D.N.Waters and L.A.Woodward, Proc. Roy. Soc., A246,
119 (1958),
- d). S.C.Graham, Spectrochim. Acta, A26, 345 (1970).
- 69). R.F.Curl,Jr. and K.S.Pitzer, Ind. Eng. Chem., 50, 265 (1958).
- 70). K.S.Pitzer and W.D.Gwinn, J.Chem. Phys., 10, 428 (1942).
- 71). R.W.Kilb and L.Pierce, J. Chem. Phys., 27, 108 (1957).
- 72). P.Cahill and S.S.Butcher, J.Chem. Phys., 35, 2255 (1962).
- 73). D.R.Lide,Jr., J. Chem. Phys., 33, 1514 (1960).
- 74). G.W.Smith, J.Chem. Phys., 42, 4229 (1965).
- 75). M.Blackman, Proc. Roy. Soc. London, A148, 365, 384 (1934),
A159, 416 (1937); Phil. Trans. Roy. Soc. London, A236, 103
(1936); Proc. Cambridge Phil. Soc., 33, 94 (1937).
- 76). W.V.Houston, Rev. Mod. Phys., 20, 161 (1948).
- 77). E.L.Pace and B.E.Jepson, J. Chem. Phys., 52, 911 (1970).
- 78). a). F.J.Bockhoff, R.V.Petrella and E.L.Pace, J. Chem. Phys.,
799 (1960),
- b). E.J.Bockhoff and E.L.Pace, J. Chem. Phys., 36, 3502
(1962).